Chemical Physics Reviews

Terahertz (THz) biophotonics technology: Instrumentation, techniques, and biomedical applications

Cite as: Chem. Phys. Rev. **3**, 011311 (2022); https://doi.org/10.1063/5.0068979
Submitted: 28 August 2021 • Accepted: 08 February 2022 • Published Online: 24 March 2022

Xuequan Chen, Hannah Lindley-Hatcher, Rayko I. Stantchev, et al.

Chemical Physics Reviews REVIEW scitation.org/journal/cpr

Terahertz (THz) biophotonics technology: Instrumentation, techniques, and biomedical applications

Cite as: Chem. Phys. Rev. 3, 011311 (2022); doi: 10.1063/5.0068979
Submitted: 28 August 2021 · Accepted: 8 February 2022 ·
Published Online: 24 March 2022

View Online Export Citation CrossMark

Xuequan Chen,[1,2] Hannah Lindley-Hatcher,[3] Rayko I. Stantchev,[1,3] Jiarui Wang,[1] Kaidi Li,[1] Arturo Hernandez Serrano,[3] Zachary D. Taylor,[4] Enrique Castro-Camus,[5] and Emma Pickwell-MacPherson[3,a)]

AFFILIATIONS

[1]Department of Electronic Engineering, The Chinese University of Hong Kong, Hong Kong, China
[2]Great Bay Area Branch of Aerospace Information Research Institute, Chinese Academy of Sciences, Guangzhou 510530, China
[3]Department of Physics, University of Warwick, Coventry CV4 7AL, United Kingdom
[4]Department of Electronics and Nanoengineering, Aalto University, MilliLab, Espoo, Finland
[5]Department of Physics, Philipps-Universität Marburg, Renthof 5, 35032 Marburg, Germany

[a)]Author to whom correspondence should be addressed: e.macpherson@warwick.ac.uk.
URL: go.warwick.ac.uk/ultrafast/emmasthzgroup/

ABSTRACT

Terahertz (THz) technology has experienced rapid development in the past two decades. Growing numbers of interdisciplinary applications are emerging, including materials science, physics, communications, and security as well as biomedicine. THz biophotonics involves studies applying THz photonic technology in biomedicine, which has attracted attention due to the unique features of THz waves, such as the high sensitivity to water, resonance with biomolecules, favorable spatial resolution, capacity to probe the water–biomolecule interactions, and nonionizing photon energy. Despite the great potential, THz biophotonics is still at an early stage of development. There is a lack of standards for instrumentation, measurement protocols, and data analysis, which makes it difficult to make comparisons among all the work published. In this article, we give a comprehensive review of the key findings that have underpinned research into biomedical applications of THz technology. In particular, we will focus on the advances made in general THz instrumentation and specific THz-based instruments for biomedical applications. We will also discuss the theories describing the interaction between THz light and biomedical samples. We aim to provide an overview of both basic biomedical research as well as pre-clinical and clinical applications under investigation. The paper aims to provide a clear picture of the achievements, challenges, and future perspectives of THz biophotonics.

TABLE OF CONTENTS

I. INTRODUCTION

Over the last two decades, terahertz (THz) biophotonics has been rapidly growing as an important interdisciplinary branch of THz science and biomedical engineering. Being loosely defined as the electromagnetic waves in the frequency range of 0.1–10 THz, THz waves have some intermediate properties between microwaves and infrared, which are driving growth in this research field. For example, the hydrogen-bond network of water has broadband relaxation modes ranging from GHz to THz frequencies. This is the origin of the high permittivity and absorption of water in the THz band that make THz waves sensitive to water.[1] One of the most famous and impressive THz images that have promoted the development of THz biophotonics to some extent is the leaf image scanned by Hu and Nuss in 1995,[2] showing a dramatic change in the THz response for the leaf after 48 h due to the loss of water. Apart from water, intermolecular vibrations and rotations of some small biomolecules, such as nucleobase and amino acids,[3,4] also lie within the THz range, providing unique fingerprints which can be specifically detected. Additionally, the shorter wavelengths offer THz waves more optical properties than microwaves. Indeed, THz has an alternative name of "far-infrared," which was commonly used before the 21st century. THz waves are usually manipulated by optics in a form of beams in free space. Compared to the waveguiding approach generally used for microwaves, a THz optical system can be easily arranged into a spectroscopy or an imaging setup. The shorter wavelength also brings another important merit of better spatial resolution compared to microwaves. This, combined with its nonionizing nature due to the low photon energy and the wavelength-comparable depth of penetration into tissues, means that THz waves have the potential to be a good modality for *in vivo* imaging and diagnosis of superficial tissues. Moreover, the high sensitivity to tissue water content variation and limited bulk scattering render THz imaging an attractive diagnostic tool for diseases/pathologies/injuries that are defined by or correlated with abnormal surface tissue water content. The above characteristics have endowed THz waves with great potential for applications in the field of biomedicine, hence pushing forward a popular research field called THz biophotonics.

THz biomedical applications span a wide range of scales from molecules to cells and tissues. However, as a newly developed technique, there are no technical standards set for the measurements, and great effort is being put into the THz instrumentation, interaction theory, data analysis, and investigation of THz biomedical effects. THz instrumentation builds the foundation for many types of applications. The theory, modeling, and data processing have also experienced promising development over the years, and they undoubtedly also play important roles. Recently, concerns about the biological safety of intense THz radiation have also been frequently discussed. These research areas not only improve the technology and broaden the applications, but also result in a large divergence, making them difficult to compare between different works and evaluate the state of art. As an interdisciplinary branch between THz science and biomedical engineering, it is important that an overview of these different aspects be presented to allow readers from different fields to gain a comprehensive view. Several reviews related to the field of THz biophotonics have been published over the last ten years. There are topical reviews on THz cancer diagnosis by Yu *et al.*,[5] Peng *et al.*,[6] and Zaytsev *et al.*[7] Reviews on skin include those by Nikitkina *et al.*[8] and Wang *et al.*,[9] and there are more general reviews on biomedical applications by Fan *et al.*,[10] Yang *et al.*,[11] and Sun *et al.*[12] However, most of these articles have been focused on the application aspect or a specific topic. In this manuscript, we aim to provide a comprehensive overview of THz biophotonics, the scope of which is illustrated in Fig. 1. Covering these different aspects of THz biophotonics is helpful for understanding the development, achievements, challenges, and future perspectives, which are essential for the development of this promising interdisciplinary area.

II. INSTRUMENTATION FOR THz BIOPHOTONICS

A. THz systems

Emission, detection, and beam-guiding components are the three essential elements for a THz system. The historical name of

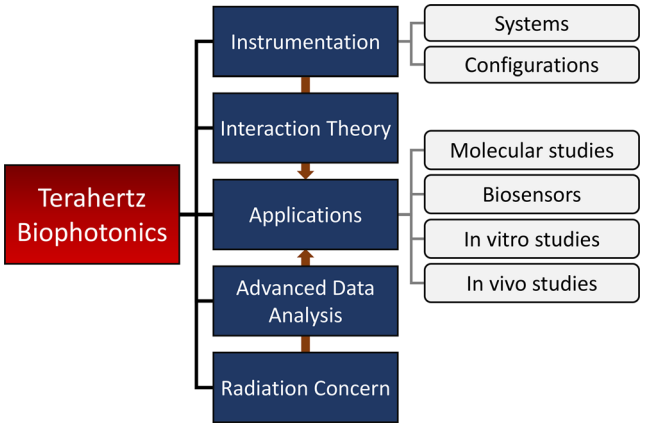

FIG. 1. The scope of THz biophotonics covered in this review.

"THz gap" originates from the lack of efficient THz emission and detection devices. Nowadays, this gap has not been completely filled as can be seen if the power, efficiency, and sensitivity of sources and detectors are compared to those available for visible wavelengths. However, considerable progress has been made toward narrowing the gap and to enable growing amounts of applications. THz systems applied to THz biophotonics can be classified into two categories: pulsed time-domain THz systems and continuous-wave (CW) THz systems. The two categories do not simply differ in emission mode; they are very different in several aspects, namely, sources and detectors, experimental protocols, and information acquired. A comprehensive overview of THz radiation and detection techniques is not within the scope of this manuscript, but this can be found from other reviews or handbooks.[13,14] Here, we focus on the systems that have been applied or have a high potential to be applied in THz biomedical research, highlighting their advantages, shortfalls, and scenarios of applications.

1. Pulsed time-domain THz systems

The name "pulsed time-domain THz systems" describes the two common features of this category: pulsed THz emission and time-domain detection. They are also commonly named as THz time-domain spectroscopy (THz-TDS) systems. Figure 2(a) shows the simplified fundamental optical setup for a pulsed time-domain THz system, which includes the essential components of a femtosecond (fs) laser, a beam splitter and an optical delay line (ODL). These optics control the beam delay between the pumping and probing beams sent to the THz emitter and detector, respectively, such that the THz waveform can be sampled in the time-domain.[14] A practical system may contain a lot more optics according to the specific user requirements, such as the laser amplifier, attenuators, waveplates, gratings, optical choppers, etc. In the THz optics region, a couple of laser-driven techniques based on different mechanisms can be used for the generation and detection of THz-waves, for example, ultra-fast carriers in photoconductive antennas (PCAs), optical rectification and electro-optic (EO) sampling in nonlinear crystals, plasma in air or liquids, and spintronic currents in a ferromagnetic/heavy-metal structure. These techniques all provide some outstanding features that make pulsed time-domain THz systems highly useful for numerous applications. For example, they all provide a picosecond level time-resolution, a broad bandwidth, and a field-detection ability comprising both magnitude and phase information for the spectrum. However, they can have different characteristics including the bandwidth, power, and flexibility, etc. In the following, we will introduce the two conventional techniques based on PCAs and EO crystals, and a relatively new emerging technology based on spintronic emission.

a. Photoconductive antenna. The invention of the photoconductive switch in 1980s has had a great impact on the whole THz society including THz biophotonics.[15] Tremendous amounts of work have been reported based on this technique. Figure 2(b) shows how a PCA works as a THz emitter and a detector. On the emitter side, the biased voltage on the electrodes accelerates the ultrafast carriers photoexcited by the femtosecond (fs) laser. This forms a transient current that radiates a picosecond pulse containing broadband THz frequencies. The electrodes act as the antenna to radiate the THz waves in the direction of laser propagation, and a hyperhemispherical silicon (Si) lens is used to collimate the radiated beam. On the detector side, the THz waves are focused by the Si lens. The laser-excited carriers in the semiconductor are accelerated by the THz electric field. This forms a current to be detected and lock-in amplified. As the carrier lifetime is much shorter than the THz pulse duration, the generated current represents

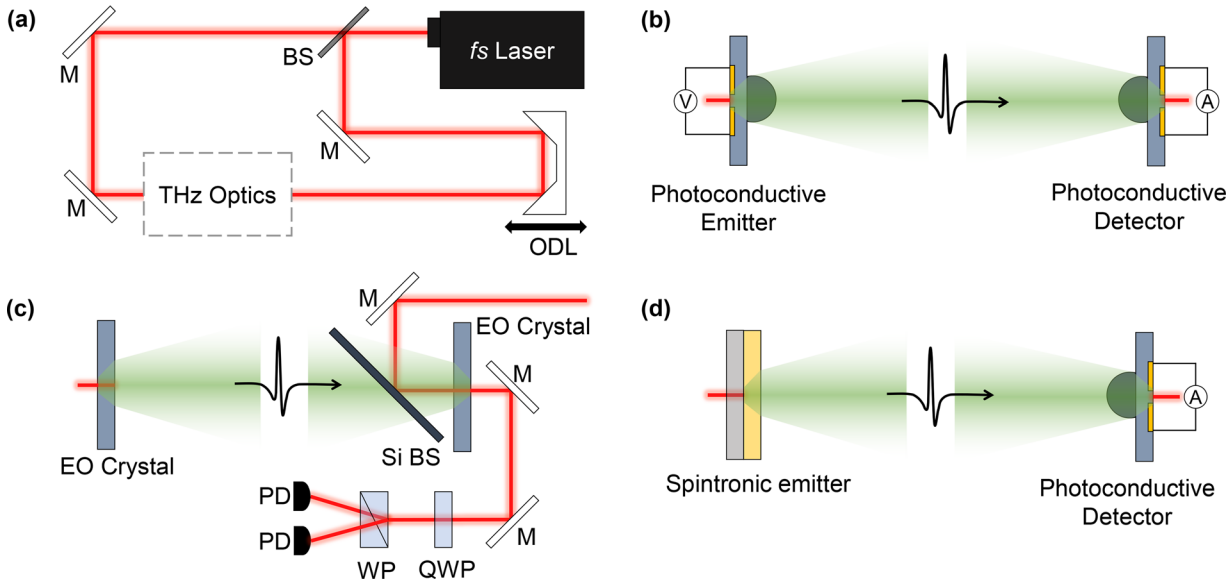

FIG. 2. Pulsed time-domain THz systems: (a) fundamental optical setting for a pulsed time-domain THz system. The THz optics region can be applied with various THz emission and detection devices, such as (b) photoconductive antennas, (c) nonlinear crystals, or (d) THz spintronic emitter. M: mirror, BS: beam splitter, ODL: optical delay line, EO: electro-optic, QWP: quarter-wave plate, WP: Wollaston prism, and PD: photodetector.

the THz electric field at the moment it interacts with the fs pulse, and the complete THz waveform is achieved by shifting the delay line to sample the THz electric field at different positions in the time-domain. PCAs have two unique features that make them especially suitable for biomedical applications. First, the metallic electrodes on the antenna allow direct control of the output polarization. Second, the compatibility with fibers enables a much higher flexibility in the optical arrangement. Polarization states usually need to be specified in biomedical research as the high absorption of many biosamples requires a reflection geometry to be used, making the measurement polarization-dependent. PCAs are usually linear in polarization for emission and detection depending on the electrode design. The polarization direction can be simply set by mechanically controlling the orientation of the antennas. Electrical control of the polarization direction has also been achieved by designing cross-electrodes.[16] The fiber-coupled modality makes it possible to freely move or rotate the antenna without affecting the laser-antenna alignment. This is usually achieved by using a fs fiber-laser with the wavelength centered at 1550 nm. In this case, all the THz optics can be assembled into a compact and portable probe head for flexible sensing,[17,18] or even in a prototype of an endoscope.[19] They can also be assembled on translation stages to perform a raster scan by moving the optics rather than the sample;[20] this is especially useful for *in vivo* studies. The fiber-connection also makes it possible to freely rotate the incident angle of a reflection system, particularly required in ellipsometry, which sets the incident angle close to the Brewster angle of a specific sample.[21]

b. Electro-optic crystal. Optical rectification is another mechanism that can be used to generate broadband THz radiation using a EO crystal, as shown in Fig. 2(c). This technique utilizes the large second-order nonlinear susceptibility of the crystal to induce a polarization proportional to the envelope of the fs pulse, giving rise to THz radiation.[22] The emitted THz wave is regarded as being rectified from the optical beam. EO crystals can also be used to coherently detect the THz electric field in time-domain, which is called EO sampling. This approach does not directly measure the THz electric field or the induced current; instead, it measures the change of the polarization of the optical beam due to the presence of the THz wave in the EO crystal. The EO technique has three major advantages over PCAs. First, without being limited by the carrier lifetime, EO generation and detection can support a much shorter pulse in the time-domain, providing a better temporal hence depth resolution. Fourier transforming a shorter pulse also provides a broader bandwidth, of which the upper frequency limit can be up to the mid-infrared depending on the crystal used.[23] This is akin to depth resolution in optical coherence tomography (OCT) where increasing optical bandwidth leads to decreased voxel depth.[24] Second, it can generate THz pulses with very high peak-intensity up to sub-mJ and peak electric field up to MV/cm.[25] The high peak power has been utilized to investigate the biological effects of intense THz radiation, which will be detailed in Sec. IV. Third, without the need for electrodes, direct spatial patterning on the pumping or probing beam can be used to perform ghost imaging (i.e., compressed sensing).[26–28] The major limitation of the EO technique is the need of laser amplification required by the nonlinear process, which restricts the repetition rate to a kHz level that fast-sampling of the THz waveforms becomes unavailable.

c. THz spintronic emitter. THz spintronic emitters are a new kind of THz source which have emerged in the last five years. The emitter is a multiple layered structure including a ferromagnetic and a nonmagnetic thin film. The generation mechanism is based on the inverse spin Hall effect to produce spin current, which comes from the diffusion of the spin-polarized electrons photoexcited in the ferromagnetic layer by the fs pulse. This spin current is then converted into a charge current in the nonmagnetic metal film, giving rise to THz radiation.[29] The detection of the emitted THz waves can be done by either EO sampling or a PCA. The former can detect frequencies over 10 THz, which is sometimes needed as spintronic emitters can cover a bandwidth up to 30 THz.[30,31] The latter approach provides simpler optics and a better flexibility, as shown in Fig. 2(d). THz spintronic emitters have many exciting features. Apart from the potential ultrabroad bandwidth, their emission efficiency remains nearly constant with the input pumping power from few mW to few tens of mW, with the pumping wavelengths from 800 to 1550 nm.[30] They also have a low requirement on pumping pulse energy; thus, lasers with a high repetition rate can be used without further amplification. The low-cost and compact fs-fiber lasers can be directly integrated, providing the flexibility of the THz optics discussed for the PCAs. The polarization can also be simply controlled by rotating the orientation of the magnetic field applied to the emitter. Note that usually only a few mT is required; hence, bulky magnets are unnecessary. Similar to the EO crystals, direct patterning on the pumping beam can also be achieved in THz spintronic emitters for compressed sensing, as reported by Chen *et al.*[32] The simple structure enables the fabrication of the emitter on a bendable substrate,[33] providing more flexibility. It can also be scaled to a large area up to 7.5 cm in diameter, as presented by Seifert *et al.*[34] The large device can generate intense THz pulses up to 300 kV cm^{-1}, offering options for investigating THz nonthermal biomedical effects (see Sec. IV). As a relatively new technique, there are still very few biomedical applications based on spintronic emitters reported. However, given the previously mentioned advantages and the rapid development in progress, spintronics has the potential to have a greater role in the future.

2. Continuous-wave and other THz systems

a. Generation. There are many ways to generate CW THz waves, ranging from vacuum devices, such as the backward-wave oscillator (BWO), solid-state devices, such as Gunn diodes, to four types of photonic devices, including gas lasers, quantum cascade lasers (QCLs), THz parametric sources, and THz photomixers. These sources have very different operating mechanisms and characteristics. BWOs and solid-state diodes are electronic devices originally developed from the microwave side. They rely on frequency multipliers to operate at higher frequencies, with a significant sacrifice on the power. For example, the multiplied output power of solid-state diodes decreases from hundreds of mW to sub-mW when the frequency is increased from 0.1 to 1 THz.[35] Diode multiplier chains can also be integrated as the extender heads with a vector network analyzer (VNA). The extender heads work both as the emitter and the detector, by harmonic generation or mixing the fundamental microwave source up to THz frequencies. VNAs measure both amplitude and phase, reflection, and transmission simultaneously with a high signal-to-noise ratio (SNR). These characteristics make them very useful in testing the performance

of a device by coupling to the waveguide ports, while they can also be employed in a quasi-optical arrangement for material characterization.[36] Free-electron lasers (FELs) are also vacuum sources but operate through a very different mechanism. FELs generate coherent THz radiation by converting the kinetic energy of a relativistic electron beam to electromagnetic waves in a periodic static magnetic field. THz FELs have a few irreplaceable features, including a high tunability of frequency in a ultrabroad band, the extremely high peak power up to gigawatts, and the flexible emission mode from CW to ultra-short pulses less than a picosecond.[37,38] The drawback is that conventional FELs are very large facilities with a high cost and complexity; hence, they are more suitable for fundamental scientific research, such as investigating THz biological effects due to the intense radiation.[39,40] However, table-top FELs are also available due to the lower requirement of the electron-beam energy for THz emission, which offers more opportunities for other biomedical applications, such as imaging.[41] On the other hand, gas lasers and QCLs are developed from the infrared side. Gas lasers emit extremely narrow-linewidth THz radiation from particular gases, such as methanol, typically pumped by a CO_2 laser. A QCL-pumped compact THz gas laser has also been recently reported.[42] The operating frequency can be tuned by using different gases and pump lines; however, the resulting spectrum is discrete. QCLs are quantum solid-state devices utilizing the intersubband transitions. They have received great attention over the last two decades as research pushes to overcome the limitations in the working frequency, operating temperature, and output power of QCLs. For example, recent work by Hu's group demonstrates a compact THz QCL operating at 4 THz at temperatures up to 250 K, which can be cooled by portable thermoelectric coolers instead of bulky cryogenics.[43] Different from the above source, THz parametric sources and photomixers can both be continuously tuned over a broad band, but they are very different in terms of power level and operation mode. THz parametric sources including THz parametric generators (TPGs) and THz parametric oscillators (TPOs), provide high peak-power pulses with a low repetition rate at tens to hundreds of Hz. They have a high gain efficiency over 1–3 THz. Photomixing is similar to pulsed PCAs, but they modulate the photoexcited carriers at a frequency equal to the frequency difference between two CW laser beams, thus emitting CW THz waves. They operate with a relatively low power at the μW level.

b. Detection. There are also several methods for CW THz detection, usually selected according to the characteristics of the source used and experimental requirements. For fundamental intensity detection, pyroelectric detectors, bolometers, and Golay cells can be used. They are sensitive single-pixel detectors, responsive across a broad band and adaptive to most kinds of sources. THz matrix cameras, usually based on microbolometer arrays or pyroelectric arrays, can be used for fast THz imaging if bright THz illumination is available. Schottky diodes are frequency mixers that down-convert the detected signal to a much lower frequency. They require a local oscillator as another THz source to provide a frequency close to that of the detected signal, with the difference frequency being measured. Some devices work as both a generator and a detector, such as THz parametric detection in nonlinear crystals,[44] using laser feedback interferometry in QCLs,[45] and photoconductive detection in THz photomixers.[46] The latter two approaches are interferometric-based detection; thus, they are phase-sensitive. Most of the other detection mechanisms only measure the intensity; additional interferometric optical settings and/or algorithms are needed to extract the phase.[47]

c. Characteristics and applications. Despite the divergent mechanisms, CW THz systems have a common advantage of narrow linewidth, compared to the typical 2 GHz resolution limit of time-domain systems. CW sources, such as parametric generators (100 MHz linewidth),[48] QCLs (tens of MHz linewidth),[49] and gas lasers (kHz linewidth)[42] have a much better resolution. Combined with the frequency-tuning ability for most of CW sources, they provide an excellent spectral resolution for spectroscopy, which has been utilized in gas sensing. However, it should also be pointed out that the absorption features of most biomedical samples with spectral fingerprints are relatively wide, typically over a few tens of GHz, which can be well resolved by pulsed time-domain systems.[3,4,50] CW systems have some limitations for spectroscopy. Vacuum and solid-state devices have a limited tuning bandwidth due to the power reduction with frequency upconversion. THz parametric generators and THz photomixers have a broader tuning range but they are typically slow. Another advantage of many CW THz sources is the high output power at their optimal frequencies, which enables a deeper penetration depth and a better SNR. The high brightness is essential for real-time imaging with a THz camera, since the beam energy has to be distributed over a large number of pixels. The high power is also required for scattering scanning nearfield optical microscopy (s-SNOM). In s-SNOM, only a tiny amount of the input THz light is scattered from the scanning tip and detected due to the large mismatch between the THz spot size and the tip, and a high harmonic component is extracted to suppress the background reflection;[51] these introduce a significant loss. For example, using the second-order harmonic component, less than one millionth of the input energy can be detected.[52] A strong input power is necessary to provide a good SNR.

CW THz systems are often used in biomedical imaging, partially due to the more robust and simpler optical settings, and faster acquisition speed compared to pulsed time-domain systems with a comparable SNR. This can be seen from Table I, where we summarize a few different CW THz systems using different combinations of sources and detectors for THz biomedical imaging and spectroscopy. The diverse selections of different devices show the high flexibility of CW THz systems. It is difficult to directly compare the performance of these systems given the diverse performance on various aspects. A potential direction for CW THz systems is to develop high-brightness, compact, sensitive, and low-cost real-time imaging systems, similar to those in the visible regime. This is needed to progress *in vivo* biomedical applications and will also promote the THz applications in many other fields, such as security and industry.

B. Experimental configurations

The experimental configuration determines how the THz beam is guided in free space, interacts with the sample, and is detected. Numerous configurations have been proposed for different applications, especially for biophotonics due to the complexity of biological systems. For a specific experiment, the configuration is usually designed according to the sample properties (e.g., transparent or absorptive, solid or liquid) and the measurement types (e.g., imaging or spectroscopy, *in vivo* or *in vitro*). In the following, both the

TABLE I. Different CW THz systems for biomedical applications.

Type	Source	Detector	υ (THz)	Sample	Reference
Imaging	BWO	Golay cell	0.279	Chicken bone	Li *et al.*[53]
		Pyroelectric detector	0.52–0.71	Leaf, pig tongue, chicken heart, pig cervical canal, liver-cancer, and breast cancer samples	Dobroiu *et al.*[54]
	Gunn diode	Golay cell	0.32	Burned porcine skin	Lu *et al.*[55]
		Schottky diode	0.3	Human colonic tissues	Chen *et al.*[56]
		Pyroelectric detector	0.1	*In vivo* rabbit cornea	Taylor *et al.*[57]
	Diode multiplier chain	Schottky diode	0.65	*In vivo* human cornea	Sung *et al.*[58]
	Gas laser	Pyroelectric array	2.52	Human hepatocellular carcinoma	Rong *et al.*[59]
		Bolometer	0.584	Fresh normal and cancerous human colonic tissue	Doradla *et al.*[60]
		Golay cell	2.52	Rat traumatic brain injury	Shi *et al.*[61]
		Schottky diode	2.5	Mouse brain slices	Siegel *et al.*[62]
	QCL	Bolometer	3.7	Sample model of liver, fat, muscle and tendon, rat brain, rat liver	Kim *et al.*[63]
		Microbolometer array	2.8	Human skin slice	Locatelli *et al.*[64]
		QCL	2.59	Porcine tissues	Lim *et al.*[65]
	Photomixer	Bolometer	0.23	Human liver	Knobloch *et al.*[66]
		Photomixer	1	Canine's basal cell tumor	Siebert *et al.*[67]
	TPO	Pyroelectric detector	1–2.5	Drugs	Kawase *et al.*[68]
		Bolometer	0.9–2.5	Pork and chicken tissues	Wang *et al.*[69]
Spectroscopy/ point scan	Photomixer	Golay cell	0.2–1	Human skin *in vivo*	Bennett *et al.*[70]
		Photomixer	0.4–1.2	*Bacillus thuringiensis*	Zhang *et al.*[71]
		Photomixer	0.1	Cornea of human eye *in vivo*	Safonova *et al.*[72]
	VNA extender source	VNA extender detector	0.22–0.33	*Ex vivo* lamb eyes	Tamminen *et al.*[73]

conventional and several novel configurations for THz biophotonics will be introduced, with their features and adaptability being highlighted.

1. Conventional configurations

Transmission and reflection are the two most conventional configurations. Transmission is a very straightforward modality for sample measurement. As shown in Fig. 3(a), a sample is directly placed in the THz beam region with the beam being either focused or collimated. The beam is partially reflected and absorbed, with the rest being received by the detector following transmission through the sample; this is described as the sample signal. By comparing this sample signal to the reference signal, generally acquired by measuring the transmitted signal in the absence of the sample, one is able to analyze the sample properties. This is particularly useful for pulsed time-domain THz measurements, in which both broadband amplitude and phase can be obtained, and the complex dielectric properties of the sample can be determined by Beer–Lambert's law. Another key advantage of the transmission configuration is the high sensitivity to most THz-transparent samples, originating from the long interaction distance between the THz light and the sample. Mathematically, it can be seen from the time-domain that the pulse can be delayed for a long distance by having a large sample thickness, as long as the attenuation is acceptable. Equivalently, this means the phase variation in the frequency-domain has no upper limit. In contrast, the phase of a signal reflected off a sample can only vary within 180°, that is, only the pulse shape is changed without a delay. Therefore, transmission is usually the best choice for transparent bulk samples. However, fresh biological samples are absorptive as they have a large water concentration, and they are usually difficult to cut into thin films. Some dehydrated biological slides are too thin to provide a long THz–sample interaction distance. *In vivo* measurements can only be performed with a reflection geometry. Therefore, in many cases a reflection configuration is required to overcome these issues.

A reflection measurement can be performed by directly illuminating THz light onto a free-standing sample, or through a certain supporting medium, such as a window or a prism. Free-standing reflection is mostly used when sample characterization is not required. This is because the reflection plane of a free-standing sample will have certain height positioning error compared to that of a reference medium, resulting in the sample-reference relative phase error, known as the "phase uncertainty" problem as the accuracy bottleneck.[74,75] This configuration has been mainly applied in CW THz imaging when only the intensity information is used to form reflectivity images, or when the absolute phase is used to form holographic images.[59,60,64]

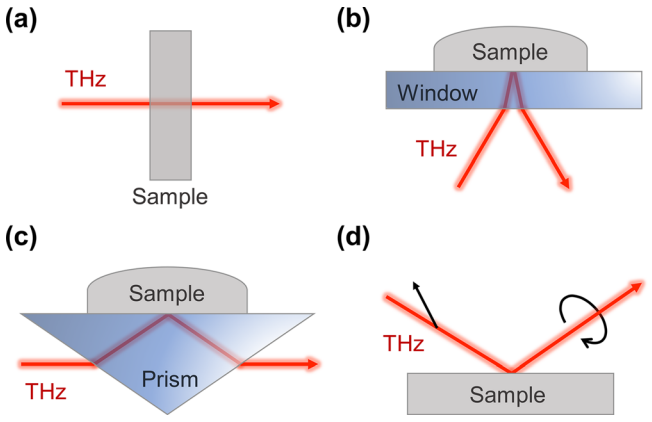

FIG. 3. Some commonly used THz configurations: (a) transmission, (b) window-based reflection, (c) prism-based reflection, and (d) ellipsometry.

Using a window or a prism to support the sample is more frequently used for biomedical studies. The supporting medium not only provides a stable reflection plane to eliminate the positioning error between the sample and reference (air) reflections, but also introduces a flat interface to optimize the focusing. This configuration requires good contact with the sample; thus, it can be used to measure liquids, fresh tissues, or skin *in vivo*. Dehydrated samples can be directly prepared on the supporting medium, in order to prevent the presence of air gaps caused by the rigid surface. Characterizing solid-state samples in reflection can be done using a reference-free configuration of ellipsometry, which will be introduced in Sec. II B 2.

A reflection configuration is specified by various systematic parameters, including the angle of incidence, the polarization, the properties of the supporting medium, and the light–sample interaction structure. These properties should be designed to optimize the measurement sensitivity. For example, Møller compares the sensitivities of transmission (for different sample thicknesses), ordinary (silicon-supported) reflection and attenuated total internal reflection (ATR) for transparent heptane and absorptive water, which shows a huge difference in the measured optical responses.[76,77] The analysis shows that the absorptive water is best characterized by the ATR geometry. A similar analysis of free-standing reflection and quartz-supported reflection can be found in Refs. 74 and 75, showing that a reflection configuration has the best sensitivity for samples with properties close to that of the supporting window. For thin films, a sandwich structure is shown to be capable of efficiently enhancing the contrast.[78] The selection of the structure and incident angle may also affect the imaging capability. For example, a prism setup generally only allows single-point spectroscopy due to the alignment variation in a two-dimensional scan. For other imaging setups at a large incident angle, the focused beam spot becomes elliptical and a worse resolution in the scanning direction parallel to the incident plane should be considered. Compared to transmission, reflection measurements are more critical in the optical alignment and more sensitive to various errors. Placing a sample slightly out of focus has little influence in transmission, but positioning and tilting errors will sensitively affect the reflection. During the measurement, the largest error source usually comes from the phase. As discussed above, the limited 180° phase variation range indicates that a small phase error could significantly change the characterization results. The phase can be influenced by many factors, such as delay-stage or laser jittering error, temperature-induced refractive-index change in fibers or other optical components, and sample positioning error. These errors should be carefully controlled in a reflection measurement.

2. Ellipsometry

Ellipsometry is a reference-free characterization technique, sometimes known as a self-reference method. It has been widely applied in the infrared and ultra-violet regimes as an accurate technology for investigating the dielectric function of different materials.[79] The fundamental mechanism is the polarization-dependent reflections of samples according to the Fresnel equations. It measures the *p*- and *s*-reflections off a sample and expresses their ratio as a function of the sample properties. By solving this inverse problem of light–matter interactions, the dielectric properties of the investigated material can be extracted. In this way, no reference medium is required. Therefore, ellipsometry is very suitable for solid-state absorptive materials since they cannot be well characterized by either transmission, free-standing reflection, or medium-support reflection.[21,80,81] Ellipsometry also shows an excellent sensitivity for thin-film characterization, providing a higher phase contrast than transmission.[21,82]

Since the polarization-dependency is the foundation of the sensitivity, ellipsometry is usually carried out close to the Brewster angle of a sample where the largest difference between the *p*- and *s*-reflection coefficients can be found. This can be easily understood from the opposite example, such as at normal incidence. In that case, the *p*- and *s*-reflections are completely identical and a ratio of 1 will always be obtained regardless of the properties of the measured sample. Measuring close to the Brewster angle brings two difficulties. First, at this region the *p*-reflection varies significantly with the incident angle, especially for materials with a large refractive index. This means the incident angle has to be set and read precisely. Using fully fiber-coupled PCAs allows flexible setting of the incident angle, and using large f-number optics can efficiently reduce the beam divergence to reduce the incident angle error. The only price is the larger beam spot due to the diffraction limit. Second, as the *p*-reflection is much weaker than the *s*-reflection close to the Brewster angle, the polarization has to be controlled precisely to make sure no *s*-component is leaked and detected when measuring the *p*-signal. Some calibration methods have been proposed to improve the polarization accuracy.[21,83] Due to the critical requirements on the optical setup and polarization control, utilizing ellipsometry for biomedical applications is still rare, but recently Chen *et al.* proposed an example of *in vivo* characterization of skin,[84] showing the ability to probe the hydration and cellular structure simultaneously. The ellipsometry configuration in this work consists of two right-angle prisms, one silicon prism on top and one gold-coated prism (i.e., perfect mirrors) on the bottom mounted symmetrically, as shown in Fig. 4. Putting the double-prism system in a transmission configuration offers two alternative beam paths, as shown in Fig. 4(a). The two positions provide two incident angles of 33° and 57° to the Si-subject/air interface. The large refractive index of the Si prism compared to biosamples gives rise to very distinct reflection coefficients at the two angles. Switching between the two angles can be conveniently achieved by vertically moving the double-prism

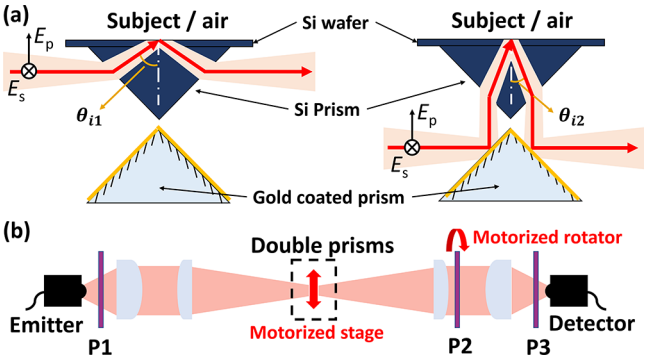

FIG. 4. Multi-configuration ellipsometer for skin characterization: (a) the double-prism system used to introduce two alternative incident angles of θ_{i1} and θ_{i2}. E_p and E_s represent the electric fields with *p*- and *s*-polarizations, respectively. (b) The integration of the double-prism system with a transmission system to provide four uncorrelated reflected spectra. P1, P2, and P3 are three polarizers, with P1 and P3 fixed at 45° and P2 being rotated to select the *p*- or *s*-signals. Reproduced with permission from Chen *et al.*, Adv. Photonics Res. **2**, 2000024 (2021).[84] Copyright 2021 Authors, licensed under a Creative Commons Attribution (CC BY) license.

system with a translation stage without changing the THz optics. Additionally, using the polarization control with three polarizers introduced in the previous work,[21] four uncorrelated spectra from four configurations given by different combinations of incident angles and polarizations can be obtained. This significantly enriches the spectral information obtained, this will be necessary for characterizing samples with a complicated structure, such as skin (e.g., multiple layers and anisotropic). The application to skin characterization will be explained in detail in Sec. V D 2. Although in this work the skin was in contact with a prism to enable a flat reflection interface, theoretically ellipsometry can be applied to noncontact *in vivo* measurements without a phase uncertainty, which provides an ideal modality for the clinical applications. Some hard tissues, such as bones and teeth, or dehydrated tissues, can also be investigated with THz ellipsometry. Therefore, it has great potential to be further explored for biomedical applications in the future.

3. Microscopy and the near-field

The THz wavelengths of 0.03–3 mm prevent far-field imaging techniques from resolving many important spatial details at the micrometer level; thus, near-field techniques are needed to overcome this limit. The most impressive near-field images have spatial resolution of 10 nm and temporal resolution of 50 fs;[85] this is achieved by placing an AFM tip in the near-field of the sample. Unfortunately, methods based on placing metallic tips next to the sample are not compatible with biological samples for three reasons: first, raster scanning is too slow although it might be worth the wait; second, biosamples cannot be flat on a nanometer scale like solid-state samples; and third, sample hydration further complicates an already complex setup given the high THz absorption of water. This is why most THz imaging of biological materials has been performed in the far-field. Nevertheless, there have been studies showing near-field THz imaging of biosamples.[56,86–95] These references use different systems and will be discussed below.

a. THz waveguide/fiber coupling. The work done by the group of Chi-Kuang Sun[56,90–92] all utilizes the same basic concept: couple free-space THz radiation onto a THz fiber or waveguide; then, this fiber/waveguide is raster scanned in the near-field of a sample with a far-field detector collecting all the radiation. They usually use a 320 GHz Gunn oscillator as their source and a Schottky diode or a Golay cell as the detector. Such a technique can also measure over a broadband frequency, typically driven by VNAs to measure both the phase and amplitude. Regardless of their single-frequency source, they have been able to distinguish between cancerous and healthy tissues[56,90,91] and also observe differences in the transmitted THz signal in the blood vessels of mouse ears due to an insulin injection.[92] The biggest problem with this work is the use of a waveguide or a THz fiber as these generally work well only for a few frequencies. Further, the physical raster scanning mechanism will most likely limit this technology to applications that need good resolution but do not need the results in real-time.

b. Optical resolution THz imaging. Optical resolution THz imaging is based on placing the sample on an EO crystal emitter (or detector) and using a visible light pump (or probe) to spatially map-out the THz field variations due to the sample. This idea was demonstrated in 2011 in a previous study[87] although not for biosamples. It was in 2020 that Okada *et al.*[86] used this technique to image breast cancer in a tissue sample. Since the THz emission or detection is localized to where the visible light pump or probe is, placing the sample in the near-field results in a THz image with optical wavelength resolution. The authors used an optical CCD array to map out the THz near-field interaction of a sample placed onto top of a EO crystal detector,[87] whereas Okada placed their sample onto an EO crystal emitter and raster scanned the optical pump beam that generates the THz radiation.[86] Both techniques achieve around 15–20 μm resolution with image acquisition taking about 1 min; however, the major difference comes from laser systems powering these setups. A previous study[87] used a 1 kHz regenerative amplified laser because the optical probe beam needs to be spread over the sample area with enough fluence, whereas in another study[86] the optical beam is focused to a spot so the 80 MHz rate fiber-laser achieves the necessary fluences. A fiber-based laser is much smaller and cheaper, making it much more commercially appealing; however, both have been used to achieve similar physical resolution while measuring the amplitude and phase over similar frequency ranges. For this reason, this technique is likely to use fiber-based systems in the future for fundamental research of biological systems.

c. Single-pixel THz imaging with optical resolution. The study of Barr *et al.*[88] and Stantchev *et al.*[89] pioneered the use of a single-pixel THz camera with the spatial THz-light modulator placed in the near-field of the sample. A single-pixel camera works by spatially patterning a beam of radiation with many patterns and then recording the resulting transmissions or reflections from an object with a single-pixel detector. The image of the object is reconstructed via computer post-processing.[96] Their first work on this approach in 2018[89] used an optical pump to photoexcite charge-carriers in undoped silicon and move the plasma frequency from below to above the THz frequency range, thus switching the semiconductor response from dielectric to conducting. Further, they synchronized the THz pulses such that they passed through the silicon a few picoseconds after optical excitation, long

before the charge carriers had diffused thus the spatial pattern was not blurred due to carrier diffusion. This results in the THz resolution being determined by the distance between the object and modulator.[97] The problem is that the spatial modulator requires optical pulses with large energy per pulse per area that is only achievable with 1 kHz repetition-rate regenerative amplified lasers, which makes the whole system slow, big, and expensive. In their next work,[88] they used a CW THz source and high-powered LED as the optical pump for a silicon photo-modulator, with the modification that the measurement was performed in a total-internal-reflection geometry as opposed to ordinary transmission. This of course results in carrier diffusion limiting the THz resolution; however, it greatly reduces the system size and cost as well as improving the acquisition speed (due to higher signal to noise ratio) and can still give subwavelength resolution for low THz frequencies. The interesting part of this technology is that the carrier injection/depletion in the modulator can also be achieved by electrical biasing instead of optical pumping,[98] whereby the resolution would be limited by the photo-lithographic techniques used to manufacture the modulator. However, such electrical modulator arrays are currently in heavy development with recent work showing a 16×16 graphene array with a 1 kHz switch-rate.[99]

d. On-chip near-field THz imaging. The final technique we mention here is the development of an integrated system-on-a-chip near-field imaging device working at 0.55 THz by Pfeiffer.[93,94] The device works by having a local oscillator connected to a split-ring resonator and finally connected to a detector. When the split-ring resonator is exposed to the sample, its resonance frequency will shift and thus the signal arriving at the detector will change. The split-ring resonator is only affected by the sample via inductive coupling to enhance the resolution to about 10 μm. As a proof-of-principle in an earlier study,[93] an image of a human fingerprint is taken and in another study,[94] they image a breast tissue sample. The downsides of this device is the single frequency operation and that the inductive coupling mechanism results in the measurement of only the real permittivity, which is unlikely to be enough for research purposes during clinical trials. However, all of the components are compatible with CMOS technology; thus, this device including all the readout electronics is very small, a few centimeters, and can be powered by a 5 V USB cable with 0.6 W of power consumption.[94] Therefore, these devices have the potential to be used by households and not just hospitals or laboratories.

4. Handheld, endoscopic, and robotic geometries

Flexibility is crucial for *in vivo* applications due to the need to measure different locations of the body. Unlike *ex vivo* samples that can be prepared into ideal flat slides with a desired thickness, living tissues usually have irregular shapes, rough surfaces, and are in inconvenient positions. Developing THz instrumentation that is compact, portable, and flexible to adapt with these applications is a hot area of research. There are mainly three strategies, handheld, endoscopic, and robotic geometries. The flexibility of these strategies is usually provided by fibers or flexible waveguides, opposed to free-space beam-guiding where the alignment is usually so critical that there is little freedom of movement.

With their compact size and the adaptability to be coupled with fiber lasers, PCAs have been designed into various handheld probing structures. One of the earliest designs is the handheld probe-head product by TeraView. The earlier product from 2004 included one emitter surrounded by six detectors.[100,101] A later design was reduced to one emitter and one detector, but with two rotating Risley prisms to enable a 1D scan along a 1.5 cm line,[17,102] as shown in Figs. 5(a) and 5(b). The THz beam is focused on top of the quartz window at the end. The probe head can be freely moved to scan any sample contacting the quartz window without affecting the alignment, similar to a clinical ultrasonic probe. Mini-Z and micro-Z are another two commercial products by Zomega that were developed around 2010[103,104] in which all the optics are assembled in a single box. They are more portable but less flexible. The handheld THz probe can also be used as an otoscope, as proposed by Ji *et al.*[105] The THz probe head consists of an emitter based on photo-Dember currents and a PCA detector, assembled with a commercial optical otoscope, as shown in Fig. 5(c). The THz beam was well collimated over a long propagation distance. Different sizes of ear specula can be integrated, with the smallest diameter of the ear speculum head down to 2.3 mm with a length of 4.1 cm. Recent work by Harris *et al.* developed a portable head employing a two-dimensional gimballed mirror and a f–θ lens to perform a fast 2D scan without using linear stages.[18] It has a field-of-view of $12 \times 19\,\text{mm}^2$ and provides consistent resolutions over the imaging area. Using these compact and handheld devices, it is possible to probe regions which are inaccessible using traditional reflection configurations.

Endoscopy is another potential THz biomedical application. Probing inside a human body is obviously more challenging. A probing structure that is highly bendable, compact, easy to focus, and anti-jamming is required. Fiber-coupled PCAs are a potential approach for this purpose. A structure for a miniaturized fiber-coupled emitter and detector was proposed by Ji *et al.*[19] Both the emitter and detector are highly compact in a size of only $2 \times 4 \times 6\,\text{mm}^3$, small enough to be inserted into a human body. Using fibers and waveguides to directly guide the THz waves in a bendable medium is another strategy. This technique typically uses a CW THz source and the fiber or waveguide is optimized to the operating frequency. For example, Lu *et al.* used plastic fibers to guide both the incident and reflected narrow-bandwidth THz waves in a single channel.[55] A long propagation distance and a small bending loss can be achieved. However, due to the weak confinement of the field, it is sensitive to the environment around the fiber, which limits its practical usage. A more robust prototype would be a metal-coated THz waveguide, as proposed by Doradla *et al.* It completely confines the field inside the waveguide.[106] The sample has to be placed closed to the waveguide tip to achieve the optimized resolution. Overall, the current state of the THz endoscopic techniques still have a long way to go before they are ready for practical applications. One important limitation is the imaging ability, which is essential for endoscopy to obtain spatial information. However, all the reported techniques can only detect a single pixel and the demonstrated imaging experiments were done by moving the sample. Other technical issues should also be further addressed, such as the robustness of the alignment against different measured distances and complicated sample surfaces, and the consideration of the diffraction limit.

Although a handheld geometry provides opportunities to measure areas that are difficult to make contact with a bulk reflection system, a small window is still required on the probe head to align the THz beam to the measured region. The contact with the window

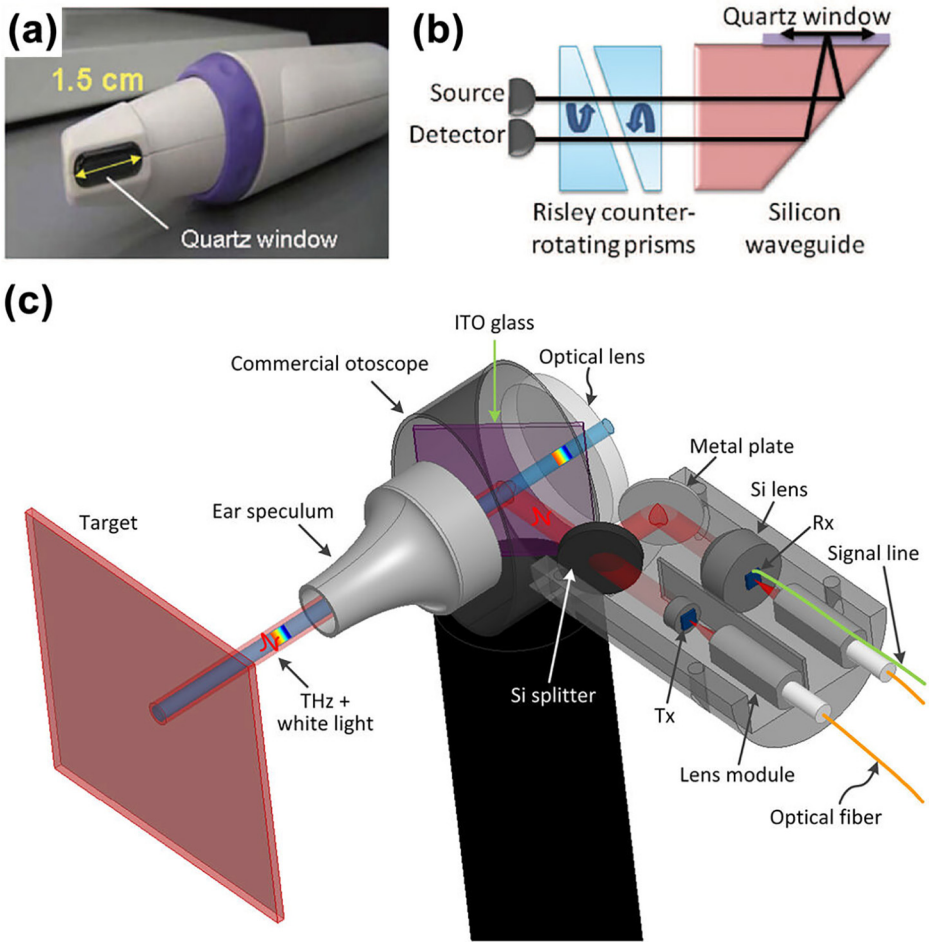

FIG. 5. Handheld THz probe heads. (a) TeraView 1D scan portable probe head and (b) its inner optical beam path. Reproduced with permission from Parrott *et al.*, J. Biomed. Opt. **16**, 106010 (2011).[17] Copyright 2011 SPIE. (c) THz otoscope. Reprinted with permission from Ji *et al.*, Biomed. Opt. Express **7**, 1201 (2016).[105] Copyright 2016 Optical Society of America.

brings an issue of occlusion for *in vivo* measurements, which refers to water being accumulated on the skin surface due to the prevention of water evaporation by the window.[108] The occlusion rate is highest at the start of the contact but also last for a long time and its influence on the THz reflectivity can be observed up to 30 min.[84] This can be clearly seen by imaging a region of healthy skin and observing the varied reflectivity across the image.[108] The reason is that the signals at different pixels are obtained at different times with different occlusion states, and this time-induced spatial variation affects the contrast of the tissue itself. In addition, the pressure exerted on the window can also affect the THz response.[109,110] To overcome these issues, a noncontact reflection setup with a high degree of flexibility to adapt with the nonflat surface is needed. A robotic geometry is a possible solution.

Sung *et al.* demonstrated an example of quasi-robotic THz imaging of the cornea *ex vivo* and *in vivo*.[58,111] They used two motorized mirrors to change the illuminating position on the parabolic mirror, thus controlling the THz beam to focus it onto different positions of a spherical surface at a normal incidence. Based on this setup, they scanned *ex vivo* porcine eyes and *in vivo* human eyes,[58] with each row scan completed within 1 s and each image obtained within 20 s. Recently, the intraocular pressure (IOP) for *ex vivo* samples was also measured by utilizing multiple stages to control the focus on a spherical surface.[112] These techniques, although successful, are limited to spherical samples of a particular size. Using a multi-dimensional robotic arm can provide a more general solution.

Nowadays, the use of robotic-arm assisted systems is becoming more common in many different fields and the THz field is not an exception. THz spectroscopy has taken the advantage of robotic systems in the quality control of paint layers for the automotive industry,[113,114] which has now been introduced to various THz applications. Stübling *et al.* presented a robotic system able to position the THz probes perpendicular to the curved surface of a sample.[115] The technique is based on the fringe patterns projected over the sample surface which is recorded by a camera to analyze the shape of an arbitrary object. With this novel technology, the same research group has been able to examine wood infested by insects and a collection of ancient pottery.[116,117] They have also demonstrated an exciting application to analyze human remains,[107] as shown in Figs. 6(a)–6(c).

In the study, they showed that the resolution of THz images is comparable with that of more mature techniques, such as CT and micro-CT scans. However, since the surface reconstruction is computational-based thus time-consuming, it is only effective for still objects. For living samples, the need for speed in data acquisition and robot positioning is mandatory due involuntary movements of the

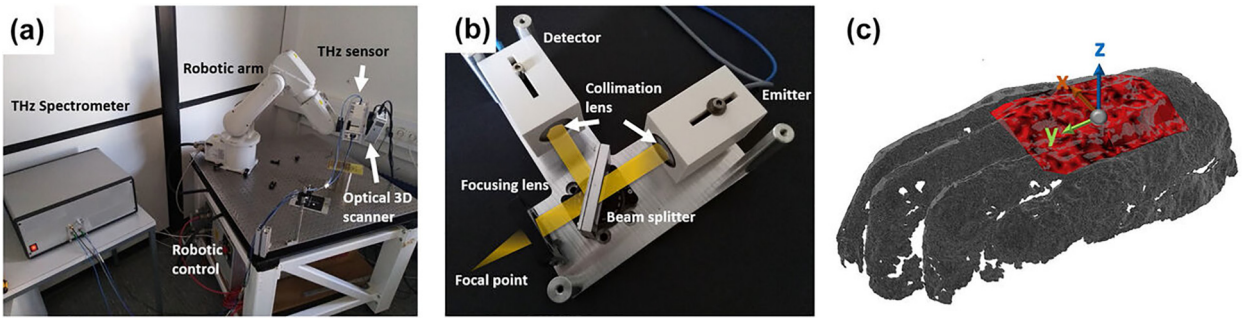

FIG. 6. Robotic configuration: (a) robotic arm integrated with the THz sensor and optical 3D scanner; (b) photo of the THz optical sensor and the beam path; and (c) optical 3D scan of the investigated mummy hand. The THz measurement area is highlighted in red. Reproduced with permission from Stübling *et al.*, Sci. Rep. **9**, 3390 (2019).[107] Copyright 2019 Authors, licensed under a Creative Commons Attribution (CC BY) license.

living being. Novel methods in surface profile acquisition have to be developed. Fortunately, with the invention of 3D vision systems, the topology of a sample can be reconstructed even at rates of 20 frames per seconds; this has proved to be helpful for capsule endoscopy,[118,119] for instance. We envisage that the inclusion of 3D stereo cameras on robotic-based THz systems for real-time noncontact examination will open new opportunities for THz *in vivo* biological imaging, which may serve as a complementary tool for clinical diagnosis.

III. THz–SAMPLE INTERACTION

Typical THz systems utilize components that are sufficiently large to limit diffraction but are still small with respect to the wavelength. Beam propagation in quasi-optical THz systems can be modeled via Gaussian beam theory or physical optics theory.[73] One major difference between THz and optical waves is that the scattering, especially Rayleigh scattering can be ignored in most cases for THz waves due to the long wavelength.[120] The inner microscopic structure of a sample is also usually much smaller than the THz wavelength, thus very little diffuse reflection will occur. Therefore, most materials are "mirror-like" in the THz regime and mainly give specular reflections. This simplifies the sample preparation, theoretical analysis, and characterization. The THz–matter interactions can be conveniently described by Fresnel's equations to express the reflection or transmission as a function of the sample properties.[79] As a result, the sample properties can be extracted by solving the inverse problem of the transfer function.[77] Biosamples also follow these characteristics, while in some tissue studies there are wavelength-comparable features that may cause Mie scattering and require additional analysis.[121,122] In general, the THz response of most homogeneous samples is solely determined by its dielectric function. Solid-state small biomolecules in the crystalline arrangement provide unique absorption features in the THz spectrum. Most of the other dehydrated samples are featureless due to the large number of vibration modes. Hydrated or liquid samples have their THz response mainly dominated by the water concentration, which can be interpreted by the dielectric model of water or the effective medium theories (EMTs). In this section, we will first overview biomolecules that exhibit spectral features in the THz range. Next, the water dielectric model and the EMTs will be introduced to understand the THz response of hydrated samples. Exploring the dielectric behaviors of different samples provides a way to understand the origin of the THz contrast and what can be explored with THz light, which will be discussed at the end.

A. Biomolecules with spectral features

Using spectral features is an ideal way for both spectroscopic and imaging to sensitively detect a target. The absorption fingerprints provide unique contrast at specific frequencies, serving as features for label-free sensing. For biomedical research, the observation of THz absorption features caused by the vibrational and rotational transition modes has been found mainly in small biomolecules. The spectral features in nucleobases and nucleosides,[3,123] amino acids,[4,124] uric acid,[125] purine and adenine,[126] peptides,[127,128] and short-chain polypeptides[129] have been reported. Large biomolecules, such as proteins and DNA, have a larger number of vibrational modes that collapse into a smooth spectrum, hence usually do not exhibit clear fingerprints.[130] To best observe the spectral features, the sample should usually be dry, solid-state, and in a single or poly-crystalline arrangement. The fact that spectral features are not observed in aqueous samples is not because they are covered by the high absorption of the solvent, instead, they disappear due to the changes in the intermolecular structure. THz waves mainly probe the intermolecular vibrations in a long-range ordering structure. An obvious example is the dramatic changes of the spectra of crystalline and amorphous glucose and lactose samples.[131,132] Figure 7 clearly shows the variation of the lactose absorbance at different crystallinity.[132] More examples of spectral-feature dependency on the molecular structure can be seen in Sec. V A 1. The restriction to small and crystalline biomolecules significantly limits the practical detection based on the spectral features. Most biosamples contain macromolecules of proteins and DNA, and could contain a large water content; thus, they do not show any characteristic absorption.

B. Hydrated samples

1. Water dielectric model

Water is the core substance for all living things on Earth. It undoubtedly plays a key role in biomedical research, especially for THz biophotonics due to the uniquely high absorption by water in the THz regime. Therefore, it is essential to model the dielectric function of water to study many water-rich biosamples. From static field to

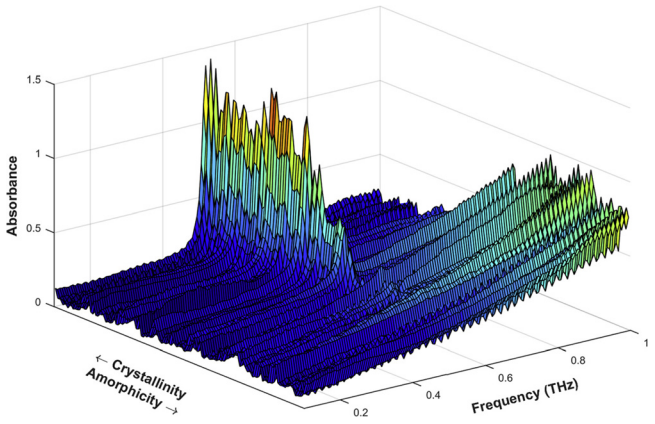

FIG. 7. Lactose absorbance in 0.1–1.0 THz at different crystallinity. Reproduced with permission from Warnecke *et al.*, Vib. Spectrosc. **102**, 39–46 (2019).[132] Copyright 2019 Elsevier.

microwave (below 100 GHz), water can be precisely described by a broad Debye relaxation centered at about 20 GHz, originating from the collective rearrangement dynamics of the water hydrogen-bond network. The end of the Debye relaxation reaches the THz regime, where it fails to successfully fit data above 0.1 THz. Historically, there is disagreement on how to fit the high-frequency response of water, but adding a secondary Debye relaxation term has been widely adapted.[133] This gives the so-called double-Debye model which can describe the water dielectric behavior up to 2 THz. Above that, an additional damped harmonic oscillation mode arising from the intermolecular stretching vibration at around 5 THz should be added to describe the dielectric function up to 10 THz.[1] Therefore, the selection of the dielectric model depends on the frequency range of a measurement.

In practical biomedical applications, the double-Debye model is more frequently used. This is partially because most THz biomedical experiments, especially tissue studies, are carried below 2 THz to obtain a better SNR. Another reason is that to fit the oscillation mode centered at around 5 THz accurately, a much broader bandwidth (e.g., >4 THz) is needed. According to the double-Debye model, the permittivity can be expressed as[134,135]

$$\tilde{\varepsilon}(\omega) = \varepsilon_\infty + \frac{\varepsilon_s - \varepsilon_1}{1 + i\omega\tau_1} + \frac{\varepsilon_1 - \varepsilon_\infty}{1 + i\omega\tau_2}, \tag{1}$$

where ε_s is the static permittivity and ε_∞ is the permittivity in the high frequency limit. Their combinations with ε_1 decide the strength of the two relaxations. τ_1 and τ_2 are the slow and fast relaxation time, respectively. The double-Debye model has been shown to be applicable to the dielectric behavior of water-rich biosamples. Pickwell *et al.* pioneered the application of the double-Debye model to describe the THz properties of skin[136,137] and basal cell carcinoma.[138] A good match was found, and the use of the double-Debye model enables the simulation of the THz response using the model parameters. Later research by other groups has further employed the model for burns injuries,[139,140] breast tissues,[141] brain gliomas,[142] and blood.[143] High correlations between some double-Debye parameters and the healthy status of the tissue were reported, indicating the potential usage of these parameters for cancer identification and classification.[144,145]

Since the two Debye relaxations originated from the hydrogen-bond rearrangement of water molecules, the application range of the double-Debye model is theoretically limited to samples with a high water-concentration. The permittivity of nonwater substances, such as fat, does not follow double-Debye behavior; thus, the presence of significant concentrations of these in samples would reduce the fitting credibility. In that case, EMTs, which consider the material as a homogeneous mixture of multiple compositions and express the effective permittivity as a function of the volume fraction of each composition, can be better applied.

2. Effective medium theories

EMTs were proposed over a century ago to determine the effective dielectric property of a medium consisting of more than one inclusion.[146] The fundamental requirement for the validation of an EMT is that the included composition should have a size far smaller than the wavelength and be homogeneously distributed, hence inducing no scattering. Based on different assumptions and derivations, there are various EMTs with slightly different areas of applications. A comprehensive overview and comparison of these EMTs in the THz regime can be found in Ref. 147. Among them, the Maxwell-Garnett (MG), Bruggeman (BM), and Landau–Lifshitz–Looyenga (LLL) models are the three most commonly used EMTs for THz applications. However, the MG model requires the guest medium embedded in the host medium to have a low volume fraction. Mathematically, this is represented by its asymmetric characteristics which mean that exchanging the permittivities and volume fractions of the two inclusions result in a different effective permittivity. For biomedical samples of which the volume fraction of water can vary in a large range, the MG model is not suitable. In contrast, BM and LLL allow arbitrary volume fractions to be included. The BM and LLL models for a two-component composite can be represented by the following equations, respectively:

$$f_1 \frac{\varepsilon_1 - \varepsilon_{eff}}{\varepsilon_1 + 2\varepsilon_{eff}} + f_2 \frac{\varepsilon_2 - \varepsilon_{eff}}{\varepsilon_2 + 2\varepsilon_{eff}} = 0, \tag{2}$$

$$\sqrt[3]{\varepsilon_{eff}} = f_1\sqrt[3]{\varepsilon_1} + f_2\sqrt[3]{\varepsilon_2}, \tag{3}$$

where, f_1 (ε_1) and f_2 (ε_2) are the volume fractions (permittivities) of components 1 and 2, respectively. f_1 and f_2 satisfy $f_1 + f_2 = 1$. ε_{eff} is the effective permittivity of the composite. Both the BM and LLL models are symmetric, as exchanging the permittivities and volume fractions of the two components gives the same result. The major difference between them is the shape of the guest medium assumed in the theoretical derivations. The BM model assumes spherical particles while the LLL model allows arbitrary shapes. In principle, LLL has a broader range of applications. However, it is usually difficult to define the shape of the inclusions for biosamples. For example, tissues contain structures from mesoscopic vasculature to microscopic cells, to nanoscale DNA and proteins. More importantly, the BM and LLL models show very little difference in the calculated effective permittivities, as shown in Fig. 8, with only a very small deviation from the MG model.[148] The experimental results from water-basil mixtures fit well with all the three models. In practical applications, the uncertainty on the permittivities of the biological background (i.e., dehydrated sample) has a much larger impact on the calculation; hence, the difference

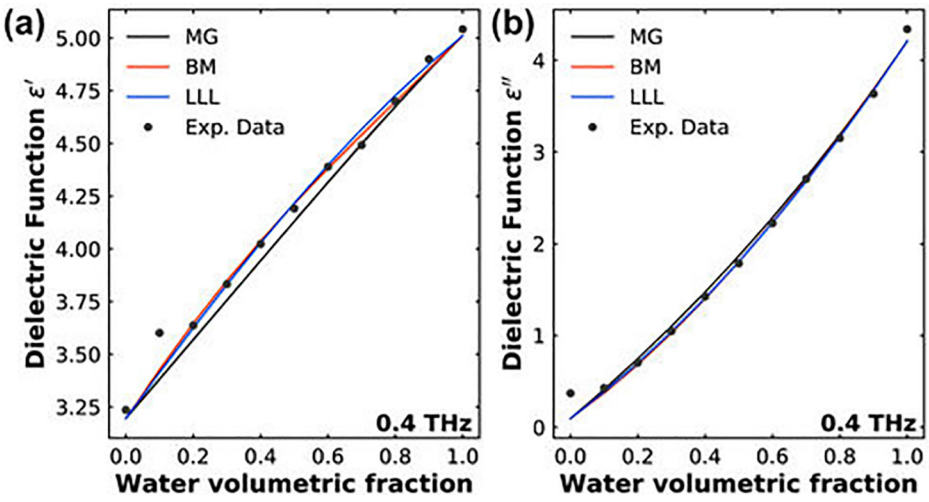

FIG. 8. Comparison of different EMTs with the experimental data: (a) real part and (b) imaginary part of the dielectric function calculated from the Maxwell-Garnet, Bruggeman, and Landau–Lifshitz– Looyenga models, respectively. The experimental results are for a water–basil mixture data at 0.4 THz. Reproduced with permission from Hernandez-Cardoso *et al.*, Appl. Opt. **59**, D6 (2020).[148] Copyright 2020 Optical Society of America.

among these models can be completely ignored. Therefore, instead of considering the adaptability of the model, more attention should be given to the data used for the model.

A common usage of EMTs in THz biomedical applications is to represent a sample as a mixture of water and a biological background from the nonwater substances. In this way, the permittivity of the sample can be effectively expressed by the permittivities and volume fractions of the two components.[149] Most dehydrated samples have a low refractive index and absorption, being transparent to the THz light. Their large contrast to the high refractive index and absorption of water makes the effective permittivity of a sample highly sensitive and mainly dominated by the water concentration, giving rise to the contrast between different samples or different regions of a tissue. In practical applications, the properties of the biological background and water are usually assumed to be known *a priori*. Fitting the EMT to the permittivity of a measured sample returns the water concentration.[150] From another aspect, with the knowledge on the properties of water and the biological background, the frequency-dependent permittivity of a sample is reduced to a single unknown variable of the water concentration. In characterizations, this greatly reduces the number of unknown parameters, making it possible to characterize some complicated structures. For instance, such an approach has been employed for characterizing skin *in vivo* which contains multiple layers or depth-dependent water concentrations.[151,152] The limitation of the EMTs is the difficulty in obtaining an accurate biological background. Ideally it should be obtained by measuring the completely dehydrated sample being investigated. However, in many cases this is unavailable especially for *in vivo* applications. A typical solution is to adopt the values from the literature, but the sources are very limited and could have large errors compared to those of the investigated sample. For example, the biological background of human skin is usually estimated using that of dehydrated porcine skin.[70,151] In our recent review, we show a large variation in the dehydrated properties from different studies, which could lead to a large difference in the extracted water concentration.[9] It should also be noted that applying EMTs is not the only way to extract the water concentration. Nuclear magnetic resonance (NMR) is another approach to evaluate the water content,[153] which has been used to verify the origin of contrast for THz images.[154] For *ex vivo* samples where dehydration is possible, the water concentration can be directly calculated using gravimetric measurements.

C. Origin of contrast

We have given an overview above of small biomolecules which exhibit spectral features and hydrated samples of which the dielectric properties are mainly dominated by the water concentration. These provide the two major origins of contrast: the unique "colors" provided by the spectral features, and the "darkness" provided by the water content. There is also a third origin of contrast from the biological background itself. Although most dehydrated samples are transparent to THz light, they still exhibit slightly different dielectric properties. He *et al.* measured dehydrated fat, muscle and skin samples.[149] Their refractive indices vary from 1.5 to 1.8, and the absorption of dehydrated fat could be four-times smaller than that of dehydrated muscle and skin. The experiment clearly shows the contrast from the biological background, which is very important in analyzing its contribution in the contrast between diseased and healthy tissues. The investigations on liver cancer and liver cirrhosis,[66,155] human breast tumor,[156] colon cancer,[157] and brain tissues[158,159] have all found differences in the THz dielectric properties between healthy and diseased areas in the dehydrated state. Although most studies have found that water dominates the contrast, in some tissues the biological background can offer a larger difference. In the study of liver cirrhosis, 50%–66% of the absorption difference is attributed to the inner structural differences between diseased and healthy tissues, which means the contribution of water is less than a half.[155] The origin of the biological background contrast could be complicated. Researchers have considered the contrast coming from the differences in the lymphatic systems, vasculature and cell density.[60,156,159] Other subwavelength structural changes or composition variations, such as protein concentration,[122] could also lead to a difference. Further, Stantchev *et al.*[89] found that the permittivity of bovine articular cartilage is polarization dependent with variation on a subwavelength scale in line with the alignment of the collagen fibrils. The contrast in the biological

background can be investigated by *in vitro* samples, while more studies are needed to explore how different factors affect the THz dielectric properties. Tissue morphology may also affect the THz response, for example in the cornea where the tissue layer results in lossy longitudinal modes that serve as the origin of contrast. Similarly, the layered structure of skin will also affect the frequency-dependent THz reflectivity.

In most practical applications, THz spectra are featureless with the contrast mainly contributed by the latter two factors, that is, the water concentration and biological background. The differences between two compared targets, such as the cancerous and normal areas, is potentially small. We will introduce several techniques and methods to enhance the contrast, such as by using biosensors (Sec. V B), by designing a sensitive multiple-layer structure (Sec. V C 2), or by using contrast enhancing agents, such as nanoparticles (Sec. V C 3).

IV. RADIATION CONCERNS AND EFFECTS

Currently, the safety power levels set by the International Commission on Nonionizing Radiation Protection for frequencies from 2 to 300 GHz is 1 mW/cm^2 for 6 min of exposure.[160] For frequencies above this range, there are currently no safety limits until one reaches IR-laser safety specifications set by the international commission. However, The American National Standards Institute sets the safety exposure for IR lasers with wavelengths from 1.4 μm to 1 mm (214 to 0.3 THz) to be at 0.1 W/cm^2 for 10 s or more.[161] They, however, only consider thermally induced damage whereas THz effects on biomatter can be split into two broad categories of thermal and nonthermal effects. The thermal effects are usually of concern to CW sources due to the strong absorption of THz waves by water[162,163] and because pulsed sources usually have low powers per unit time but high peak field strength values. The nonthermal effects of THz radiation are very unique from other frequency regimes because, while the low photon energies are not strong enough break chemical bonds, linear or nonlinear resonances in DNA can occur.[164,165] These nonthermal effects were first discussed by Fröhlich in the 1970s and 1980s[166] with the idea that THz radiation forms coherent states in biomatter, often called Fröhlich condensates. He considered a system of quantum oscillators surrounded by a thermal reservoir and he showed that this system can oscillate as a single coherent mode, somewhat like a Bose–Einstein condensate, instead of as a set of free oscillators each with a particular resonance frequency. He claimed that such effects will perturb the biochemical kinetics of biological objects, hence the need to consider the entire system as a whole rather than focusing only on single parts.

Some of the earliest investigations into whether THz radiation can damage biological function was the project named "THz-Bridge" funded by the Europe with the project ending in 2004.[167] It showed that under low power conditions, THz radiation did not induce any adverse effects in most experimental conditions; however, there was a study where both genotoxic and epigenetic effects were induced in lymphocytes following exposure to CW 100 GHz radiation of 0.05 mW/cm^2. This was at intensities much lower than the current safety levels, and the cells were without the protection of the human body. The project concluded that more measurements under different exposure conditions, such as CW and pulsed sources with different powers, are needed before THz radiation can be safely adopted for commercial purposes under standardized protocols. More recent studies have found further biological effects of THz radiation with previous studies[162,168–170] being reviews dedicated to the biological effects of THz radiation.

The bioeffects of THz radiation are unique. A series of studies by Fedorov[171–173] found that exposure to THz radiation (1 ps pulses, 0.1–2.2 THz, 76 MHz repetition rate, 8.5 mW of power) would shorten the lifespans of drosophila flies. This suggests a response that affects the entire system that cannot be explained by thermal effects only. There is also a 2013 study by Titova *et al.* showing the activation of DNA damage response in artificial skin cells due to exposure to pulsed THz radiation (1 kHz pulse rate, 1 μJ per pulse, 0.1–2 THz),[174] and the cell response was different when exposed to pulsed UV light. The mechanism that activated this DNA damage response was not known at the time of writing. In 2020, Tachizaki *et al.*[175] showed that THz pulses (1 kHz rep-rate, 0.5 MV/cm, 0.2–1.1 THz) caused the regulation of genes related to zinc–finger proteins in stem cells indicating that the concentration of Zn^{2+} ions was affected by the intense THz pulses. Most recently in 2021, the Hegmann group showed that THz pulses (1 kHz rep-rate, 0.03–2.4 μJ energy per pulse, peak electric fields of 27–240 kV cm^{-1}) incident on artificially cultivated human skin cells inhibited DNA signaling pathways associated with some types of cancers,[176] offering potential for cancer therapy. An earlier study by Gun-Sik Park's group at Seoul National University also found that THz pulses (1 kHz rep-rate, 0.26 nJ/pulse, 0.3–2.5 THz) induce a genetic response in mouse skin similar to that of a puncture wound and that the genome analysis was very different to that caused by UV radiation, thermal damage and neuron radiation exposure.[177] Additionally, they observed that exposure to this type of THz radiation resulted in the wound taking longer to heal. There were also the observations of Ramundo-Orlando *et al.* that permeability of cell membranes was affected by pulsed THz radiation.[178] Note that not all studies observed effects due to THz pulses. Angeluts *et al.*[179] found no evidence to suggest that THz radiation (1 kHz rep-rate, 550 pJ/pulse, 0.6–6 THz) damages the DNA of human blood leukocytes.

The references in the above paragraph all used pulsed THz radiation and in such sources thermal effects can be ignored because the temperature increases are below 0.1 K, which is not enough to trigger a thermally induced stress response in cells. However, CW sources are capable of inducing heating effects although it should be noted that low enough CW powers can still induce a response without triggering any thermal response in the biological system. In one study, Franchini *et al.*[180] looked at how human fibroblasts respond to pulsed and CW THz radiation. They used a compact free-electron laser to generate pulses between 100 and 150 GHz with time length 50 ps and their CW source generated a single frequency at 25 GHz. They found that THz exposure for both pulsed and CW sources do not induce any thermal effects (due to low CW powers); however, they did observe aneuploidy in their samples for both types of radiation with the speculation that different mechanisms are involved. Increasing the CW power levels was done by. in the study by Echchgadda *et al.*[181] where they exposed jurkat cells to a 2.52 THz CW source with 636 mW cm^{-2} power and observed a 6 °C temperature increase; therefore, they had to compare their results to jurkat cells that were heated to the same temperature for the same duration. The heated cells do show significant changes in their genome expressions; however, the THz exposed cells showed the activation of very different signaling pathways. This indicates that while CW THz radiation can heat the sample, its effects are not simply

thermal. The same group has also shown that the majority of jurkat cells die after 20 minutes of exposure to their CW 2.52 THz source with 227 mW cm^{-2} power.[182] The final study we review from this group is Ref. 183, where they exposed human keratinocytes (skin cells) for 20 min to a CW source with different frequencies (1.4, 2.52, and 3.11 THz) keeping the power density at 44.2 mW cm^{-2} for each frequency. This low power density was not enough to induce a thermal response. Their results showed that each frequency triggered specific metabolic or signaling pathways that were not triggered by the other frequencies. This indicates that a careful study needs to performed to find the safe exposure levels at each frequency.

Kiseliov *et al.* studied the potential of THz radiation to suppress tumor growth (Guerin carcinoma) in rats and compared it to x-ray exposure.[184,185] Their source was a CW hydrogen cyanide gas laser operating at 0.89 THz with power densities of 1600 μW cm^{-2}, and they exposed the tumors for 10 min once every three days. They found that THz radiation and x rays both slow down tumor growth compared to a control group. However, the mechanisms are very different as the x rays kill all cells whereas the THz wave induced an inflammatory response where the immune system targeted the cancer cells. In the same study, they also exposed tumors for 10 min once every day with a power density of 400 μW cm^{-2}. In this scenario, they found that tumor growth actually accelerated compared to their control. This study shows the great effort required to determine and develop any potential therapeutic uses of THz radiation. A study that makes a further relevant point is that performed by Bock *et al.*[186] where they exposed mouse stem cells to pulsed THz radiation (1 kHz rep-rate, 1–20 THz frequency range, 1 μJ per pulse) from air-plasma. They found that THz irradiation accelerates cell differentiation by activating a specific transcription factor (peroxisome proliferator-activated receptor gamma) with molecular dynamics computer simulations coinciding with the gene specific response they observed. Their work indicates that THz radiation could be used for cellular reprogramming.[186]

Mizuno *et al.* performed a series of *in vivo* measurements investigating the effects of THz radiation on corneal tissues.[187,188] They irradiated the corneal tissue of each rabbit with a 162 GHz CW source with powers ranging from 60 to 600 mW cm^{-2} for 6 min. The corneal thickness, opacity, and temperature were measured and they also checked for corneal epithelium damage. They observed some thinning of the cornea and the development of corneal opacity following the measurement. However, they also monitored the corneas for nine days following the measurements and found that some of these effects recovered with increasing time following the exposure. The study classified the severity of the effects according to the power level of the exposure. They observed no damage to the corneal tissues at 60 and 120 mW cm^{-2} in any of their corneal assessment techniques. They also measured changes in the THz reflectivity following the exposure and propose that some of the damage observed could be linked to dehydration effects caused by the increase in temperature attributed to the high power exposures.

Currently, there is no consensus in regard to what are safe THz power levels partly because a lot of studies have not observed any effects due to THz exposure (see Refs. 179,189, and 190) while simultaneously others have observed effects (see references in the above paragraphs). It should be noted that most studies use different methods of evaluating biological damage and their exposure conditions are also different. Further, the exact mechanism via which THz radiation affects living organisms is unclear. The so-called Fröhlich condensate is the most accepted theoretical mechanism; however, it was first experimentally observed in 2015 by Lundholm *et al.*[191] in a lysozyme protein. They shone a CW 0.4 THz light on a lysozyme protein and used the x-ray crystallographic method to obtain the vibrational modes of the protein structure. They observed changes to the atomic displacement of a long helical part of the protein, and that the overall atomic positions were more ordered (less displacement) with the THz light on. The most likely explanation of their results is a Fröhlich condensate. This, unfortunately, is only a single-step toward understanding the physical mechanisms via which THz radiation affects entire biological systems which consist of many proteins and molecules, and highlights the research left to be undertaken.

V. BIOMEDICAL APPLICATIONS

THz biomedical applications can be found for molecules in a nanometer level up to tissues at a centimeter level. Different approaches for sample preparation, measurements, and data analysis have been used depending on the different characteristics of the samples. Earlier studies gave more attention to investigating the fundamental THz dielectric properties of biosamples. This was followed by numerous studies targeting sensitive detection. Recently, increasing numbers of measurements and images of macroscopic tissues have been performed, especially relating to *in vivo* applications, showing the trend of THz biophotonics toward more practical applications. In this section, we present an overview of biomedical applications using THz technologies. In particular, we first introduce the fundamental earlier studies of biomolecules including their solid phase and aqueous solutions. Then, different sensing techniques proposed for sensitive detection of various biosamples will be presented. Another large branch of applications, covering tissues investigated either *in vitro* or *in vivo*, will be comprehensively reviewed. We will show the progress that has been made in different areas to date and discuss their trends of development.

A. Fundamental molecular studies

THz biomolecular spectroscopy is one of the earliest THz biomedical applications, which can be classified into a field of THz-biochemistry. It starts from the far-infrared studies using Fourier transform infrared spectroscopy (FTIR) from the 1960s.[192] The invention of THz-TDS filled the lower spectral range of 0.1–4 THz, providing a better SNR and accuracy in this region. The motivation of THz spectroscopy of biomolecules comes from the fact that THz waves can sensitively probe the phonon vibrations and intermolecular interactions, such as the hydrogen-bonding activities and collective vibrations, which play critical roles in many biological processes, such as protein folding and conformational changes or DNA transcription. This is in contrast to the infrared region which mainly probes the intramolecular vibrations and rotations. The sensitivity to the long-range arrangement makes the molecular THz response highly dependent on the ordering structure and the solvation environment. This mechanism determines the characteristics mentioned earlier that spectral features of sharp absorption peaks are only observed in small biomolecules in their solid crystalline form. For macromolecules, THz waves probe a large number of collective modes that give rise to a smooth spectral absorption.[130,193] For amorphous samples, the high level of spatial disorder results in complicated intermolecular

interactions from the random molecular orientations, giving rise to inhomogeneous broadening of the features.[131,132] Long-range order is also absent in aqueous solutions. In this case, the solvated molecules interact with the surrounding water molecules, forming a hydration shell with properties different from that of bulk water,[194] thus offering a chance to be probed by THz spectroscopy. Therefore, in terms of applications, THz molecular spectroscopy can be classified into three categories: investigating the molecular dynamics in solid-phase samples, investigating the molecular interaction with water, and improving the sensitivity of molecular detection.

1. Solid-phase samples

Most investigated solid-state biomolecular samples for THz spectroscopy are usually poly- or single-crystalline small molecules which provide highly ordered lattice structures. The connected intermolecular vibrations controlled by noncovalent forces, such as H-bonds, give rise to absorption at some specific frequencies in the THz range, resulting in sharp peaks as the spectral features. As a result, THz light is highly sensitive to the molecular arrangement. For example, isomers, which may present similar infrared spectral features due to the similar intramolecular vibrations, can be distinguished from the low-frequency intermolecular modes in THz spectroscopy.[125] For the measurement, polycrystalline samples are usually prepared by mixing the investigated biomolecules with THz-transparent polymer powders, such as polyethylene and compressing the mixture into pellets. This method provides flexibility in the fraction ratios between the two compounds and arbitrary thicknesses, such that a long sample–THz interaction can be achieved. THz-TDS is commonly used, which can probe the low-frequency modes down to subterahertz and enables the simultaneous extraction of both the refractive index and the absorption coefficient. FTIR was mainly used in some earlier works, providing a broader bandwidth up to mid-infrared. In both systems, a focused THz beam directly passes through the pellet sample in a transmission geometry. The sample thickness is typically maximized to allow a sufficiently long THz–sample interaction distance, while attention should be given to ensuring the sample attenuation does not exceed the dynamic range of the system, especially at the peak regions. Fabry–Pérot oscillations in the spectrum due to the beam bouncing within the sample may occur. These features should be distinguished from the sample spectral features. Another way to prepare polycrystalline samples is by drop-casting or spin-coating solutions on a substrate to make planar ordering polycrystalline thin films. Compared to polycrystalline pellets which are randomly orientated in the 3D directions, the crystal orientations of the film are only random in the 2D planar direction, significantly reducing the inhomogeneous broadening of the spectral features. The narrower feature absorption makes it possible to separate some close vibrational modes. However, it is difficult to measure such thin films in the traditional transmission geometry due to the low sensitivity. Instead, waveguides have shown a very promising sensitivity for broadband characterization of such thin films,[195,196] which will be detailed in Sec. V B 2.

The above measurement protocol for pellets has been widely adapted to investigate many important biomolecules. The observation of spectral features is usually limited to small biomolecules when the number of oscillation modes is small. Large biomolecules are usually featureless in the THz band. This is the result of the increased number of vibrational modes due to the large number of degrees of freedom, which causes the spectrum to collapse into a featureless spectrum. For example, spectral features are found in nucleoside and nucleobases,[3] but not in DNA or RNA,[197,198] in amino acids and short-chain peptides,[4,129,199] smoothed in tetrameric peptides,[127] and not seen in proteins.[200,201] Other small therapeutic biomolecules also exhibit THz spectral features due to collective vibrations, such as various types of saccharides,[131] uric acid,[125] purine and adenine,[126] and many pharmaceutical drugs.[50] Due to the high sensitivity to the intermolecular network, a promising application is using THz spectroscopy to monitor polymorphic conversion *in situ*. Figure 9 from Ref. 202 shows the solid–solid conversion of carbamazepine form III to I at isothermal conditions (433 K), recorded at 5-min intervals. In such an application, THz spectroscopy demonstrates its advantages of low photon-energy (no heating effect), fast acquisition, and noninvasive measurement.

Another common feature observed for the small biomolecules is the sharpened and enhanced absorption peaks at low temperatures. This sometimes enables two peaks to be resolved at low temperatures, but they are collapsed into one at room temperature.[3,126] The positions of the feature peaks are also temperature sensitive, while the relationships with temperatures vary with different peaks and at different temperatures, due to the different mechanisms dominating the shift.[131] To understand the origins of the observed features, researchers usually apply various molecular modeling calculations or simulation methods to analyze the experimental results, such as normal mode calculations,[200,203] density functional theory calculations,[3,123] and molecular dynamics simulations.[128,204] For macromolecules which present no spectral features, THz spectroscopy is still sensitively responsive to their molecular structures. In this case, the detection is based on a featureless dielectric difference. For example, applications have shown that THz dielectric spectroscopy can be used to probe protein conformation and mutation,[200] and detect the binding state of DNA.[198] However, the absence of a specific fingerprint reduces the sensitivity and the contrast to other dielectric substances.

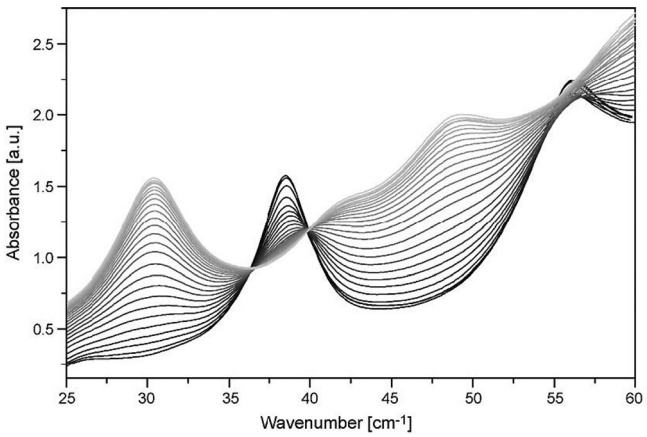

FIG. 9. Solid–solid conversion of carbamazepine form III (black) to I (light gray) at isothermal conditions (433 K), recorded at a 5-min interval. Reproduced with permission from Zeitler *et al.*, Thermochim. Acta **436**, 71–77 (2005).[202] Copyright 2005 Elsevier.

2. Interaction with water

Although solid-phase samples may exhibit spectral features in the THz range, the most ideal approach for studying biomolecules is to investigate them in a condition mimicking their *in vivo* biological environment. This requires an aqueous phase, with a proper pH value, temperature, and other requirements on the inclusions. Among these conditions, it is critically important that the mechanism and dynamics of biomolecules interacting with water is explored, which essentially determines many biological structures and functions, especially for proteins. An important branch of THz biomolecular spectroscopy is the study of solvated biomolecules, usually by means of THz absorption or dielectric spectroscopy. The most obvious obstacle, however, is the high THz absorption by water that strongly limits the light–matter interaction distance, hence the accuracy. Havenith's group has made a great contribution to this area. They probed the fast relaxation dynamics of water solutions using a Germanium laser operating at 2.3–2.9 THz with a high output power up to 1 W. This enables the measurement of a large sample thickness to provide a high sensitivity. Their early work in 2006 measured the absorption of lactose solution as a function of the lactose concentrations.[205] The first observation is the concentration-dependent absorption from the measurement does not follow the weighted sum of the two components (i.e., lactose and water). Instead, a three-component model including the solute, bulk water (i.e., free water), and hydration water (i.e., solvation water or bound water) shows a better agreement. Further analysis reveals a hydration shell of 5.13×0.24 Å around the lactose, corresponding to 123 hydration water molecules around each lactose molecule, which have reached beyond the first hydration layer. These observations are based on the sensitivity of THz to the rearrangement of hydrogen-bonds in water, which is affected by the solute. Their following work in 2007 studied water–protein interactions,[206] which is important for understanding how water affects protein structures and functions. A nonmonotonic trend of the THz absorption against the protein concentration is found. This relationship is explained by a hydration shell of 20 Å around each protein molecule and the overlapping of the shells at high concentrations. The observed hydration shell thickness is much larger than that observed by scattering methods, potentially due to the different definitions of hydrated water. The analysis of the hydrogen-bond correlation function shows increasing hydrogen-bond lifetime with decreasing distance to the protein, showing the distance-dependent water properties in the THz regime. A further step forward is the investigations of the group into the influence of protein mutations and the pH value,[207] protein structural flexibility,[194] and the thermal denaturation effect on the solvation dynamics.[208] They have also investigated the protein–solvent interaction upon the folding process (which happens on a millisecond time scale), by using a kinetic THz absorption (KITA) setup to initiate the refolding reaction relative to the probing time of the THz pulse.[209] Details about these investigations can also be found in Refs. 210 and 211.

The concept of a long-range hydration shell with distinct THz properties brings a new perspective in which to view the protein hydration dynamics. This theory has been supported by other groups. Tamminen *et al.* studied the free and bound water in gelatin hydrogels with different total-water contents in the frequency range of 220–330 GHz. They verified the constant nonfreezing bound-water mass with a distinct property compared to pure water.[212] Arikawa *et al.* used THz-TDS to measure disaccharide-water solutions.[213] The use of the ATR geometry circumvents the high attenuation problem of water in a transmission measurement; thus, a broad bandwidth of 0.5–2.6 THz can be investigated. They used the three-component model with local field correlation to extract the properties of the hydration water. Bye *et al.* used an intense THz synchrotron source to study different concentrations of bovine serum albumin (BSA) solutions in 0.3–3.3 THz.[214] An observed nonlinear concentration dependency was explained by the presence of a 15 Å hydration shell around the protein. Sushko *et al.* compared proteins of different molecular weights with different concentrations using a quasi-optical VNA in the WR-3 waveguide band (0.22–0.325 THz). They also found a similar thickness for the hydration shell of 16–25 Å.[215] A larger range of molecular weights from 0.075 to 250 kDa, covering amino acids to proteins solvated in water is reported by Grognot and Gollot.[216] They applied a broadband THz-TDS in a Si-based ATR configuration to improve the sensitivity for absorptive liquids. Very different concentration dependencies for different sizes of molecules were found, as can be seen from the relative refractive index and extinction coefficient in Fig. 10. For small biomolecules, the hydration shell is relatively large compared to the molecule. The property of the hydration water in the shell makes a great contribution to the solution, hence the refractive index can increase and the extinction coefficient drops slowly with the increasing concentration. In contrast, the hydration shell is relatively small compared to large molecules. Therefore, the effective properties of the solution agree well with the theory that the biomolecules act as empty and transparent cavities to replace the water molecules.[210] Reduced refractive index and extinction coefficient were observed with the increasing concentration. The solute is not limited to proteins and their components. Phospholipid bilayers, which is a main component for biomembranes, also showed a long-range hydration shell up to four to five layers, as reported by Hishida and Tanaka.[217] All these studies demonstrate the unique role of THz spectroscopy in exploring the biomolecule–water interactions. The thickness of the hydration shell revealed by THz spectroscopy is larger than that observed by inelastic neutron scattering or nuclear magnetic resonance. This is because of the different definitions of the hydration shell caused by the different relaxation dynamics probed by these techniques. Inelastic neutron scattering or nuclear magnetic resonance probe the slower dynamics of $10^{-9} - 10^{-11}$ s, corresponding to the water molecules immediately adjacent to the solute, while THz spectroscopy measures dynamics at 10^{-13} s such that the slightly perturbed water molecules at long distances are included.[215,217]

B. Biosensors

Given that spectral features are rarely available in most biosamples, differentiating the relatively small dielectric differences requires high accuracy. In addition, the volume of most biosamples is small, the THz light can only interact with a thin film, and the measurement sensitivity is usually low. An important branch of THz biomedical research is to improve the sensitivity of biosensors with the aim to induce larger changes in the THz response with only trace amounts of samples. For this purpose, it is actually competing with many other sensing techniques, ranging from surface plasmon resonance (SPR), fluorescence to colorimetric methods. One of the biggest challenges of using THz waves for sensing is the long wavelength compared to the sample thickness, which is usually at a molecular level or subwavelength. To overcome this issue, various techniques have been proposed

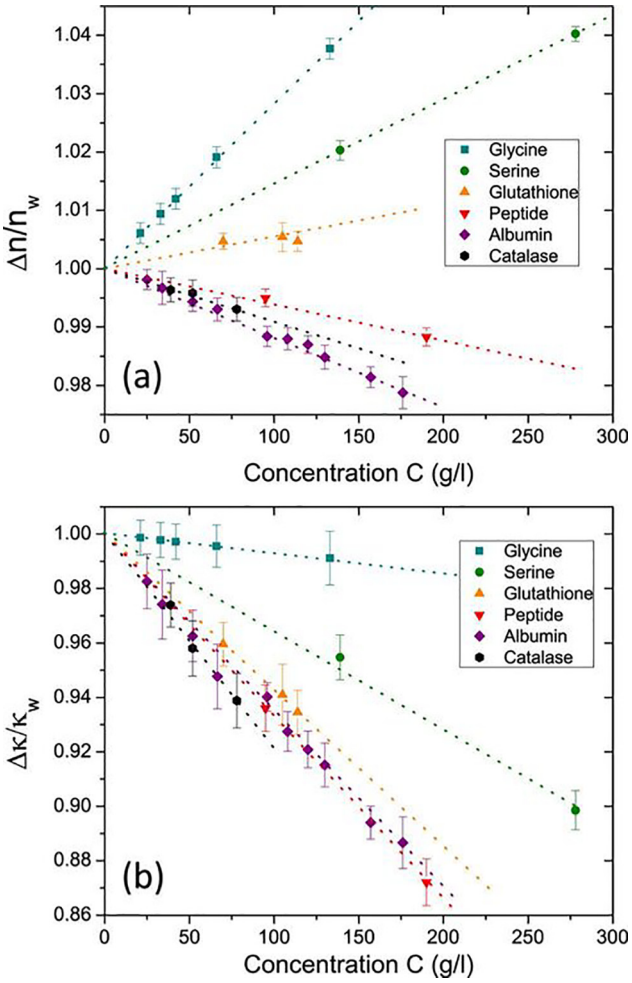

FIG. 10. Concentration-dependent relative (a) refractive index and (b) extinction coefficient of biomolecules with different molecular weights, including glycine (0.075 kDa), serine (0.105 kDa), gluthatione (0.307 kDa), peptide (0.458 kDa), albumin (66 kDa), and catalase (250 kDa). Reproduced with permission from Grognot *et al.*, J. Phys. Chem. B **121**, 9508–9512 (2017).[216] Copyright 2017 American Chemical Society.

to efficiently enhance the light–matter interaction.[218,219] Here, we overview the three most widely applied techniques, including metamaterials (MMs), waveguides, and THz surface plasmon polaritons (SPPs).

1. Metamaterials

MMs are artificial media consisting of subwavelength periodic structures (usually metallic) that have effective electromagnetic properties tailored by their structures. The high flexibility of the structural design makes it possible to realize almost arbitrary responses of the THz waves; thus, MMs are not just limited to THz sensing, and they have also been widely used in THz functional devices for beam control, modulation and polarization manipulation.[220,221] This is also the reason that MMs have become one of the hottest THz topics in the past ten years. The fundamental principle of MMs is based on exciting localized plasmonic modes in the metallic structures resonating at a single frequency or at some particular frequencies. The localized resonance gives rise to strongly enhanced and subwavelength-confined fields at the resonant metal-dielectric boundaries, typically at the gap regions. Any tiny changes in the dielectric environment caused by the analyte will significantly change the resonance condition, thus introducing a detectable variation in the resonant frequencies and/or intensities. The tightly focused field strongly enhances the light–matter interaction and requires only trace amounts of samples to produce a measurable change.

For sensing applications, planar MMs, which are also called metasurfaces, are more commonly used for convenient sample preparations. As the measurement is mainly based on the shift or the amplitude change of a resonance, a MM sensor with a sharp resonant peak or dip, mathematically represented by a high quality-factor (Q-factor), is preferred. The performance of a MM sensor can be evaluated by many aspects, sometimes depending on the sample types. For example, the sensitivity (S) is usually defined as the frequency shift per unit refractive index change, which is convenient for films with well-defined bulk THz properties. For dehydrated molecules on a sensor with an inhomogeneous and ultrathin thickness, it is difficult to define the refractive index, and one may need a measure of frequency shift per unit weight per unit area. The full width at half maximum (FWHM), or sometimes the Q-factor, is used to describe how robust the detection is against measurement errors. The figure of merit (FOM) combines the above two quantities by FOM = S/FWHM, providing a more comprehensive evaluation. To compare the ability to detect trace amount of the sample, the sample thickness or the volume will also be considered, such as measuring the volumetric sensitivity as the sensitivity per unit volume. The high flexibility on the MM patterns allows many different structures to optimize these aspects, thus there are a great numbers of studies in this area. In this manuscript, we will overview how the sensitivity, the sample volume, and the Q-factor were improved by different groups for biomedical sensing. Readers may also refer to the topical reviews in Refs. 218 and 222.

A lot of effort has been dedicated to increasing the sensitivity, which can be improved by various approaches. Conventional MMs include split-ring resonators, dipole resonators, or mesh resonator metallic structures fabricated on a bulk substrate. One well-known limitation in the traditional design is the field-confinement in the high-permittivity bulk substrate. Typically, a Si or other semiconductor substrate with a permittivity over 10 and a thickness of hundreds of micrometers is used. The confined field in the substrate weakens the interaction with the analyte, which can be solved by using an ultrathin or low permittivity substrate.[223] Tao *et al.* compared two sensors based on the same pattern on a thick (500 μm) Si and a thin (1 μm) SiN substrate, respectively. The sensitivity was improved more than an order of magnitude by the use of the thin substrate.[224] The same group proposed a MM sensor with the same pattern but on a paper substrate in the next year. The low permittivity and low absorption of paper also enables a strong field-analyte interaction. The use of a paper substrate, enabled by their novel shadow mask patterning fabrication method, has the advantage of the porosity feature, which is favorable for sample absorption. 100 μl glucose solution was deposited on the paper sensor and dried. They showed that glucose concentration down to 3 mmol l^{-1} can be detected, comparable with the clinical techniques

used for blood glucose detection.[225] Different detection sensitivities for glucose and urea were also found, which implies specific-target detection. Another approach to reduce the substrate influence is partially removing the substrate at the nonpattern regions. Using a focused photon beam, Chiam *et al.* fabricated a high aspect ratio MM sensor with 10 μm high split-ring resonators. Doing this leaves more field-enhancing space for the analyte previously occupied by the substrate, this significantly improves the sensitivity.[226] One potential drawback for this approach is the relatively large sample volume needed to fill the removed substrate, as the strongest field enhancing plane is located at the metallic layer. Another fabrication method of etching only the gap region of the split-ring resonator may ease this issue.[227] Figures 11(a) and 11(b) show the top-view and cross-section SEM images of the resonator with an etched trench. The increased sample volume is negligible, and an improvement factor of up to 2.7 times can be achieved. The substrate influence can also be eliminated by adopting a perfect absorber design. A MM absorber usually consists of three layers, namely, the ground metallic plane, the middle dielectric layer, and the MM patterns on top. The metallic ground perfectly isolates the field interaction with the lower substrate. Further, it also provides a high Q factor over 10 (traditional MM is below 10).[231] The metallic ground plane can also be an individual flexible substrate, as proposed by Yahiaoui *et al.*[232] Apart from the substrate, the sensitivity can also be improved specifically for a targeted sample. Lee *et al.* fabricated a nano-slit antenna MM sensor, with the structural dimensions designed to match the MM resonant frequencies to the vibrational frequencies of D-glucose and fructose, respectively.[228] By drop-casting the glucose or fructose solution on the sensor, a polycrystalline thin-film was formed which provides sharp vibrational peaks with very high absorption at the resonant frequencies of the sensor. In this way, the sensor provides selectivity to only be highly sensitive to the targeted samples. Figures 11(c) and 11(d) show the measured results of the normalized spectra using the glucose sensor to measure sucrose and D-glucose respectively. The resonant peak of the sensor at 1.4 THz matches the glucose vibrational mode. A much higher sensitivity can be found in the glucose measurement. Recently, novel nanomaterials have also been introduced to improve the sensitivity. By adding a monolayer of graphene on top of a MM absorber,[233] or replacing the metallic dipoles with carbon nanotube (CNT) dipoles,[234] a higher sensitivity was observed, as reported by Ying's group. They demonstrated the sensitive detection of 100 nM thrombin binding to the aptamers on the graphene sensor and the clear reflectance variation of the CNT sensor by glucose solutions at concentrations from 0 to 100 ng/ml. They attributed the improved sensitivity to the efficient absorption of the analyte by the graphene or CNTs through p–p stacking and van der Waals forces. However, the added analyte introduces negligible modulation to the graphene or the CNT; thus, there is very little contribution from the conductivity variation. In addition, cleaning the surface of

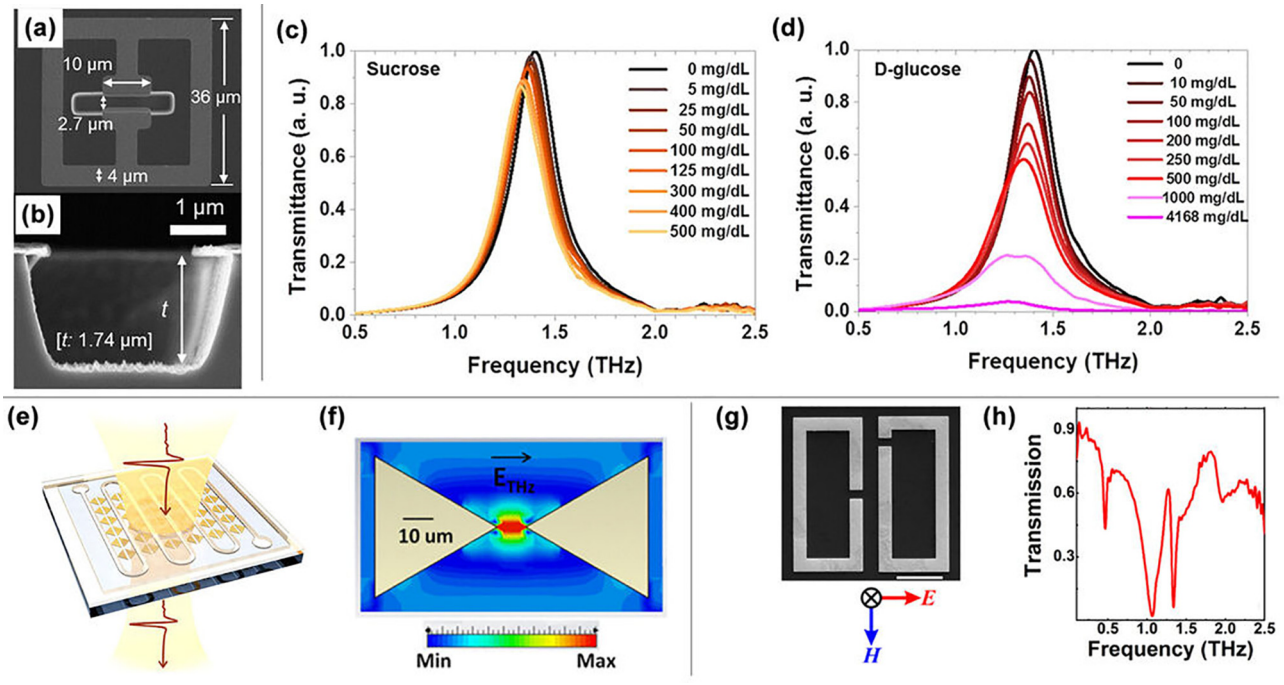

FIG. 11. THz metamaterial sensors: (a) top-view and (b) cross-section SEM images of the metamaterial pattern with a trench etched at the field-enhancing region. (a) and (b) are reproduced with permission from Meng *et al.*, Opt. Express **27**, 23164 (2019).[227] Copyright 2019 Authors, licensed under a Creative Commons Attribution (CC BY) license. Normalized THz spectra measured with the glucose antenna metamaterial sensor for (c) sucrose and (d) D-glucose molecules. (c) and (d) are reproduced with permission from Lee *et al.*, Sci. Rep. **5**, 15459 (2015).[228] Copyright 2015 Authors, licensed under a Creative Commons Attribution (CC BY) license. (e) Schematic of the microfluidic bow-tie metamaterial sensor. The corresponding simulation in (f) shows that the resonant THz field is enhanced at the microfluid regions. (e) and (f) are reproduced with permission from Zhang *et al.*, IEEE Trans. Terahertz Sci. Technol. **9**, 209–214 (2019).[229] Copyright 2019 IEEE. (g) Symmetric-broken double split ring resonator design. The scale bar is 15 μm. The corresponding (h) measured transmission spectra of the metamaterial sensor. (g) and (h) are reproduced with permission from Yang *et al.*, Opt. Express **25**, 15938 (2017).[230] Copyright 2017 Optical Society of America.

graphene or CNTs could be difficult, which may limit their practical usages. Nanoparticles have the surface plasmon resonance usually at visible wavelengths due to the nanometer-scale structure, which cannot be utilized for THz sensing. However, when combined with MM, their larger permittivity will cause changes in the electric field especially at the enhancing regions. The use of nanoparticles may also provide a homogeneous monolayer distribution. Adding gold nanoparticles has been shown to cause a highly efficient improvement on the detection sensitivity for both avidin[235] and epidermal growth factor receptor (EGFR).[236]

Improving the sensitivity can usually reduce the amount of sample required for successful sensing. There is also research focused on directly reducing the volume needed. The enhanced field at the resonant locations of traditional MM sensors is confined within few tens of micrometers in height. Given that the frequency resolution limit of THz-TDS is about 2 GHz, the minimum thickness of a sample that can cause a measurable changes is about 100 nm.[231,237] Thinner layers require an extremely confined field compared to the wavelength. A solution provided by Park *et al.* is a single nanoslit antenna.[238] In this structure, the analyte in the nanoslit interacts with the strongly confined field; thus, a very small amount of sample is required, while the transmission is very weak. The approach of narrowing the gap is also adopted in another design consisting of annular nanogaps fabricated by atomic layer lithography.[239] The device showed the ability to detect a 1-nm-thick layer of Al_2O_3, six orders smaller than the wavelength. Alternatively, the sample volume can also be minimized by reducing the lateral area. For example, Withayachumnankul *et al.* attached the MM sensor close to the THz emission crystal to interact with a THz near-field.[240] The sample can be as small as 0.2λ. More recently, a spintronic THz emitter has been integrated with MM sensors monolithically by Bai *et al.*[241] Hela cells and pseudomonas prepared on the asymmetric double-split ring resonator MM sensors directly interact with the THz waves emitted from the backside of the substrate, with a lateral spatial resolution down to 500 μm. This resolution can be further improved by reducing the substrate thickness (2 mm in this study). The area can also be reduced by concentrating the analyte to only the field-enhancing regions by guiding the sample using a microfluidic device, as reported by Zhang *et al.*[229] and shown in Figs. 11(e) and 11(f), and they presented the ability to detect BSA solutions down to 0.13 μl.

A larger amplitude change can be induced by the analyte near the resonant frequency if a higher Q-factor can be provided; thus, a better robustness against experimental errors can be obtained. Some research has also been dedicated to improving the Q-factor by sharpening the resonant peak or dip. This is usually realized by breaking the symmetry of the MM pattern. A theoretical study of asymmetric THz MMs has been given by Signh *et al.*[242] This design enables a Q-factor up to 65 in the quadrupole mode of a split-ring resonator with asymmetric double slits[223] and up to 100 in an octupolar mode of a double split-ring resonator structure.[230] Figures 11(g) and 11(h) show the MM unit design and the corresponding experimental transmission spectra. The octupolar mode is at about 1.3 THz.

The great effort given to THz MM sensors has improved their performance from many aspects. Sample loading and measurement are simple with excellent sensitivity. However, the mechanism of localized plasmonic resonance is sensitive to the dielectric loss of the sample. Many aqueous samples, especially water solutions, have extremely high absorption in the THz range. Measuring these absorptive materials introduces significant loss that obviously broadens the resonant peak, resulting in a poor Q-factor, as can be seen in Refs. 229, 243, and 244. Therefore, most of the MM sensing applications have been shown on low-loss samples, such as dehydrated materials. Developments leading to structures specifically designed for absorptive samples are in high demand.

2. Waveguides

Waveguides direct the propagation of a THz beam by confining the field near the guiding structure; thus, they can also be used to sense a small amount of analyte. There are many forms of THz waveguides. Among them, the parallel plate waveguide (PPWG) is one of the most commonly used structures due to a few advantages. PPWGs support the propagation of a TEM mode with almost zero dispersion, similar to free space THz waves, while confining one of the spatial dimensions of the electric field to a subwavelength scale, providing efficient interaction with thin-film samples. The absence of resonance enables a direct characterization of the sample optical properties. A PPWG is simply made of two metallic plates parallel to each other, with a subwavelength air-space (typically of the order of 100 μm) between them. Usually, two Si plano-cylindrical lenses are attached to the edges of the PPWG to couple the free-space THz light into and out of the waveguide, as shown in Fig. 12. In this way, the THz wave is compressed in the z direction to a subwavelength level in order to efficiently interact with any thin-film sample deposited on the waveguide inner surfaces. The near perfect conductivity of metals in the THz regime offers nearly zero dispersion, no cutoff frequency, and low absorption of 0.1 cm^{-1} in the range of 0.1–4.5 THz.[245] The metallic plates can also be replaced by metallic films to provide a high flexibility.[246] A PPWG can also be designed in a tapered structure such that the thickness of the gap gradually reduces from the input/output to the middle. In this way, the middle thickness can be reduced down to 8 μm to strongly confine the field without significantly affecting the coupling efficiency between the THz light and the PPWG.

The Grischkowsky group has made great contributions in PPWG sensing. A successful application of thin-film water sensing has been demonstrated by Zhang and Grischkowsky.[247] They controlled the temperature and the pressure of a chamber, such that a 20-nm thin film of water was condensed on the inner surfaces of the PPWG inside the chamber. The PPWG enables a long interaction length up to 63.5 mm (i.e., the length of the PPWG) with the water film. Both the refractive index and absorption coefficient can be sensitively characterized. The two major limitations of this method are first, the water film

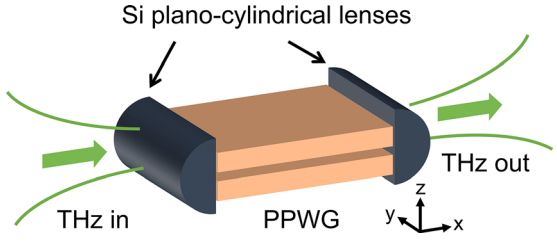

FIG. 12. Schematic of a typical parallel plate waveguide and its coupling to the free-space THz waves.

thickness cannot be physically measured and it was determined by equating the refractive index at 0.86 THz to that of bulk water. Such a method cannot be applied to other samples with unknown optical properties. Second, strong water-vapor absorption lines appeared in the characterization results, which are caused by the different vapor pressures in the sample and reference measurements. Another significant advantage of PPWGs is the ability to characterize the samples with spectral features. This is not only because it provides a high sensitivity to thin films. As mentioned earlier, polycrystalline thin films have planar ordering and have one less dimensional disorder compared to pellet samples; thus, they provide sharper feature peaks by reducing the inhomogeneous broadening. Melinger *et al.* investigated 1,2-dicyanobenzene (12DCB), tetracyanoquinodimethane (TCNQ) and 1,3-dicyanobenzene (13DCB) drop-casting on the inner surface of the PPWG to form polycrystalline thin films.[195,196] Figure 13 shows an example comparing the spectra of 12DCB measured in a pellet and in a PPWG.[196] Compared to the three broad features for the pellet sample, the PPWG can resolve six narrow absorption features. The FWHM of the peaks can be significantly reduced by up to five times compared to the pellet samples. They have also studied different crystalline forms induced by different concentrations and preparation methods,[195] which correspond to different absorption characteristics. In another study by Laman *et al.*, 2,4-DNT sample was measured by the same PPWG method and compared to its pellet form at 11 K. The PPWG sensing identified 19 features with many of them having linewidths below 15 GHz, compared to only seven spectral features and about an eight times broader width observed in the pellet sample. They have also studied seven small biomolecules, including deoxycytidine, nucleosides and amino acids, to demonstrate the applications to biomedical samples.[248] The drawback of using PPWG for spectral sensing is the difficulty in extracting the absolute absorption coefficients, due to the slight changes in the frequency-dependent transmission when the PPWG is reassembled to load/remove the sample.

Resonance can be introduced to PPWGs for sensing via frequency shifts, in a way similar to that of MM sensors. There are several methods reported. For example, Harsha inserted a dielectric Bragg grating into the PPWG.[249] The height of the dielectric grating is only 900 nm and thus introduces very little perturbation, and the waves still propagate in the broadband TEM mode. The structure provides very sharp resonance dips as narrow as 6 GHz and a Q-factor up to 430, significantly higher than traditional MM sensors. Mendis *et al.* adopted another approach by machining a rectangular groove on one of the waveguide plates.[250] The TE_1 mode is excited, and an extremely narrow resonance with a linewidth of 3 GHz was formed at 0.293 THz. Liquids can be conveniently filled into the groove to shift the resonant frequencies. A thin stainless steel film with a single slit inserted into the middle of a tapered PPWG can also introduce a sharp resonance with a linewidth of 11 GHz.[251] The same group has also investigated the application of this structure in the sensing of a thin-film dielectric layer, showing the sensitivity to the sample length, thickness and refractive index.[252]

Other waveguide structures have also been proposed for sensing applications. Microstrip-line waveguides are usually directly integrated with a PCA emitter and detector in an on-chip configuration. Coplanar waveguide lines combined with VNA extenders have been proposed for liquid and cell characterization.[253,254] Byrne *et al.* showed the application of such a sensor for measuring lactose pellets;[255] it was

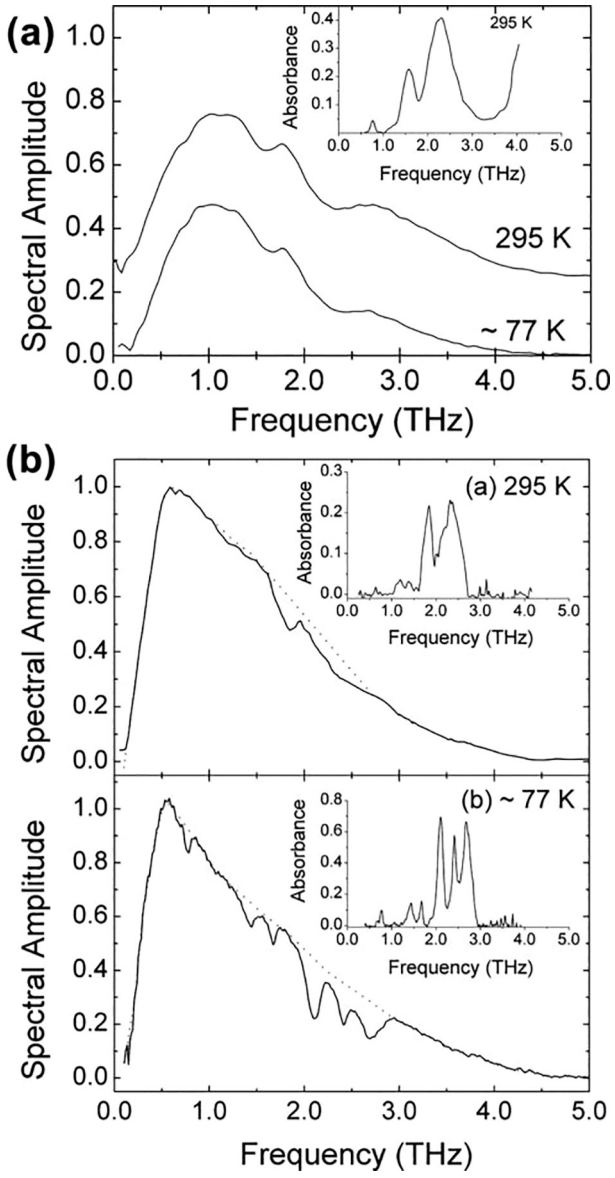

FIG. 13. The spectra of 12DCB transmitted through (a) a pellet and (b) a parallel plate waveguide covered with 12DCB film, at 295 and 77 K, respectively. The insets show the corresponding absorbance spectra (only the absorbance at 295 K for the pellet sample is shown). Reproduced with permission from Melinger *et al.*, Appl. Phys. Lett. **89**, 251110 (2006).[196] Copyright 2006 AIP Publishing.

able to resolve the consistent absorption dip observed in transmission measurements. Compared to free-space TDS, this technique has the advantages of compactness and no multiple reflections from the system. The lactose spectrum appeared as a straight line with an obvious absorption dip. However, it requires the sample to be placed close to the device to sufficiently interact with the evanescent wave, while direct contact may damage the device since it is integrated with the emitter and detector. Improvements to the robustness can be made using the design proposed by Ohkubo *et al.*[256] They illuminated the

pumping and probing beam from the bottom of the device and protected the antenna and the strip line by a thin cover layer. By changing the thickness of the cover layer, they were able to control the interaction efficiency between the THz light and the aqueous sample. Bandpass or band-stop filters can also be integrated with microstrip-line waveguides such that the sensing is measured in a quantity of frequency shift. Wood *et al.* showed a significant frequency shift of the stop band induced by photoresist layers of a few micrometers.[257] Nagel *et al.* demonstrated that a bandpass microstrip filter can sensitively differentiate the denaturized and hybridized DNA films.[258] Dielectric waveguide sensing has also been proposed. In the work by Li *et al.*, a Bragg waveguide with a defect in the first layer showed the ability to sense thin-film lactose. However, it is inconvenient to coat the sample onto the inner surface of the waveguide. The work by Fan *et al.*[259] favors tiny sample sensing. They guided the THz wave along a PMMA cylindrical tube with one side of the tube machined with a grating structure. The output spectrum from the waveguide contained resonance from the interference effect. The grating sharpened the resonance dips and served as a platform to load a small amount of analyte, with the dip position shift determined by the properties of the analyte.

Most of the waveguide structures provide a tight field confinement and a long propagation length. This characteristic is highly favorable for thin-film sensing because a long interaction length can be achieved in the planar direction of the sample. However, similar to the MM sensors, sensitive detection of absorptive aqueous samples has not yet been demonstrated. Although we have seen the characterization of an ultrathin 20-nm water film,[247] the special condensation method to form the thin film cannot be applied for many other aqueous samples. Resonance methods, such as Mendis's work,[250] are expected to face the same issue as that of MM sensors, namely, that the resonance dip will be significantly broadened by the absorptive sample.

3. THz surface plasmon polaritons

SPR is a technique which was originally used for sensitive probing at visible wavelengths. It is based on the excitation of SPPs, referring to the coupling oscillations of electromagnetic waves and the electron gas density at the metal-dielectric boundary. The resonant wave is nonradiative, traveling only along and tightly confined to the boundary, hence giving the term "surface" and providing the ability to sense thin-film samples. Optical SPPs are generally excited near the plasma frequency of a metal in a prism-coupling configuration. Since the plasma frequencies of all metals are far above the THz range, SPPs at the metal–dielectric interface are very weakly confined at THz frequencies. THz SPPs have been mainly achieved by three approaches: (a) prism-coupled SPR based on doped semiconductors; (b) aperture-coupled SPPs along a conductor–dielectric interface; and (c) spoof SPPs using artificial periodic structures.

The dispersion relation of surface plasmon waves at a conductor–dielectric interface is described by the following equation:[260]

$$k_{SPP}(\omega) = \frac{\omega}{c}\sqrt{\frac{\varepsilon_c\varepsilon_d}{\varepsilon_c+\varepsilon_d}} = k_{free}(n_{SPP} + i\kappa_{SPP}), \tag{4}$$

where k_{SPP} and k_{free} are the wavevectors of the SPPs and free space wave, respectively; ε_c and ε_d are the relative permittivities of the conductor and dielectric, respectively; and n_{SPP} κ_{SPP} are the SPP effective refractive index and extinction coefficient. Exciting SPPs requires n_{SPP} larger than 1. Therefore, free-space radiation cannot directly couple with SPPs due to the smaller wavevector. A prism (i.e., n >1) in an Otto or Kretschmann configuration is usually used to match the wavevector.[261,262] For the conductor, a negative real part of ε_c is also required, which is found below the plasma frequency at which the real part of the permittivity changes its sign. Semiconductors with a proper doping level can tune the plasma frequency to the THz regime, such as doping silicon at a level of 10^{-16} to 10^{-17} cm^{-3}.[263,264] InAs and InSb have been experimentally demonstrated to be materials capable of supporting well confined THz SPRs, and their magneto-optical response further enables the control of the resonance via external magnetic fields.[265,266] However, the quality of the SPR based on these semiconducting materials is relatively low compared to the gold SPR in the visible range. This is fundamentally determined by the dispersion behavior of the semiconductor near the plasma frequency. Generally, an ideal SPR has a wavevector that dramatically increases when approaching the plasma frequency, providing a tightly confined field and a sensitive angular/frequency dependence of the reflectivity. When these are satisfied, a sharp SPR dip in the frequency-domain or in the incident-angle domain can be obtained, providing a high Q-factor and a high sensitivity of the dip shift to tiny changes in the analyte properties.[267,268] Compared to the visible devices, the spectral reflectivity of THz SPR is flat and broad, providing a low sensitivity.[265] Although the decay length in the dielectric is subwavelength, it is still relatively large compared to MM sensors or waveguides, limiting its thin-film sensing ability. This is potentially why this approach has not been widely applied in practical sensing applications. Apart from bulk semiconductors, graphene has also been theoretically proved to be able to support THz SPR when it is heavily doped or stacked as multiple layers.[269,270] Theoretical analysis shows better dispersion characteristics, reflected by the narrow FWHM of the resonance. However, so far there has been no fabricated graphene SPR sensor demonstrated in the THz band.

Another approach to excite THz SPPs is by scattering the THz light at an aperture formed by a gap between a metal blade and a conductor, as first proposed by Saxler *et al.*[271] The SPPs propagating along the conductor over a certain distance will be re-coupled into free space by another blade aperture and will be received by the detector. Due to the continuum of the wave vectors of the scattered evanescent field, the broadband spectrum all can be coupled to the SPPs. The measured signal is a low-pass continuous spectrum up to the plasma frequency. This is in contrast to the above prism-SPR in which only one wavelength will be in resonance and an absorption dip is expected. In Saxler's work, gold was used for the generation of SPPs. Dielectric thin films of 3.8 and 9 μm coated on the gold showed different transmitted amplitudes. However, as discussed above, gold is obviously not an ideal selection for THz SPPs which yields in a very poor field confinement. The later work by Isaac *et al.* improved this method by using InSb,[272] which reduced the decay length of the SPPs in air by over a factor of 10. They also showed a onefold phase change when measuring a thin-film polymer on InSb compared to that on gold. The same configuration has also been used for defect detection by Yang *et al.*[273] They presented the ability to measure a particle on the InSb with a size down to 11 μm. However, the properties of the SPPs are determined by the materials. The InSb used has the same limitation as that in the prism-coupled SPR, that is, the field confinement is still relatively

weak. For example, in Issac's work,[272] they estimated the decay length into the air at 1.2 THz to be 178 μm using InSb (70% of the wavelength in free space), which is not significantly subwavelength.

A more practical method for THz SPP sensing is launching spoof SPPs on a structured periodic conductor.[274] The patterned periodic conductor, which can be regarded as a metamaterial, exhibits a similar dispersion relation to that of conductors near the plasma frequency. Therefore, the term "spoof" was allocated to differentiate it from the natural SPPs. Structured conductors have two important advantages over the natural THz SPP conductors. First, better dispersion characteristics can usually be achieved for a more tightly confined field. Second, the plasma frequency can be freely adjusted by scaling the structure. To excite SPPs, the coupling methods used for the natural conductors can be applied. A very similar configuration to that described above for aperture-coupled SPPs is applied for a groove-structured heavily doped Si design.[275] The period, width, and depth of the rectangular grooves are 442, 221, and 100 μm, respectively, giving rise to a low-pass profile with a sharp stop band close to 0.3 THz. The rapid transmission drop is attributed to the rapid decrease in the group velocity approaching the stop band. The highly doped Si can also be directly replaced by metals, as shown in the work by Williams *et al.*[276] A copper metamaterial structure with periodic pits was investigated with the same aperture-coupling method, as shown in Figs. 14(a) and 14(b). The apertures h_1 and h_2 in Fig. 14(b) are used to couple in and out the SPPs, while the aperture h_3 can be adjusted to verify the field confinement. Figure 14(c) shows the measured spectra when h_3 = 1000 and 200 μm, respectively, compared to the calculation. The artificial structure provides a better dispersion profile such that a sharp cutoff frequency is observed in the spectrum at the Brillouin zone boundary. In addition, the use of metal reduces the Ohmic losses compared to doped semiconductors. Other coupling methods have also been reported. Li *et al.* fabricated a V-groove structure made of heavily doped Si.[277] They directly illuminated a normal-incident light to an extra coupling groove 5 mm away from the V-groove structure, which is more convenient than the aperture coupling method. A sharp stop band edge was also observed, owing to the bent dispersion curve. From the propagation point of view, these devices can also be regarded as plasmonic waveguides. The Otto configuration can also be applied. In that case, the detected reflection is expected to have a narrow dip at the resonant frequency, in contrast to a stop band. Ng *et al.* used a wax prism in an Otto configuration to couple the THz light to a groove structure deposited with gold.[278] The schematic and the experimental configuration of the groove metamaterials are shown in Figs. 15(a)–15(c). By optimizing the gap between the prism and the grooves, a deep and narrow resonant dip, accompanied by a dramatic phase change was formed. A high FOM up to 49 was achieved for nitrogen sensing and a sensitivity of 0.52 THz RIU^{-1} was found from the fitting. They have shown sensitive detection of different analytes that obviously shift the resonant dip, as shown in Fig. 15(d). However, samples, such as water and glycerin with a large absorption, have a significant damping effect, which obviously broaden the resonance. Using a prism with a higher refractive index can further improve the field confinement in such a configuration, as demonstrated by Huang *et al.*[279] They have also proposed a more accurate method for measuring the frequency shift by looking at the phase change (i.e., the first derivative of the phase spectra), which offers a higher Q-factor than the absorption spectra.[280] However, similar broadband resonances were found for absorptive liquids, indicating the common damping effect caused by the large sample absorption.

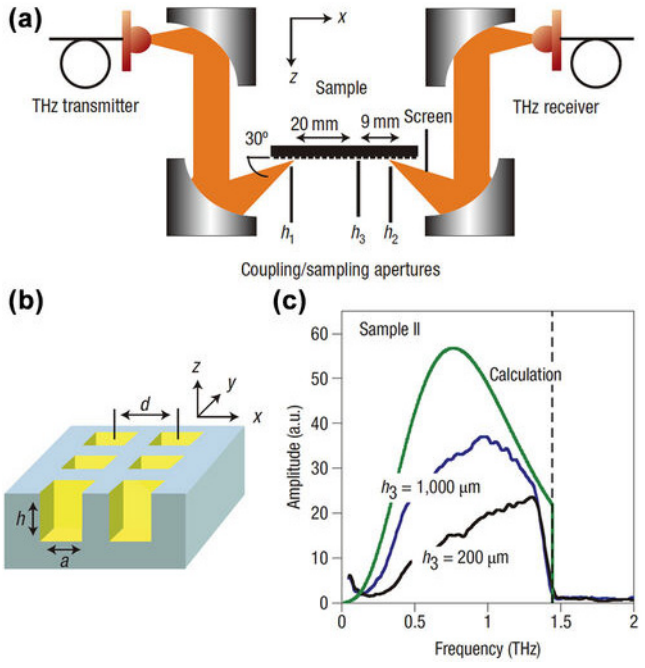

FIG. 14. Aperture-coupled THz spoof surface plasmon polaritons: (a) illustration of the experimental arrangement and the coupling between the free-space THz light and the surface plasmon polaritons; (b) schematic of the plasmonic metamaterial with periodic pits; and (c) measured spectra for one of the samples (sample II) when h_3 = 1000 and 200 μm, respectively, compared to the calculation. The dashed vertical line indicates the Brillouin zone boundary. Reproduced with permission from Williams *et al.*, Nat. Photonics **2**, 175–179 (2008).[276] Copyright 2008 Nature Publishing Group.

According to the coupling and detecting method, THz SPP sensing may have similar characteristics to those of MM sensors and waveguides. Aperture-coupled SPPs can be regarded as plasmonic waveguides such that a long interaction distance with the thin-film sample can be achieved. Prism-coupled SPR has the merit of a sharp resonance similar to MMs such that a sensitive detection can be achieved by monitoring the shift of the resonance. However, overall THz SPP is also a refractive-index sensing technique that has a worse performance with a higher sample absorption.

C. *In vitro* measurements

We have introduced various techniques for THz sensing, which have been mainly applied for thin-film samples, typically molecules, cells, and biomolecular solutions. Tissues have a much larger scale with spatial and frequency-dependent properties; thus, they are usually directly measured by label-free THz spectroscopy and imaging. Applications relating to disease diagnosis have been widely reported over the last two decades. They can be classified into the two distinct categories of *in vitro* and *in vivo* studies, which are very different in terms of the sample properties, preparation methods and measurement protocols. In the following, we will first overview the *in vitro* THz applications.

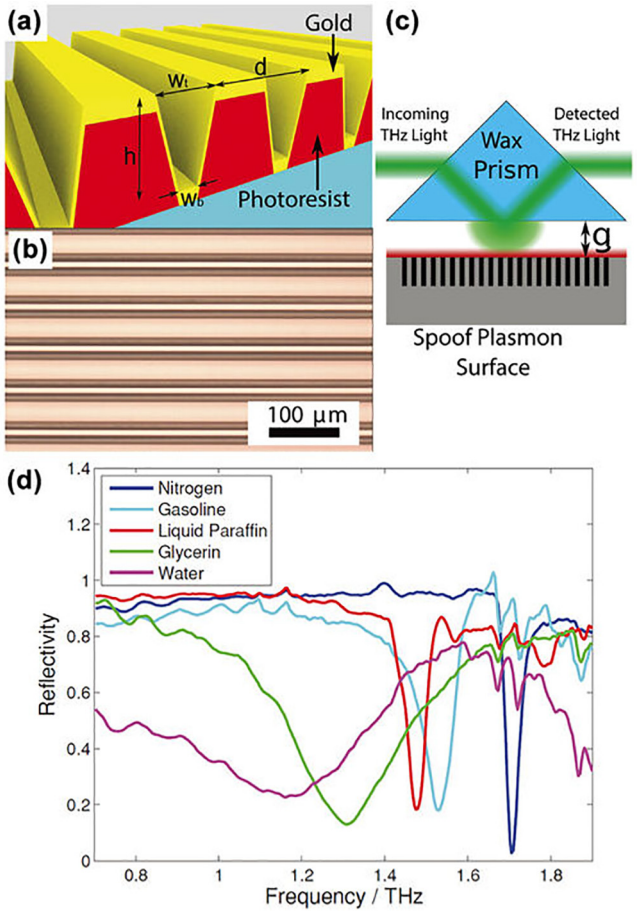

FIG. 15. Prism-coupled THz spoof surface plasmon polaritons: (a) schematic and (b) optical microscope of the spoof surface plasmon polaritons groove structure; (c) illustration of the Otto-configuration to couple the THz light to SPPs; and (d) measured spectra of different sample fluids. Reproduced with permission from Ng *et al.*, Adv. Opt. Mater. **1**, 543–548 (2013).[278] Copyright 2013 Wiley-VCH Verlag GmbH & Co. KGaA, Weinheim.

The current state of THz technology is still primarily confined to university laboratories due to critical experimental requirements. For example, THz imaging is mostly performed by a slow raster scanning. Reflection measurements require a highly flat sample surface for precise alignment, and typically good contact with a window is needed for accurate phase acquisition. *In vitro* tissues can better meet these critical requirements as they have a more ideal sample shape, and measurement variables, such as the applied pressure on the window or the subject-variance, are more easily controlled than for *in vivo* studies. They can also be accessed and handled more conveniently. In addition, *in vitro* studies are necessary to investigate and understand the origin of contrast, which is essential for further applications in clinical cancer detection and delineation. Some conceptual experiments can only be performed on *in vitro* samples. Excised tissues may also aid the histopathological examination. Therefore, *in vitro* studies are of great importance in THz biological applications. Next, we will talk about the sample preparation methods for *in vitro* measurements, followed by the most common *in vitro* application of pathological detection, especially neoplasm detection.

1. Sample preparation

In vitro samples for THz measurements can be either fresh or dehydrated, and there are several methods which can be used to prepare the samples. Freshly excised tissues can be directly measured, which have the advantage of preserving the original sample properties and contrast, while the large water content results in a high absorption close to that of pure water. This means that a thin slide, typically less than 500 μm, is needed to measure them in transmission. This can be achieved but for some tissues it could be challenging. The high absorption also limits the bandwidth due to the stronger attenuation at higher frequencies.[149] Therefore, fresh samples can be more conveniently measured in reflection since they are usually soft enough to contact well with a window.[60,156] Another problem for fresh samples is that they can be quickly dehydrated after being excised, especially when exposed to dry air or nitrogen in the experimental chamber. Structural and chemical changes could also happen with time. Fan *et al.* proposed a novel method to embed the fresh sample in gelatin,[122,281] as shown in the inset of Fig. 16(a). Figures 16(a) and 16(b) show that the THz properties of the gelatin preserved skin sample have negligible changes for up to 35 h. In comparison, the sample without gelatin preservation (i.e., control sample) showed dramatic property alterations after 9 h. Although fresh tissues to the best extent mimic the *in vivo* conditions, freezing the fresh sample to effectively reduce the water absorption could be useful in many aspects. For example, it allows a precise transmission measurement by allowing a larger sample thickness and may sometimes provide a better contrast between diseased and healthy tissues by reducing the high background absorption from water. Since water has a monotonically increasing absorption at THz frequencies, freezing the sample also improves the transparency at high frequencies; thus, a broader bandwidth can be measured. Hoshina *et al.* showed the greatly extended measurable bandwidth of a 1.7 mm porcine tissue in transmission at −33 °C.[282] Sim *et al.* showed an enhanced contrast between oral cancer and normal mucosa after freezing the sample at −20 °C compared to the results obtained at room temperature.[283] A hidden tumor inside the tissue was also observed in the frozen sample. He *et al.* further investigated the influence on the sample properties in the freeze–thaw process and found that by combining snap-freezing and fast-thawing, it was possible to remove the hysteresis in the slow-thawing process.[284]

Dehydrated samples have also been broadly studied. There are a few reasons; first, it provides a high transparency in transmission. Second, it enables the background contrast from the nonwater component to be investigated. Third, the sample can be easily handled with the properties remaining unchanged over a long time. The most widely adopted method is to fix the sample in formalin,[155,285] which could be followed by ethanol dehydration and paraffin-embedding.[102,149] Sun *et al.* studied the effect of formalin-fixing on the THz properties of samples.[285] The observation of the reduced refractive index and absorption coefficient with the increasing fixing time indicates the reduction in the water concentration caused by the formalin. In addition, new intermolecular interactions between the sample and formalin could occur. The fixed sample becomes rigid and could be distorted. A good contact with a window could be difficult, and scattering may occur affecting the results of the measurement. To prepare samples with a controllable surface flatness and thickness, the fixed sample is usually further soaked in increasing concentrations of ethanol to remove the remaining water and embedded in paraffin wax to

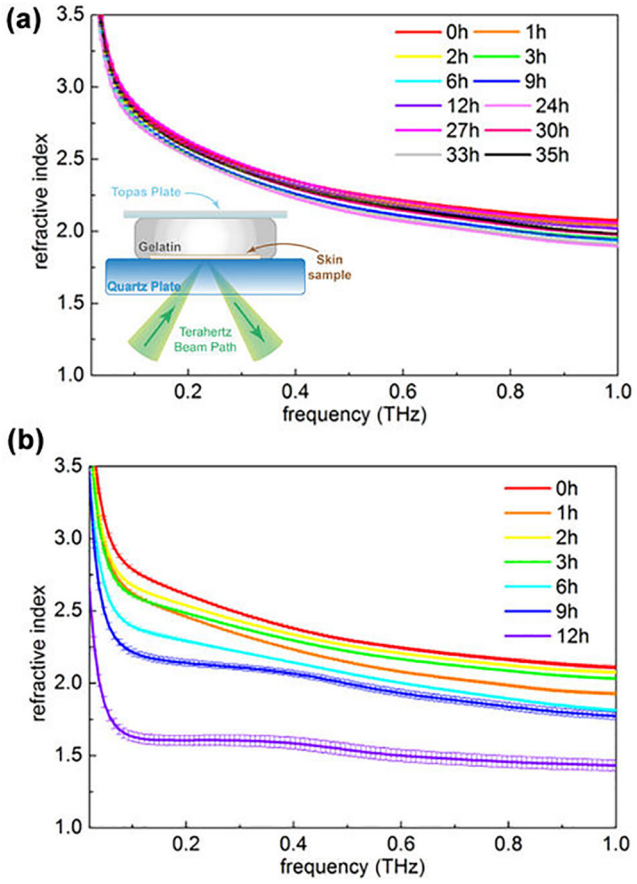

FIG. 16. The changes in the refractive index with increasing time of (a) the gelatin preserved sample and (b) the control sample. Inset of (a) shows the diagram of the skin sample embedded in gelatin during the measurement. Reproduced with permission from Fan *et al.*, Phys. Med. Biol. **60**, 2703 (2015).[281] Copyright 2015 Institute of Physics and Engineering in Medicine.

enable precise sectioning by a microtome. Another potential influence of formalin-fixing is that it could change the protein and DNA structure. Png *et al.* proposed the lyophilization (freeze drying) method to overcome this issue.[286] The lyophilization procedure includes snap freezing the sample and placing it in a low-pressure (10–100 Pa), low-temperature (−74 °C) environment to sublimate the water. The method was claimed to better retain sample freshness.

2. Pathological detection

Neoplasms are the most common type of pathological changes being studied by THz *in vitro*. A neoplasm refers to a type of abnormal and excessive growth of tissue, which will normally but not necessarily develop into a tumor. Early diagnosis of neoplasms has a great impact on human health. THz is one of the technologies with the potential to provide good contrast between neoplasms and normal tissues. Given that noninvasive measurement is the most ideal modality for cancer detection, skin is potentially the most suitable target as it is relatively easy to access and THz waves can penetrate into certain depths of skin. Therefore, for *in vitro* studies, skin tissues are one of the earliest investigated samples. Skin cancers can be categorized into two main types, melanoma and nonmelanoma cancers. Most of the investigations have been on nonmelanoma cancers, including basal cell carcinomas (BCCs) and squamous cell carcinomas (SCCs). Early work by Woodward *et al.* demonstrated the image contrast in the reflected THz amplitude at a fixed time position between BCCs and healthy tissues.[287] The higher reflectivity from the BCC area was confirmed by Wallace *et al.* in the study of 19 fresh BCC lesions.[288] Further analysis of the spectral properties of BCCs and normal areas attributes the difference to the increased water content in the diseased tissues.[289] Figure 17 shows that both the refractive index and absorption coefficient of BCC are higher than that of the normal skin.[138] The difference can be clearly reflected by the fitted double-Debye parameters. Another technology using a CW THz imaging system showed that both BCCs and SCCs can be distinguished from healthy tissues by their cross-polarization reflections.[290] Oral cancer is another kind of neoplasm that could potentially be measured noninvasively, although with the current state of THz systems such an application has not yet been tested *in vivo*. Sim *et al.* measured frozen fresh oral cancer

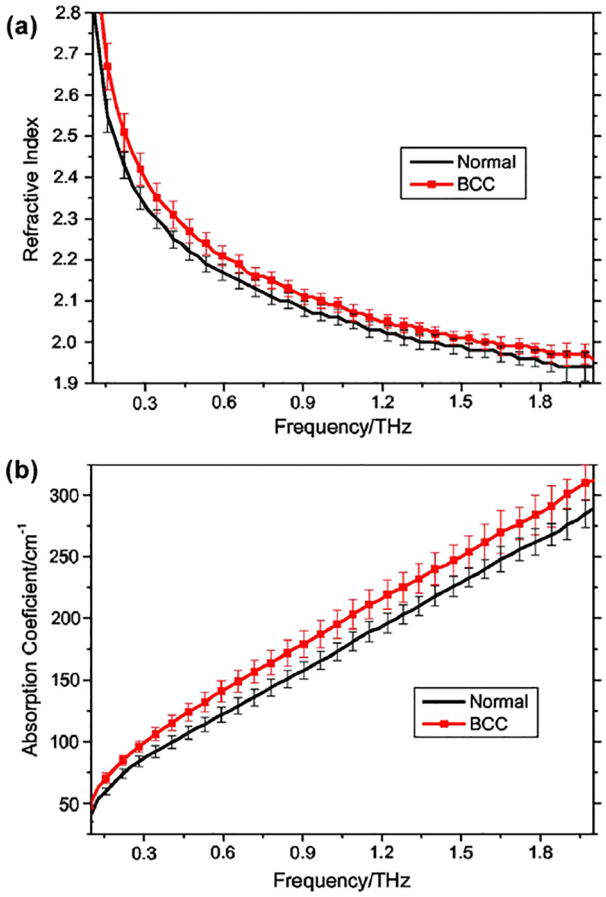

FIG. 17. (a) The refractive index and (b) absorption coefficient of normal skin tissue and basal cell carcinomas. The error bars represent 95% confidence limits. Reproduced with permission from Pickwell *et al.*, J. Biomed. Opt. **10**, 064021 (2005).[138] Copyright 2005 SPIE.

specimens and compared the results to measurements taken at room temperature; there was a larger contrast between oral cancer and normal mucosa at frozen temperatures.[283] Further, a lower refractive index and absorption coefficient was observed for the cancerous tissues, which is different from the previous skin studies. Sun *et al.* utilized a multiple-layer structure to enhance the imaging sensitivity. Dehydrated oral cancer tissues were deposited on a quartz window and then covered by water. Such a quartz–sample–water sandwich structure gave a significant contrast between healthy and cancerous areas, while the THz transmission images could not clearly differentiate the two areas due to the small thickness of dehydrated sample slice.[78]

Neoplasms inside the human body are very difficult to measure *in vivo* even with state-of-the-art THz technology, mainly due to the difficulty in aligning beams to an irregular surface, the slow imaging speed and the strong attenuation of THz light by water. Studies of excised specimens avoid many of the technical issues associated with *in vivo* measurements. As can be seen from the following examples, the studies of either fresh or dehydrated samples show the essential THz contrast between normal and diseased areas. Breast cancer was one of the first types of cancer studied to investigate the ability of THz measurements to observe contrast between healthy and cancerous tissues. The study by Fitzgerald *et al.* shows a high correlation between the THz images and the photomicrograph for the tumor area of 22 freshly excised breast tissue specimens.[156] Using transmission measurements of the sample, a larger refractive index and absorption compared to healthy fibrous tissue was found,[291] in agreement with the characteristics observed for skin cancers. The contrast can also be provided by other measured parameters. Figures 18(a) and 18(b) show the THz reflected images plotting E_{max} and E_{max}/E_{min}, respectively, compared to the histology image in Fig. 18(c). The pink region in the histology image indicates the cancerous tissue, and this can be seen to correspond to the yellow region in the E_{max}/E_{min} image, indicating

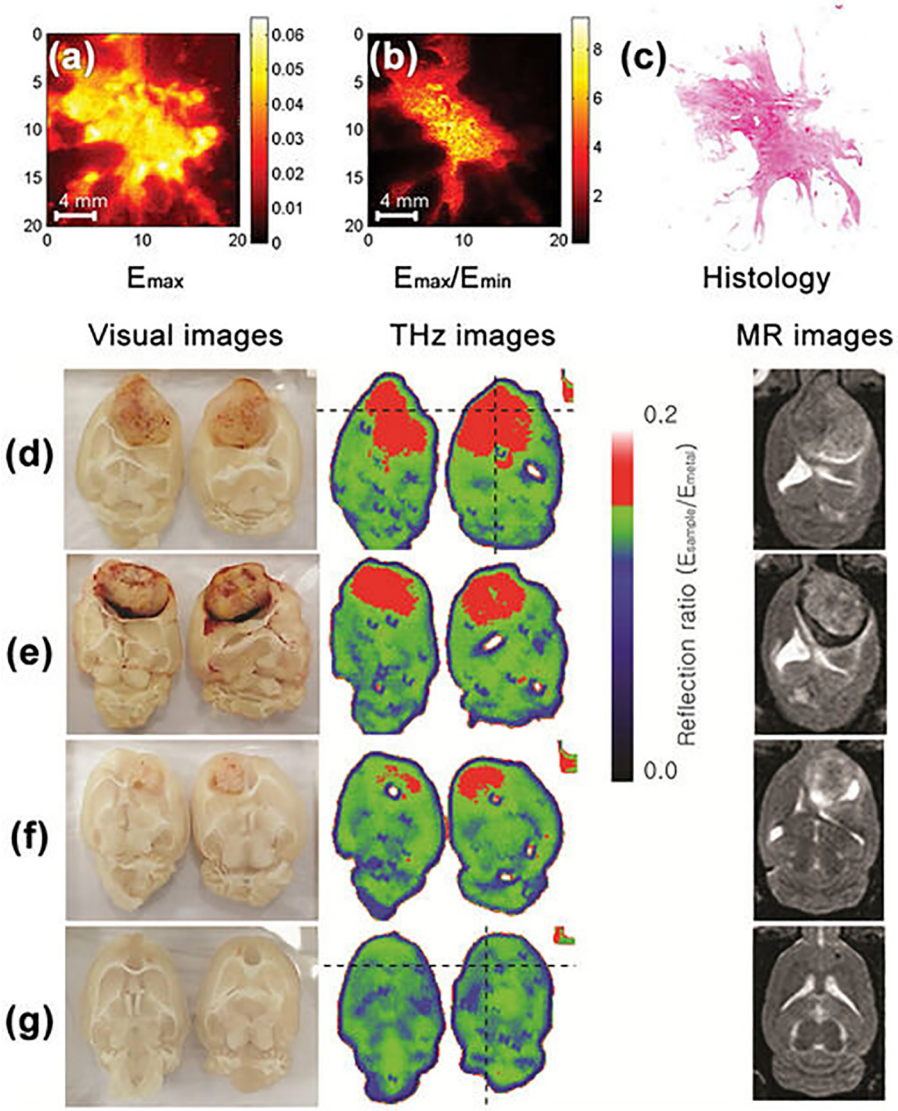

FIG. 18. THz reflected images of breast tissue plotted by (a) E_{max}, (b) E_{max}/E_{min}, respectively, compared to (c) the hisotology image. (a)–(c) are reproduced with permission from Ashworth *et al.*, Opt. Express **17**, 12444–12454 (2009).[291] Copyright 2009 Optical Society of America. (d)–(g) Visual, THz, and magnetic resonance (MR) images of brain tissues (d)–(f) with and (g) without brain tumor. The THz image size is $4 \times 3\,cm^2$. (d)–(g) are reproduced with permission from Oh *et al.*, Biomed. Opt. Express **5**, 2837 (2014).[158] Copyright 2014 Optical Society of America.

that this parameter is capable of differentiating the breast tumor from the surrounding adipose tissue. In fact, the broadband detection enables the extraction of a large number of parameters, which can be investigated in order to differentiate between different tissue types. Automatic classifications of cancerous and healthy breast tissues can be done by adopting machine learning methods, such as support vector machine (SVM), to account for multiple features.[102,292] A similar data analysis has been applied for many other diseases. We will introduce numerous advanced data analysis methods independently in Sec. VI. Brain tumors have recently attracted more attention. Oh *et al.* measured both freshly excised and paraffin-embedded rat brain tissue.[158] A higher hydration level was found in tumor areas leading to a higher refractive index and absorption, providing a good contrast to the normal areas in the THz images. Figures 18(d)–18(g) compare the visual, THz and magnetic resonance (MR) images of fresh brain tissues, where the samples in (d)–(f) contain brain tumor and (g) is a normal brain tissue. This contrast between healthy and cancerous regions is shown in the THz images in Fig. 18 by the red regions and is consistent with the bright regions in the MR images caused by a higher water concentration. The THz images are given by the peak-to-peak reflected amplitudes normalized to the metal reflection. This further confirms that water could be the primary source of contrast for cancer detection. When the water was removed, the cell density still affected the THz response, but it was found that it contributes less to the contrast. The observations are in line with the spectral analysis of fresh normal and tumor rat brain tissues by Yamaguchi *et al.*[293] They have also considered the higher cell density and water content in the tumor as the reasons for their larger refractive index and absorption. The linear discriminant analysis was used to classify the data with an accuracy up to 98%. Ji *et al.* studied both fresh mouse brain samples and human specimens of different grades.[154] They showed clear contrast at 0.5 THz among glioma, normal white, and gray matter. The higher reflection in the gray matter compared to the white matter could be the result of the intrinsic differences in water and lipid concentrations. Glioma of different grades were also investigated by Gavdush *et al.*[122] Fresh specimens (26 in total) from patients were embedded in gelatin and measured, with a higher refractive index in the tumor region for grade I to IV. The increased water content caused by the abnormal vascularity and edema is considered as the origin of contrast. A recent topical review on THz diagnosis of human brain tumor is given in Ref. 294.

Neoplasms in many other locations, such as the stomach,[295,296] liver,[106,297] colon,[60,298,299] and cervix,[300] have also been broadly explored. These studies provide the essential knowledge of the THz response between different cancerous and healthy tissues. Apart from neoplasms, other pathological tissue changes have also been studied. Liver cirrhosis was studied by Sy *et al.* by measuring both fresh and fixed samples.[155] The results show a considerably large contrast contribution of 50%–66% from the biological background, even higher than that by water. Alzheimer's disease was studied, and it was found that the disease will increase the contrast between the gray matter and white matter to 4.2%, compared to 2% in the normal brain tissues.[301] The demyelination of white matter in Alzheimer's tissues could be the potential cause of the difference. Cornea hydration is related to diseases including keratoconus and Fuchs' dystrophy.[302] *In vitro* hydration sensing of porcine corneas has been done by Bennett *et al.*[303] They used EMT on different hydration levels, and it shows a good fit, with a linear relationship between the THz reflectivity and the water concentration being observed. Most of these studies conclude that water is the major source of contrast, and typically a higher water content is observed in the cancerous/diseased area. However, tissues of different types, locations and grades, can have different biological compositions and structural changes that may contribute to the specific THz dielectric properties, and in some cases, these factors could dominate the contrast. Investigating samples in both fresh and dehydrated states in the same experiment makes it possible to better explore the origin of contrast. Although to some extent consistency in the observed contrast is determined by the THz systems used, sample preparation techniques, measurement protocols, and data processing, numerous variables among these processes could alter the experimental results, introducing difficulties in comparisons. Also, experimental errors could be difficult to comprehensively estimate, such as the systematic error, nonideal contact, or scattering from the rough surface. Currently, it is difficult to establish a gold standard for THz *in vitro* studies of tissues, as this field is still under rapid development. However, attention should be given to controlling these variables and developing a robust protocol in future studies to improve data credibility and comparability.

3. Other applications

In vitro measurements are also important in many other studies. For example, the fundamental investigation of the EMT adaptability for biological samples is based on the measurement of both fresh and dehydrated samples,[149] as we have also mentioned in Sec. III B 2. *In vitro* studies can also be applied to explore agents to enhance the penetration depth or the imaging contrast. Oh *et al.* demonstrated that glycerol can effectively enhance the penetration depth of THz waves into fresh tissues.[304] Figure 19(a) shows their experimental setup. A metal plate was placed above the mice skin. Figure 19(b) shows the reflected THz pulse of the skin with/without glycerol. Applying the glycerol significantly enlarged the second pulse reflected from the skin–metal interface and reduced the separation between the two reflections. The results correspond to a decrease in both the refractive index and absorption coefficient. They have also demonstrated the potential application of detecting tumors underneath a thick skin. In Fig. 19(c), Matrigel drops (normally a gel form except at a temperature of 4 °C) on the backside of the sample are pictured and can be compared to the location of the contrast in the THz images. Figure 19(d) shows the peak-to-peak value of the entire waveform measured from the sample, while Fig. 19(e) shows the peak to peak after the initial reflection has been removed so only the reflection from the metal plate remains. In Fig. 19(e), the shape of artificial tumor made by the Matrigel drops can be observed as the dark region in the image when glycerol has been applied to the sample, but only very weak contrast was found in the sample without applying the glycerol. Another work by the authors showed that gold nanoparticles could also be a potential contrast-enhancing agent.[305] Cancer cells with/without adding gold nanoparticles illuminated by IR radiation showed significant/no changes on the reflection. However, it should be noted that THz does not interact with the nanoparticles directly due to the much larger wavelength compared to the particle dimensions. The changes are purely temperature-based by coupling the IR radiation with the surface plasmon resonance of the nanoparticles to heat up the cells. THz

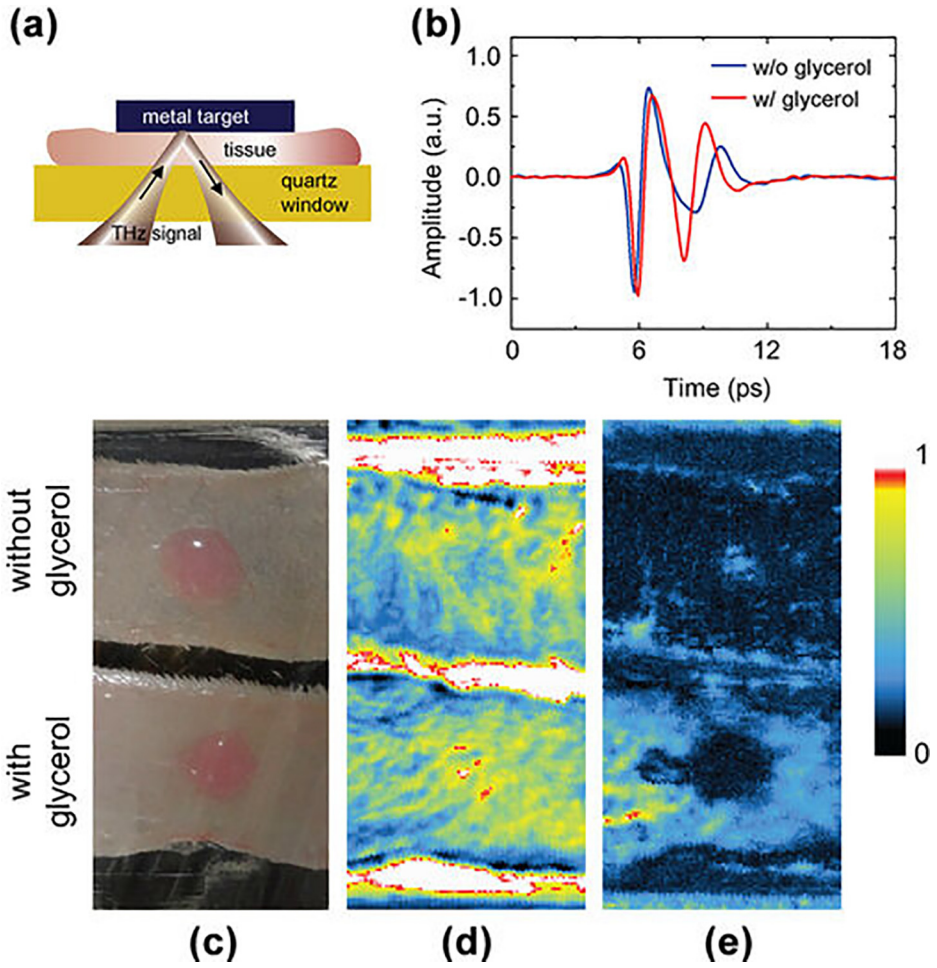

FIG. 19. (a) Schematic of the experimental setup. (b) Reflected THz pulses without and with applying glycerol. (c) Visible image and THz images plotted using (d) the peak-to-peak values of the whole waveform and (e) the peak-to-peak values of the waveform after cut off the main pulse. Reproduce with permission from Oh *et al.*, Opt. Express **21**, 21299 (2013).[304] Copyright 2013 Optical Society of America.

imaging was utilized as a thermometer to monitor the changes in the properties of water induced by the temperature. Gold nanoparticles have also been used to assist laser tissue soldering, which is an emerging concept in surgical medicine. Utilizing the time-resolution of THz-TDS and the high sensitivity to water, Dong *et al.* demonstrated 3D reconstruction of photothermal damaged porcine skin induced by tissue soldering.[306] Another application of THz *in vitro* studies is drug delivery, which can also be monitored by THz imaging based on the high sensitivity to water and drug concentrations. Kim *et al.* applied dimethyl sulfoxide (DMSO) containing ketoprofen onto a mouse skin sample and demonstrated that THz imaging can reveal the spatial distribution and penetration depth of the drug solution.[307] As the drug was being absorbed, the refractive index of the sample reduced, giving rise to an index matching with the quartz window; thus, the reflected signal decreased with the time. Their further study demonstrated that THz imaging can also distinguish different concentrations of the drug solutions.[308] Wang *et al.* used *in vitro* porcine skin to evaluate the transdermal drug delivery efficiency by different application methods, including topical application and via microneedles to enhance the permeability of skin.[20] The results show that THz imaging can be used to evaluate different methods for transdermal drug delivery.

D. *In vivo* applications

The nonionizing nature of THz radiation means that it has great potential for safely imaging biological tissues *in vivo*. Furthermore, it enables a noninvasive detection without additionally extracting the region of interest prior to measuring it, e.g., for a biopsy examination. This also removes the need to use techniques to preserve the sample which could alter the properties of the region. However, most THz *in vivo* measurements have been limited to areas that can be accessed noninvasively, typically skin, and in some studies the cornea has been measured as well. This is because of the high absorption of THz light by tissue such that THz light cannot detectably penetrate deeper than a few hundreds of micrometers into biological tissues. More importantly, as *in vivo* measurements can only be performed in a reflection configuration, a flat surface in most cases is required to align and receive the THz light. This is typically achieved by contacting a well-aligned imaging window on the measured area. Even in a surgery in which the area inside the body can be exposed to THz light, the need of a window is not an ideal modality for clinical applications, as we will later introduce in the examples.[154,309] Although some concepts, such as THz endoscope, have been proposed, they are still only single-pixel detection and require precise alignment, which is far from

practical. For the available areas such as skin, there are challenges which arise when a living subject is measured such as the movement of the subject during the measurement, and an increased exposure of the sample to other environmental factors which could alter the properties of the region.

As outlined above, many studies use an imaging window to aid the alignment of the sample and to flatten the soft tissue making it easier to image without the need to account for the curvature of the biosample surface. In some studies, a processing technique is used to remove the influence of the lower reflection from the imaging window.[310] For skin which is composed of multiple layers, a deconvolution is usually performed on the measured response of the sample with an air reference. The result is described as an impulse function and can be used to identify the presence of hidden layers in the sample and to quantify changes in the water content of the sample. Other more advanced processing techniques which are being researched to enhance the information that can be extracted from THz measurements are explained in detail in Sec. VI.

This section will summarize some of the key developments in the field of *in vivo* assessment with THz spectroscopy or imaging, highlighting different biological changes which have been shown to induce a contrast at THz frequencies. We will also introduce some of the work which has been done to address other variables which can influence the THz response of biological tissues and what experimental approaches have been employed to reduce the effects of these.

1. Skin assessment

The first investigation in which human skin was measured *in vivo* in laboratory conditions was performed by Cole *et al.* in 2001.[311] They demonstrated the ability of THz pulsed imaging to identify the thickness of the stratum corneum (SC) in regions, such as the palm where the SC is thick enough such that the reflection at the SC–epidermis interface can be distinguished from that from the quartz–SC interface. By performing a raster scan to acquire an image, it was possible to present results similar to an ultrasound B-scan in which the different layers in the skin can be identified as a function of depth. However, due to the high water content, the accessible depth is wavelength-comparable; thus, it mainly provides superficial skin information. They also found that they could observe changes in the hydration of the skin with THz measurements, for example, following the application of a wet towel to the skin surface. It was also observed that the THz response of skin changed throughout the measurement while the skin was in contact with the imaging window, when using a setup, such as the one shown in Fig. 20(a). This was attributed to the occlusive effect of the imaging window, as it prevents the natural process of water loss through the skin surface causing water to accumulate in the skin with increasing contact time. Figure 20(b) shows microscope images of skin increasing times into occlusion, and the smoothing of the skin throughout this process can be observed. Figures 20(c) and 20(d) show the effect of occlusion on the measured THz response of skin during 10 min of occlusion, (c) shows the processed waveforms increasing times into occlusion where they have been shifted horizontally for clarity, and (d) shows the amplitude of these waveforms as a function of time. Sun *et al.* demonstrated that this occlusion effect can be modeled using a biexponential function; this is demonstrated by the red line in Fig. 20(d).[108] A more complete summary of the work performed by Sun *et al.* will be presented in Sec. V D 4 along with approaches which can be used to remove the effects of occlusion from results obtained with contact THz measurements of the skin.

Pickwell *et al.* performed a series of *in vivo* measurements on 20 human volunteers to explore the repeatability of THz measurements of the skin and the efficacy of theoretical models at describing the interaction of THz radiation with living skin.[136] The palm and the dorsal and volar forearm were measured weekly for four weeks using a contact reflection geometry. The volar forearm was found to give the most repeatable results; this is thought to be because it is the region with the least exposure to environmental conditions, such as sunlight, and does not have as much hair as the dorsal forearm. The double Debye model introduced in Sec. III B 1 was used in combination with the finite difference time domain (FDTD) model proposed in Ref. 137 to simulate the THz response of skin. Two types of models were used for the skin structure; the volar and dorsal forearm were assumed to be single-layer structures as the SC is too thin in these regions to be resolved with THz wavelengths, while the palm was modeled as a two layer structure to account for the thicker SC. In all regions, there was good correlation between the measured and simulated impulse functions of the skin, confirming the efficacy of this model in describing *in vivo* THz–skin interactions. Any discrepancies between the measured and simulated results were attributed to the oversimplification of the structure of the skin used in the model. Zaystev *et al.* also performed *in vivo* THz measurements in a range of the locations across the body extracting the refractive index and absorption coefficient.[313] They were able to observe variation in the THz optical properties of the skin across the body, which could be attributed to changes in the SC thickness or hydration.

Echchgadda *et al.* measured the regions on the dorsal forearm, volar forearm, and the palm of 35 human subjects and extracted the refractive index and absorption coefficients of each of the regions.[314] They also measured the transepidermal water loss (TEWL) and the extent of melanin pigmentation—two common techniques for skin assessment. TEWL measurements give an indication of the skin barrier function and are, therefore, also linked to the hydration state of the skin while the melanin pigmentation describes the skin tone. The study found no significant differences in the absorption coefficients of the three regions measured. However, it was found that the palm had significantly lower refractive index than the two forearm regions and that these changes are most significant at lower frequencies. The study also found moderate correlation between the slope of the absorption coefficient and the TEWL of the skin suggesting that THz measurements of the skin are effective for hydration assessment.

Up until this point, the summary of the use of THz radiation for *in vivo* skin assessment has been focused on techniques with resolution limited by the wavelength. However, near-field imaging techniques are also being developed, as introduced in Sec. II B 3. Tseng *et al.* applied such an approach to *in vivo* imaging.[92] This study took the unusual approach of utilizing a transmission geometry to perform the measurements; this was possible as the region being imaged was the ear of a mouse, which was found to have a thickness of around 0.2 mm, making it thin enough for the THz radiation to pass through the tissue and be detected with sufficient signal to noise. Using this approach, they were able to perform measurements with sub wavelength resolution in which it was possible to observe blood vessels in the ear. A dip could be seen in the transmission through the tissue in the location of the blood vessel due to the higher water content in the blood compared to the surrounding tissue, and examples of these results can be seen in Fig. 21.

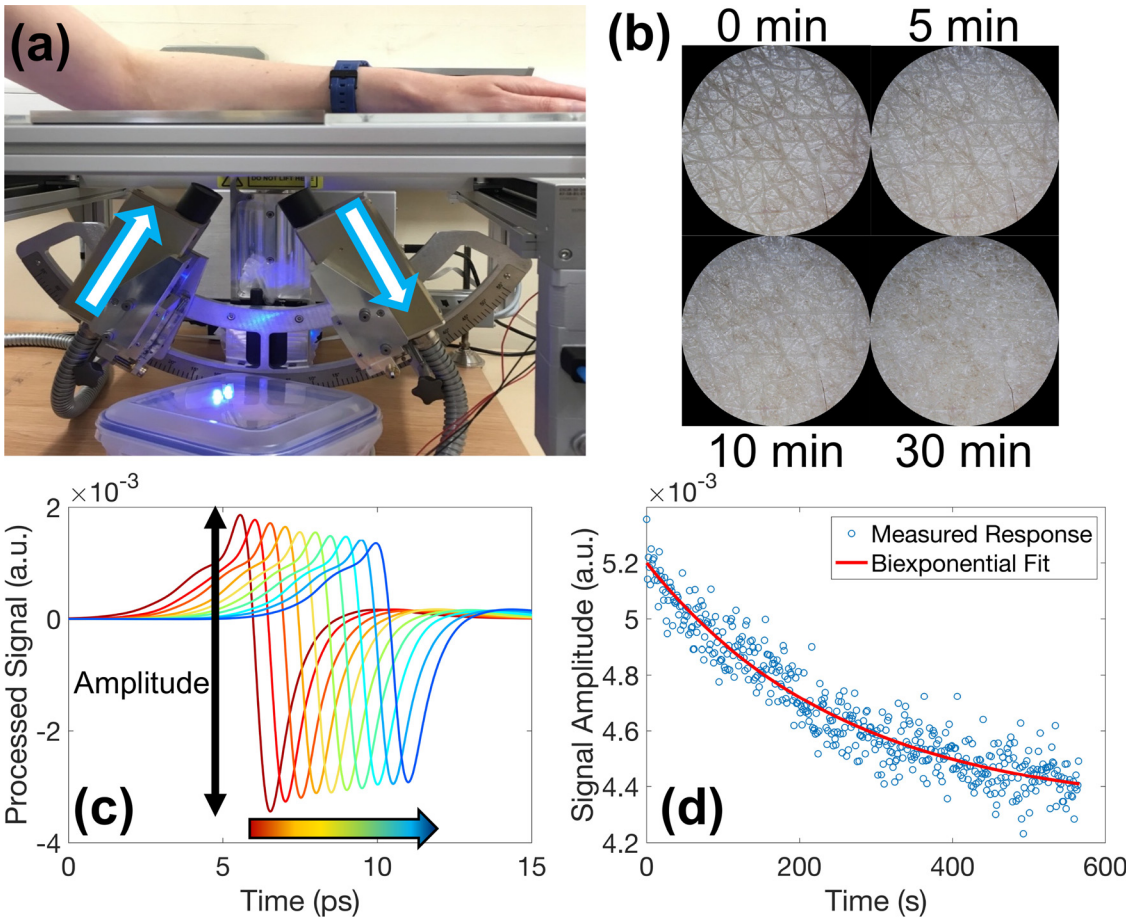

FIG. 20. (a) An example of an experimental setup used to measure the skin on the volar forearm in a reflection geometry. Reproduce with permission from Lindley-Hatcher *et al.*, J. Phys. **3**, 014001 (2020).[312] Copyright 2020 Authors, licensed under a Creative Commons Attribution (CC BY) license. (b) Microscope images of the skin after increasing occlusion times. Reproduced with permission from Chen *et al.*, Adv. Photonics Res. **2**, 2000024 (2021).[84] Copyright 2021 Authors, licensed under a Creative Commons Attribution (CC BY) license. (c) Processed THz signals obtained at 1-min intervals when measuring skin for 10 min under occlusion, the waveforms have been horizontally shifted for clarity. (d) The peak to peak amplitude of the processed waveform plotted against occlusion time and fitted with a biexponential function shown in red.

They were also able to apply FDTD simulations of blood vessels to investigate the impact of changing the refractive index and absorption coefficient of the blood and surrounding tissue on the quality of the fit. They also assess the suitability of the technique for performing longer term monitoring of blood vessels by measuring the effect of injecting the mouse with insulin. Changes in the properties of the blood vessel in the mouse that has been injected with insulin can be seen compared to those of the control mouse which received no such treatment. This technique shows promise for imaging sub-wavelength features of the skin; however, for most human measurements, a transmission geometry will not be feasible so the technique should be developed into an approach, which can be used to image thicker regions through which THz radiation cannot penetrate.

2. Quantifying hydration changes in the skin

In addition to measuring the refractive index and absorption coefficient of the skin at THz frequencies or changes in the THz pulse reflected from the skin surface, it is possible to use some of the models introduced in Sec. III B 2 to extract further information about the skin, such as the percentage water content or SC thickness. Other studies deliberately change the hydration properties of the skin to observe the sensitivity of THz measurements to such changes. In this section, we will summarize some of the key developments in this area; for the full details of these models, we refer the reader to a review of the models describing the interaction of THz radiation with the skin.[9,148]

Sun *et al.* were able to extract the diffusivity of occluded skin.[152] They modeled the water distribution in the skin using a swelling model for the SC and proposed three different functions to describe the diffusivity. These models were used to produce a hydration profile for the skin which was entered into the stratified media model first proposed by Bennett *et al.*[70] By fitting to the measured results with these models, the hydration profile and diffusivity in the skin could be extracted. The measurements were performed on five healthy subjects, and the skin was measured throughout 20 min of occlusion by the imaging window. The study revealed that the function in which

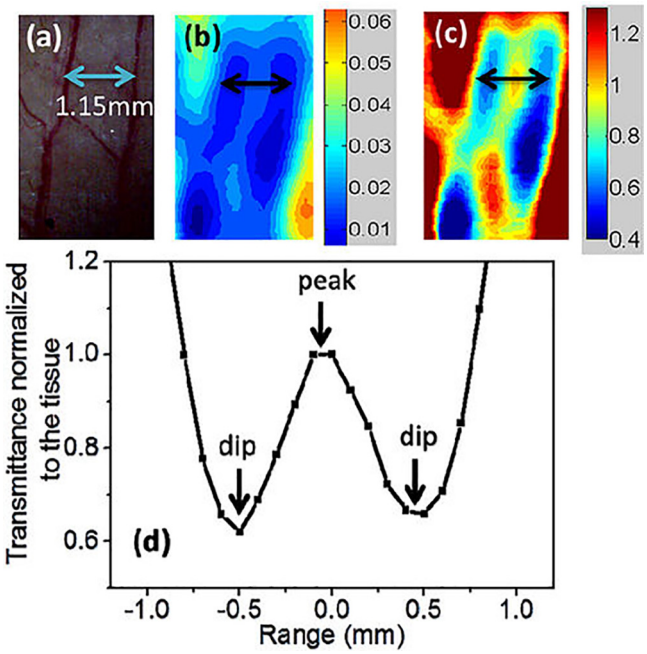

FIG. 21. *In vivo* measurements of the capillaries in mouse ears: (a) optical images of the regions, (b) THz transmittance images, (c) THz images normalized to the peak transmittance between the vessels, and (d) normalized transmittance cross section along the arrow. Reproduced with permission from Tseng *et al.*, Opt. Express **23**, 25058–25071 (2015).[92] Copyright 2015 Optical Society of America.

diffusivity was expressed as proportional to the water gradient across the SC gave the best fitting results, it was then possible to infer that it is this hydration gradient which is driving the movement of water through the skin during the occlusion. The convection velocity of water as a function of occlusion time was also extracted, and this confirmed that the rate of water movement decreased with occlusion time as the gradient across the SC decreases as the upper layers of the SC become saturated with water. A summary of these key results can be seen in Fig. 22(a), which plots the hydration profile in the skin as a function of occlusion time on the horizontal axis, and the SC thickness is plotted on the vertical axis so that the swelling of the SC as the water content increases can be seen. In this example, the high absorption of water shows a unique feature of the THz range. Although the detectable depth of the hydration profile is limited to mainly the stratum corneum, it provides high sensitivity measurements and can determine the sub-wavelength water-content variation.

Wang *et al.* performed a study taking THz point and line scans to quantitatively assess the efficacy of different burn treatments at increasing the hydration of the skin.[151] They measured the volar forearms of ten human subjects and used a SC–epidermis bilayer model of the skin alongside the LLL EMT to extract the changes in the SC hydration and thickness in response to the treatments. The point scans compare the effects of silicone gel sheets (SGSs) (an occlusive layer which is stuck to the skin for the duration of the treatment) to a silicone gel sample which is topically applied. They found that the effects of the silicone gel were minimal, in contrast the amplitude of the time-domain signal was significantly reduced following the application of the SGS, and the magnitude of this reduction increased the longer the sheet was applied. Using the EMT, they were able to find that the water content of the epidermis did not significantly increase following the application of the sheet, however the hydration of the SC was found to increase from 24% to 58% after 4 h SGS application, the thickness of the SC was also found to have been significantly increased. They also observed that skin that had been treated with the SGS had a less significant response to the occlusive effect of the imaging window than untreated skin, as the treated skin was already saturated with water. Further, a line scan was also acquired of a region of the forearm where a thin strip (5 mm) of SGS had been applied in the direction perpendicular to the line scan so that treated and untreated skin could be measured. They measured the skin before applying the SGS and up to 2 h after removal where the SGS had been applied for 10 min, 4 h, and 12 h. An example of these results is shown in Fig. 22(b), where the blue regions indicate skin with increased hydration and each row in the figure shows the line scan of the region with increasing time after the removal of the SGS. For comparison they also measured the response of the skin to the application of a wet bandage (WB). They found that the longer the SGS is applied the longer it takes the hydration levels of the skin to recover back to their initial state. They also found that the wet bandage increased the hydration the most significantly however these changes did not last and could only be seen up to 5 min after the removal of the bandage. It was observed that there were no lateral effects of the SGS sheeting on the hydration levels of the surrounding tissues, while the wet bandage increased the hydration of the tissues surrounding it up to double its own width. This study demonstrates the potential of THz imaging for evaluating the efficacy of different hydration techniques for burn treatments and providing advice as to the correct application durations for occlusive bandages.

The study performed by Lindley-Hatcher *et al.* involved obtaining point scan THz measurements from 20 subjects before and after the application of three different types of skin moisturizers.[312] They measured four regions of the volar forearm, one which remained untreated as a control and the other three were treated with an oil, water and water in oil-based moisturizer, respectively. The regions were all measured before the treatment and again 20 min after the application of the sample. The regions were all also measured using the commercial gold standard for skin hydration assessment: the corneometer. The study found that the THz measurements were able to distinguish between the different skin responses to the different sample types and moderate correlation was found between the THz amplitude of untreated skin and the measured corneometer response. The corneometer clearly indicated changes in the hydration state of skin following the application of the samples; however, it appeared to be less able to distinguish between the different effects of the samples, for example, the water-based and water-in-oil samples appeared to have the same effect on the response of skin measured with the corneometer. This study suggests that THz sensing could be a useful tool for assessing changes induced in the skin by different moisturizer samples and even help to identify which moisturizers would be most effective for certain skin types.

In addition to using the standard reflection geometry in which a single polarization state is used to take THz measurements of the skin,

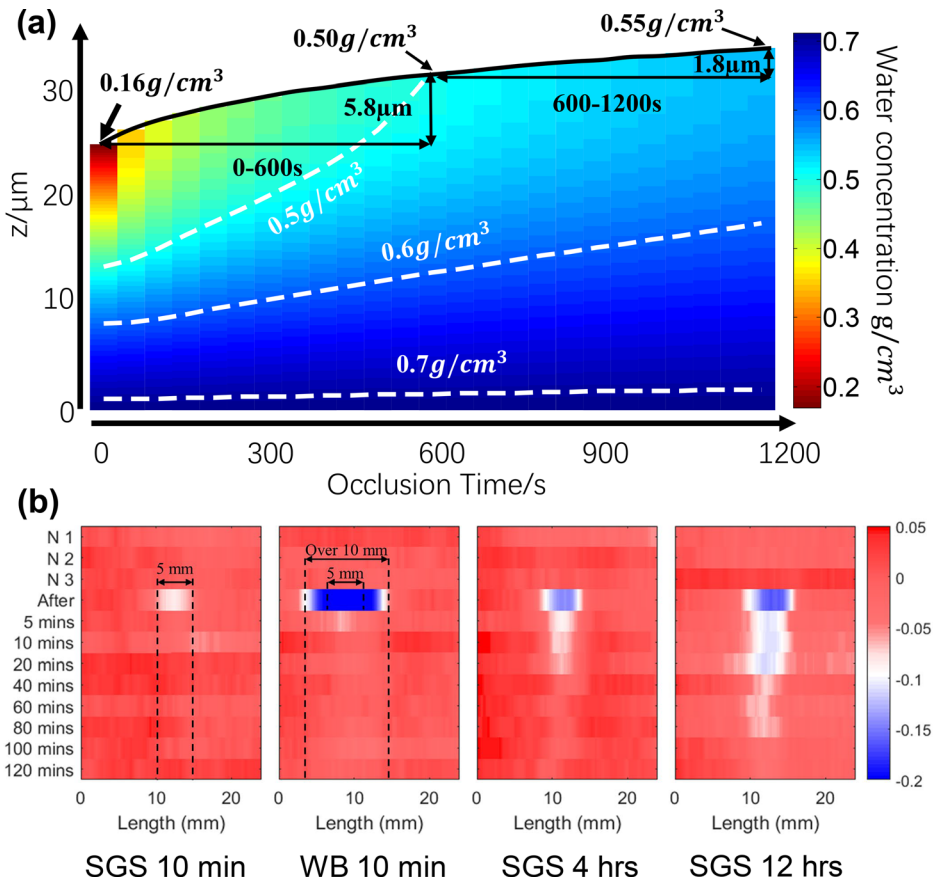

FIG. 22. (a) A colormap of the dynamic changes in water concentration in the surface of the skin as a function of skin depth throughout occlusion. Reproduced with permission from Sun *et al.*, J. Biophotonics **12**, e201800145 (2019).[152] Copyright 2018 Wiley-VCH Verlag GmbH & Co. KGaA, Weinheim. (b) THz line scan images increasing time after 10 min silicone gel sheets, 10 min wet bandage (WB), 4 h silicone gel sheets, and 12 h silicone gel sheets application (left to right). Reproduced with permission from Wang *et al.*, Biomed. Opt. Express **10**, 3584–3590 (2019).[151] Copyright 2019 Optical Society of America.

new geometries and approaches to *in vivo* THz skin assessment are also being developed. For example, Chen *et al.* developed an ellipsometry system capable of measuring the skin using *s* and *p* polarizations at two incident angles.[84] Using the experimental setup introduced in Sec. II B 2 and shown in Fig. 4, they were able to obtain four complementary spectral ratios describing the skin; this enhanced the ability to resolve the complex model of skin. They used an anisotropic model for the SC to account for the alternating layers of lipids and corneocytes that makeup the SC, as shown in Fig. 23(a). Using the data obtained with this experimental setup, they were able to verify the birefringent nature of the SC. By measuring the skin throughout 31 min of occlusion, it could be observed that both the ordinary and extraordinary components of the refractive index and absorption coefficient increased with occlusion time as water built up in the surface of the skin while the properties of the epidermis remained relatively stable throughout occlusion, as shown in Fig. 23(b). They also extracted the dispersion and birefringence of the SC as a function of occlusion time and linked these variables to the hydration and structure of the skin respectively. They conclude that occlusion increases the amount of water in SC and decreases the inhomogeneity. This experimental configuration and model for the skin make it possible to learn about changes in the skin on a cellular level through noninvasive measurements; this opens the door to more opportunities to use THz measurements to learn about changes in the skin.

3. Monitoring burns and scars

There has also been significant interest in the ability of THz imaging to objectively assess and classify the severity of burns. The links between burn severity and the dehydration of the tissue and the ability of pulsed THz techniques to identify different layers in the skin suggest that THz imaging could be very useful in this field. Additionally, THz techniques have high sensitivity to water content of tissues while materials, such as bandages and gauze, are nearly transparent, meaning that burns could be viewed through a bandage. This section summarizes some of the spectroscopic and imaging techniques which have been tested as potential approaches for burn assessment.

Tewari *et al.* measured the THz reflectivity of the skin of a rat up to 7 h after the tissue was burned.[315] A 35 × 35 mm^2 image was obtained, which took less than 8 min to acquire, with the region maintaining contact with an imaging window throughout the measurement. They calculated the water content of the skin using the stratified media model of the skin with an EMT. These measurements were performed every 15 min for the first hour and then every 30 min subsequently for up to 7 h following the injury. Figures 24(a)–24(d) show THz images of the change in water content of the skin before the burn and increasing time points after a thermal contact injury with a cross shape, where the lighter regions indicate regions of higher water content. The study revealed an initial increase in the water content in the

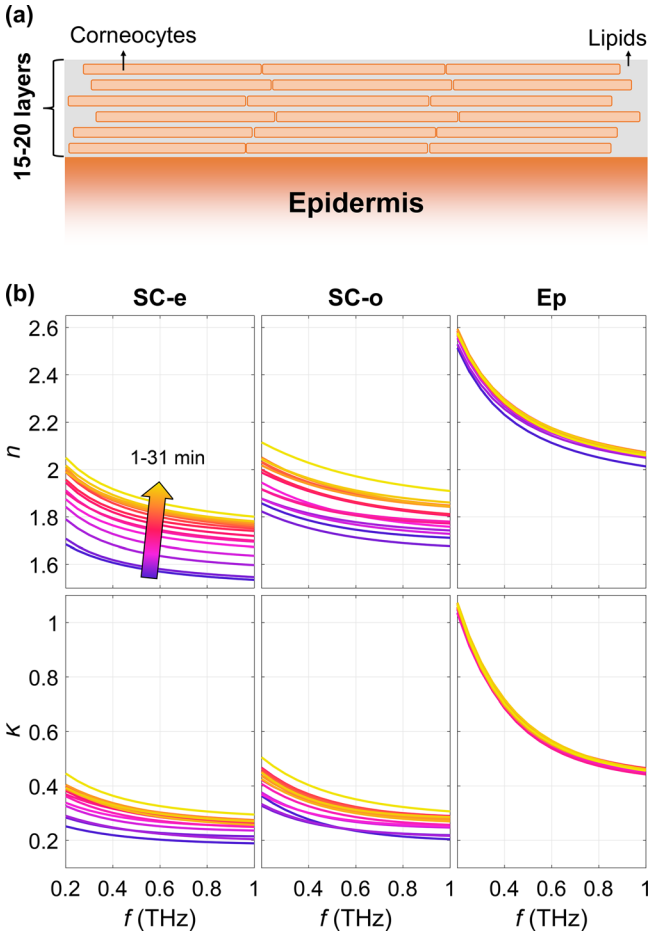

FIG. 23. (a) The model of the skin used, showing the alternating lipid and corneocyte layers; and (b) the changes in the refractive index and extinction coefficient of the ordinary and extraordinary components of the stratum corneum and of the epidermis throughout 31 min of occlusion. Reproduced with permission from Chen *et al.*, Adv. Photonics Res. **2**, 2000024 (2021).[84] Copyright 2021 Authors, licensed under a Creative Commons Attribution (CC BY) license.

region local to the burn which is associated with the inflammatory response of the skin. Following this, a region of increased water content was observed directly where the skin was injured, surrounded by a region of decreased water content. This suggests that THz imaging has the potential to provide insight into the behavior of skin following injuries, such as burns, and provide guidance on the correct methods and timescales to use when providing treatment.

Following this study, the group identified water as a source of contrast in these images and confirmed that THz reflection measurements are sensitive to the movement of water in the skin following a thermal contact injury. This was done by comparing THz reflectivity images of full and partial thickness burns on rats to T2 weighted MRI measurements of the same regions. In this study, the spatial-temporal contrast displayed in the image series is more important than the reflectivity of individual pixels. This contrast provides sufficient information for burn depth/severity characterization. These studies find that there is good correlation between the two imaging techniques for both types of burn.[318,319]

There has also been work by Tewari *et al.* to explore the combining of THz images with optical images of the burn regions.[317] This is done using two markers which are visible at THz and optical frequencies, making it possible to calibrate the two images. Such an approach makes it possible to more accurately link the features in the THz image to the location on the skin relative to the burn. In the study, nine rats received either a full or partial thickness burn and the burnt area was imaged continuously for 435 min following the injury, with the region remaining in contact with an imaging window for the duration of this time. Figure 24(f) shows the images of the full and partial thickness burns increasing times after the injury at THz frequencies alone and an optical image combined with the THz results. In the THz images, the reflectivity is plotted with the colormap where the light regions show regions of increased reflectivity indicating increased tissue water content compared to the surrounding darker regions. Moreover, the concentric-like spatial distribution of water relative to the injured region correlates with the known concentrically arranged damage zones in burn injuries. The results revealed the dynamic changes in the THz response of the tissue around the burnt region, which could be an indication of the movement of water in response to the injury. It is possible that the prolonged contact between the skin and imaging window also had an impact on the water distribution throughout the study; this effect is explained in more detail in Sec. V D 4.

Arbab *et al.* explored an approach to the application of THz spectroscopy for the classification of burns.[140] Unlike the approach explained above which used an incoherent imaging technique, this study used THz-TDS to measure the spectral response of a single region of a burn. They used nine rats in their study, five of which were inflicted with a second degree burn and four with a third degree burn; regions left uninjured are also marked on each rat to act as a control region. Both regions are measured on each rat immediately following the burn and 72 h following the burn. The results were compared to histology results obtained following the excision of the burnt area at the end of the study. They used an image processing technique to define a quantitative variable, the density of skin structures (DOS), to characterize the histology results. They also define a spectral variable Z, which is used to classify the burn from the measured THz reflectivity spectrum,

$$Z = a \cdot R + b \cdot S, \tag{5}$$

where R is the average reflectivity across the measured frequency range and S is the spectral slope of the reflectivity. a and b are arbitrary constants optimized to maximize the specificity of Z. Using these parameters, they demonstrate the ability of THz spectroscopy to identify healthy and burnt skin. They also find good correlation between DOS and Z with a correlation coefficient value of -0.797 for the results obtained 72 h post-injury.

This group then expanded upon the study by performing measurements on porcine skin, as this is thought to be a better model for human skin.[320] Three pigs were measured and on each pig three regions were burnt for increasing durations to increase the severity and depth of the burn. The results of the THz measurements were compared to the current gold standard for burn depth assessment:

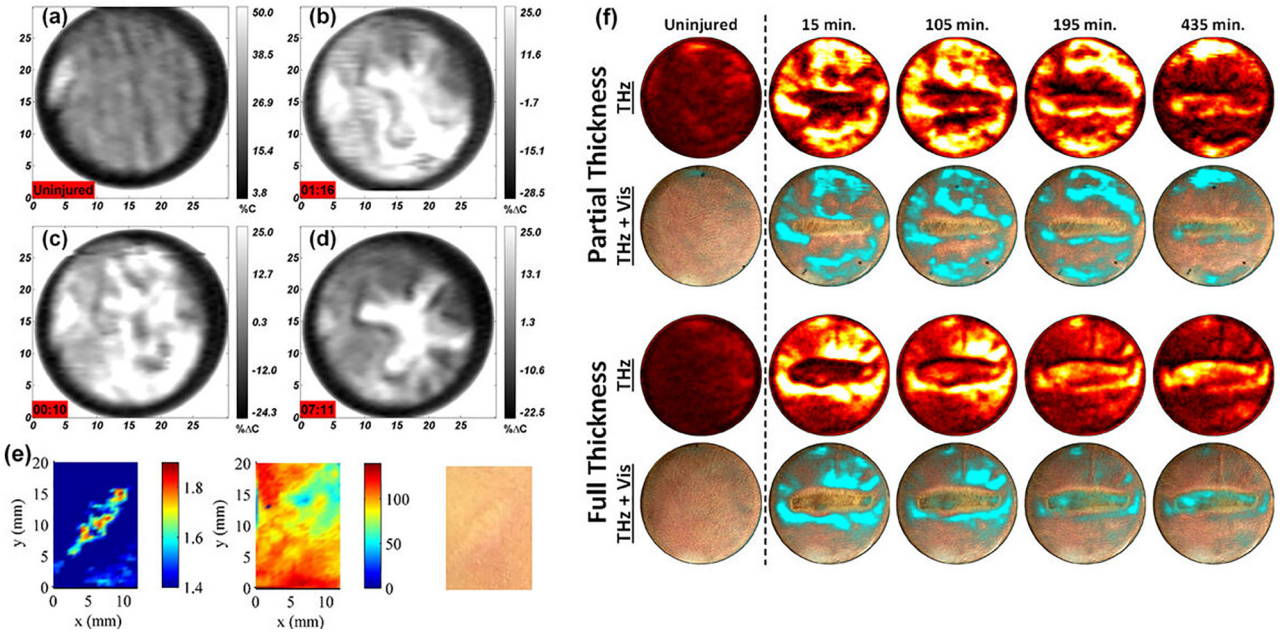

FIG. 24. (a)–(d) THz images of the water content of rat skin increasing time following a burn, reproduced with permission from Tewari *et al.*, J. Biomed. Opt. **17**, 040503 (2012).[315] Copyright 2012 SPIE. (e) THz images of the refractive index (left) and absorption coefficient (middle) at 1 THz of a scar six months following the injury, compared to the visible image (right) of the same region. Reproduced with permission from Fan *et al.*, J. Biphotonics **10**, 1143–1151 (2017).[316] Copyright 2017 Wiley-VCH Verlag GmbH & Co. KGaA, Weinheim. (f) Images of partial and full thickness burns of the THz reflectivity and the THz reflectivity combined with a visible image of the region increasing time after a burn. Reproduced with permission from Tewari *et al.*, Biomed. Opt. Express **10**, 322–337 (2019).[317] Copyright 2019 Optical Society of America.

vimentin immunohistochemistry (IHC). As before, they defined a spectral parameter Z to characterize the burns from the THz measurements,

$$Z = a \cdot SA + b \cdot SS, \tag{6}$$

where SA is the spectral area and SS is the spectral slope. They found that there was good correlation between the burn depth and the spectral parameter Z, suggesting that THz measurements could be an effective way to quickly assess the severity and depth of a burn. However, it should be recognized that the dermis layer, which is partially or fully damaged in the second- or third-degree of burn injuries respectively, has a thickness of 1–4 mm, where the THz waves becomes considerably weak to interact with. Therefore, the attenuation of water may fundamentally limit the sensitivity in evaluating burn severity. It is hoped that this work could be used to develop THz spectroscopy into a technique that can predict healing outcomes and identify which treatment option would be most effective.

Fan *et al.* found in their study that the ability of THz imaging to identify disruption in the skin is not limited to thermal injuries, such as burns but can also include scars caused by abrasion.[316] They measured four human scars, three of which were old scars which had finished the healing process while the last one was a recent scar which was measured at multiple time points so that the healing process could be observed. By producing THz images of the refractive index and absorption coefficient, they found contrast in both variables. They found that as the recent scar healed, the contrast in the absorption coefficient diminished while some contrast in the refractive index remained as shown in Fig. 24(e); this was attributed to the deposition of collagen leading to structural changes in the tissue causing the scar. They were also able to observe the scar at two weeks post injury through a plaster: they found they could still identify the contrast in the measured impulse function of the skin.

4. Parameters affecting the THz response of skin

The strong sensitivity of THz radiation to the water content of tissues can be a challenge as well as a strength of the technique as there are many variables which can influence skin hydration. It is important that these variables are carefully controlled in order to obtain repeatable results, which are meaningful and can be compared between different subjects.

As mentioned in Sec. V D 1, the occlusion of the skin by an imaging window prevents the natural loss of water from the surface of the skin resulting in an increase in the water content in the SC throughout a measurement. Sun *et al.* conducted a systematic review of other variables with the potential to contribute to the observed decrease in the amplitude throughout the measurement including the movement of the imaging window, thermal expansion of the quartz window, and the buildup of a perspiration layer. The study confirmed that the effect of these variables was negligible and identified the buildup of water in the SC as the dominant factor. A key challenge of acquiring an image of the skin is that the optics must be raster scanned across the whole region, meaning that there is a long time delay between the measurement of the first point and the last point. Figure 25(a) shows the variation in the THz image of the skin with increasing time into occlusion. Sun *et al.* proposed that the biexponential model could be used to

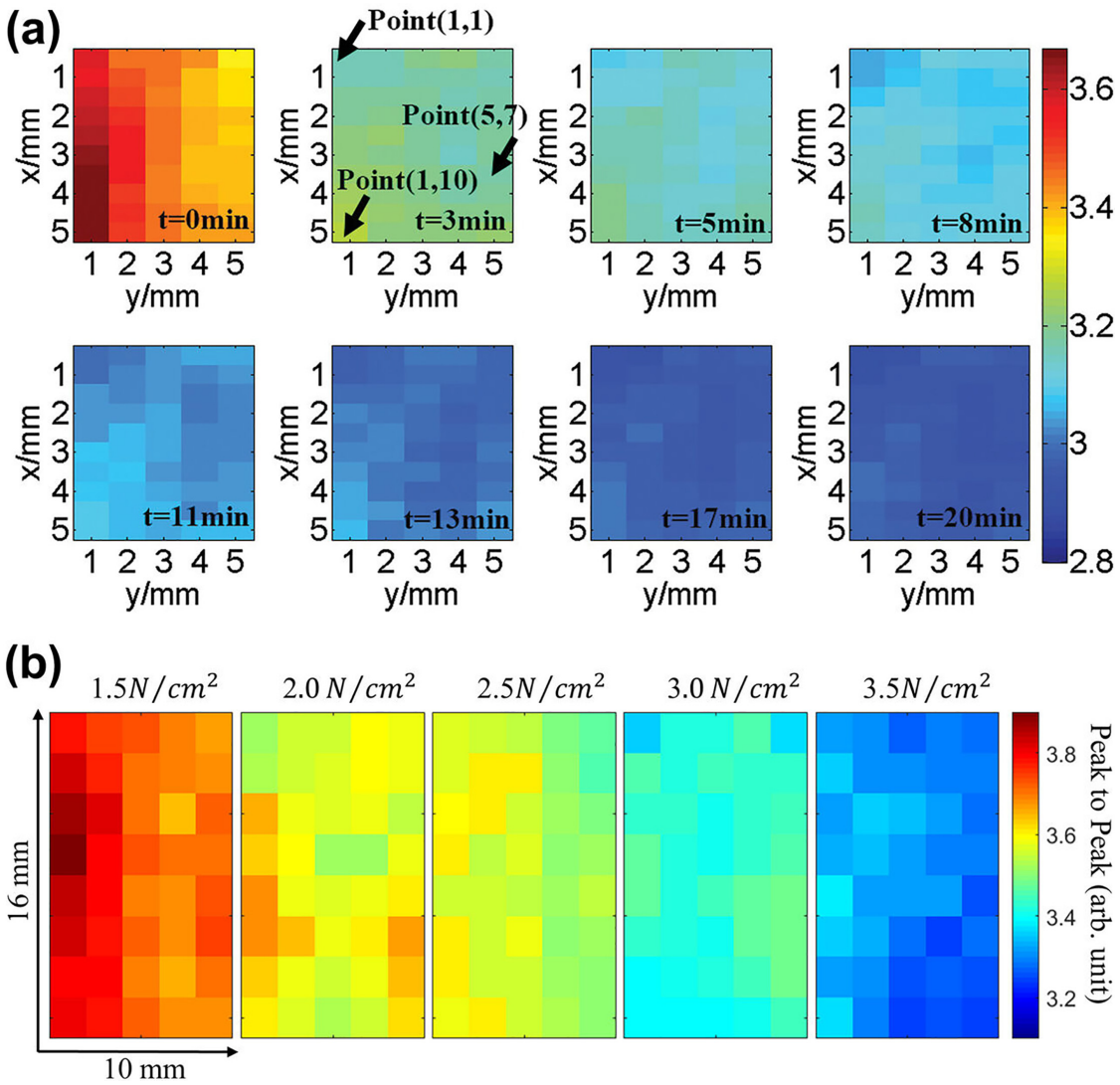

FIG. 25. (a) Images of the same region of skin with increasing time into occlusion, showing the decrease in peak to peak amplitude with increasing occlusion time. Reproduced with permission from Sun *et al.*, J. Biophotonics **11**, e201700111 (2018).[108] Copyright 2017 Wiley-VCH Verlag GmbH & Co. KGaA, Weinheim. (b) THz images of the skin acquired under different contact pressures between the skin and the imaging window. Reproduced with permission from Wang *et al.*, Biomed. Opt. Express **9**, 6467 (2018).[109] Copyright 2018 Optical Society of America.

compensate for the effect of occlusion from THz images of the skin. In addition to removing the effect of occlusion from the results, there is also potential that the occlusion curves of skin could be used to identify abnormalities, such as the presence of cancer beneath the skin surface, which may affect the water dynamics in the skin.

In addition to occlusion, another variable which will affect the THz response of skin is the contact pressure between the skin and the imaging window. Wang *et al.* investigated the impact of pressure by incorporating pressure sensors into the THz system and measured the THz response of skin at five different pressures.[109] The study found that the reflectivity of skin decreased by up to 30% as the pressure increased, while the refractive index increased by up to 10%. Images of the peak-to-peak amplitude at different contact pressures are shown in Fig. 25(b), and the clear effect of pressure on the measured THz response of skin can be seen. This was attributed to an increase in hydration and an increase in the density of the biological tissues. The results from the skin modeling confirmed that the thickness of the SC decreases as pressure increases and the surface hydration of the SC increases.

To account for the observations that occlusion time and contact pressure influence the THz response of skin, Lindley-Hatcher *et al.* compiled a robust protocol for *in vivo* skin measurements using a reflection THz system.[110] They also introduced a variable called the normalized relative change, which can be used to remove the effects of natural variation of the skin between measurements by subtracting the variation in the control region from the variation in the treated region.

They found that by using this protocol and processing technique they were able to obtain repeatable measurements of the changes in human skin following the application of a commercial moisturizer.

These initial studies have identified some of the parameters which can influence the measured THz response of skin and have quantified the magnitude of these changes. Other parameters which can also have an impact include the environmental conditions, such as temperature and humidity. It is important that these parameters are controlled as effectively as possible by the experimental protocol if *in vivo* THz measurements are to give robust and repeatable results.

5. Corneal assessment

In addition to imaging the skin, THz radiation has been tested as a potential technique for assessing corneal hydration, as the eye can be accessed without passing through any other tissues. The first *in vivo* images of the cornea at THz frequencies were obtained by Taylor *et al.* who measured the corneas of five rabbits using an imaging window to flatten the curve of the tissue.[57,302] The corneas were measured every 10–15 min over a period of 2 h while the eye was exposed to a stream of air to dehydrate the eye. In addition to the THz measurements, the central corneal thickness was measured using ultrasound; this can be used to approximate the corneal water content; however, the accuracy of such a conversion is questionable. Very little correlation was found between the THz reflectivity of the cornea and the measured corneal thickness. Following electromagnetic modeling, the study raises the question that the technique employed to dehydrate the eye using air may be altering the corneal thickness in isolation from the hydration leading to observable changes in the ultrasound results but not in the THz images.

The THz spectral signatures of the cornea observed arise from lossy longitudinal modes, it is assumed that these exist due to the uniform structure of the cornea comprised of a thin collagen layer backed by water. The lossy nature of these modes means that the upper limit of the usable illumination band for studying the cornea may not extend too much beyond the millimeter wave region. A subsequent study by Chen *et al.* applied the more appropriate diffusion model to represent water content gradients.[321] Corneal tissue water content gradients have been confirmed in cornea. Castoro *et al.* observed a substantial bound water component in *ex vivo* bovine corneal samples along the optical axis.[322] This suggests that the cornea cannot be modeled using only free water components.

Following on from this initial study, the group advanced their approach further by developing a noncontact imaging technique for the cornea, as mentioned in Sec. II B 4, which takes advantage of the limited variation of the shape of the cornea between subjects and the relatively uniform geometry.[111] The move to noncontact imaging not only removes the risk of the imaging window interfering with the corneal hydration during the measurement, it also increases the applicability of such an approach for *in vivo* human measurements as it is more comfortable than maintaining contact between the eye and an imaging window for the duration of the measurement. Using this system, Sung *et al.* were able to acquire the first noncontact THz images of the human cornea of a single subject and subsequently plot the THz reflectivity map of the cornea. This study highlights the potential of THz imaging for checking the health of the eye; however, they also encountered challenges with controlling the movement of the subject. There are practical difficulties with *in vivo* measurements which must be dealt with before quick, repeatable noncontact measurements of the eye can be obtained with such a system as part of routine eye checks.

Tamminen *et al.* produced hydrogel-based corneal phantoms to test the efficacy of THz spectroscopy for corneal assessments and validated the accuracy of the results obtained.[73] Using this approach, they were able to extract the absolute thickness of the cornea and verify the results by comparing the results with measurements of the central corneal thickness obtained with OCT, which is the present gold standard for corneal assessment. The technique was also able to provide absolute estimates of the anterior and posterior water content of the corneal phantom and characterize phantom sphericity. It has also been proposed that THz spectroscopy could be used for sensing increases in intraocular pressure (IOP), in the recently obtained patent.[323] The first experimental demonstration of correlation between THz reflectivity and IOP was reported in a previous study.[121] Statistically significant increases in reflectivity between 0.4 and 0.6 THz corresponded to an increase in IOP. Endothelial layer damage, resulting from IOP increases, was confirmed using SEM of the corneal biopsy samples.

Additionally, work was performed by Ozheredov *et al.* to demonstrate the ability of THz imaging to observe the tear film in the human eye.[72] By asking subjects to keep their eye open for as long as possible before blinking and measuring the THz reflectivity of the eye using a noncontact geometry, a decrease in the reflectivity of the eye as a function of time could be observed. This decrease is associated with the drying of the eye as the tear film declines; they also observe the recovery of the reflectivity following blinking; this suggests that the tear film is restored by blinking. This study was then expanded upon by performing a similar investigation on 29 subjects measuring both eyes, the gradient of the decay of the reflectivity between blinks was obtained using a linear fit.[324] These results were used to categorize whether subjects had dry eye syndrome and compared to other approaches used to assess the health of the eye. It appears that subjects who reported suffering from dry eyes were more likely to have a greater decrease in the THz reflectivity of the eye between blinks. They also performed a study exploring the optimal model for describing the dehydration of the eye between blinks.[325] By applying an EMT, they were able to show that an exponential decay is the function which best described the decay of the reflection coefficient between blinks, and they were able to learn more about the structural changes in the tear film layer and how this influences the penetration depth of the THz radiation.

6. Cancer diagnosis

There remains a high demand for a nonionizing imaging technique which can quickly identify the presence of cancer and accurately outline the tumor margins. THz imaging has the potential to fill this gap and significant progress has been made in investigating this possibility. The first *in vivo* study which demonstrated the ability of THz imaging to identify the presence of cancer was performed by Wallace *et al.* in 2004.[288] As with many of the following studies, the focus was on skin cancer as it can be accessed and imaged noninvasively using THz reflection imaging. In the Wallace study, five subjects with basal cell carcinoma (BCC) on their arm were imaged, and THz images of the regions were produced. The study found a broadening of the THz

pulse in the cancerous regions and an increase in the peak amplitude. There was good correlation between the THz images and the subsequent histological results. At the time, it was acknowledged that the origin of this observed contrast was not well understood, and an up to date summary of the current understanding of the origin of contrast is given in Sec. III C.

More recently Zaystev *et al.* conducted a series of studies in which they investigated the ability of THz measurements to identify the presence of skin cancer *in vivo*.[326–328] In addition to the BCC examined by Wallace *et al.*, they also studied the common precursor to melanoma: dysplastic skin nevi. They compared the dielectric permittivity of these dysplastic nevi to that of nondysplastic nevi which are more likely to remain benign. By plotting the Cole–Cole diagrams of these results, they were able to demonstrate that THz measurements were able to distinguish between healthy skin and dysplastic and nondysplastic skin nevi. It should be noted that these studies were performed with a relatively small sample size of four subjects.

While the primary focus of research into potential applications of THz imaging to cancer diagnosis has been on skin cancers, there has also been some work demonstrating the contrast between healthy and cancerous tissues in other regions. These studies lose the advantage of being noninvasive imaging techniques, but may serve as an assisting operating examination tool. As mentioned, many current THz *in vivo* measurements are still based on a window-tissue raster scan modality. This can be seen from the early example of *in vivo* BCC imaging by Wallace *et al.*,[288] as well as the more recent *in vivo* studies of rat-brain tumors[154,309] described in the following paragraph. Such a modality is not ideal for invasive measurements, as a noncontact and fast imaging system would be preferable for aiding cancer removal and ensuring that the correct margins are used to define the tissue extraction.

One example of invasive *in vivo* THz measurements of cancer is the application to the identification of brain gliomas. Ji *et al.* performed an *ex vivo* study of the sensitivity of THz measurements to the presence of gliomas in brain tissue of mice, as part of this they also measured a single mouse brain *in vivo* by creating a cranial window to access the brain.[154] The study revealed that the THz image displayed a contrast between the healthy and cancerous regions; this was verified using MRI and fluorescence images of the same region and further *ex vivo* images following the extraction of the brain. Wu *et al.* extended this in their study in which 15 mice with brain gliomas were imaged *in vivo* and compared to the results from five healthy mice which underwent the same surgical procedures.[309] The study compared the THz reflection images of the brain taken following the creation of a cranial window with MRI and visual images and showed good correlation in the cancerous regions identified. After the THz images had been acquired, the brain was extracted and a histological examination was also performed. Some of the results from this study are shown in Fig. 26, where the cancerous tissue can be seen in the THz image as the red region which corresponds well to the location of the black rings marked on the *ex vivo* optical image showing the location of the cancer. These studies identify the ability of THz imaging to reveal the presence of cancer in other tissue types; however, a noncontact measurement scheme with a fast-imaging speed is needed for clinical applications.

Finally, it should also be noted that in a few specific cases *in vivo* THz measurements have been performed using a transmission geometry rather than using reflection. Chen *et al.* used a transmission geometry to image human breast cancer which had been placed inside the subcutaneous tissue of a mouse.[329] Mouse skin is very thin and elastic so it could be stretched thin enough that the transmission measurement could be performed and it was found that the cancerous region could be identified from the THz image. However, it is questionable how such an approach could be transferred to *in vivo* human measurements. It is useful to observe that breast cancer can be observed *in vivo* even under such conditions, and that the sensitivity shown in THz images in previous studies is not unique to the *ex vivo* conditions used.

7. Clinical solutions

There are many more potential applications for THz imaging and spectroscopy that have been explored. A brief summary of some of the recent advances will be addressed here. Once such application for THz imaging which has been investigated is the assessment of reconstructive skin flaps to determine if they will be successful. To do this, Bajwa *et al.* performed THz measurements on six rats, three of which had a flap of skin fully excised then returned to the region and held in place with sutures.[330] The other three rats had the region partially excised leaving two sides of the square of tissue intact; the tissue was raised from the skin surface then returned to its original position. These regions were measured with THz radiation 24 h, 48 h, and 7 days following this procedure, and THz reflectivity images of the regions were produced. At these time points, the regions were also clinically assessed to evaluate the health of the tissue. At the end of the study, the regions were removed, and a histological examination was performed. It was found that the fully excised region showed a significant contrast in the THz image from the surrounding healthy tissue 24 h following the procedure; such differences were observable in the clinical examination 48 h following, as shown in Fig. 27. Upon histological examination, it was confirmed that this tissue was necrotic. However, no such contrast was visible in the THz images of the partially excised regions. This suggests that THz images are able identify the drop in tissue water content, indicating that a skin graft is not successful prior to a clinical examination of the region. This could be a useful tool for rapid quantitative assessments of skin health and indicate the potential success of reconstructive surgeries at earlier stages.

THz imaging has also been investigated as a potential method for the objective diagnosis of diabetic foot syndrome. Diabetic foot syndrome is common in patients with diabetes and can cause ulceration on the foot which in many cases results in partial or total amputation of the limb. Presently, there is no gold standard technique for diagnosis and currently used methods are very subjective. Hernandez-Cardoso *et al.* constructed a setup to perform THz reflection measurements on the foot including a chair for the subject to sit on while their foot was in contact with the imaging window, shown in Fig. 28(a).[331] In an initial study, they measured the right foot of 33 healthy volunteers and 38 subjects diagnosed with diabetes; from these images, they could use 21 from the control group and 12 from the diabetic group, as some subjects struggled to maintain stable contact with the imaging window for the duration of the measurement. They extracted the water content of the skin using the LLL EMT and produced an image of the foot with each pixel representing the water content in that location. It is clear from these results that subjects in the diabetic group had significantly

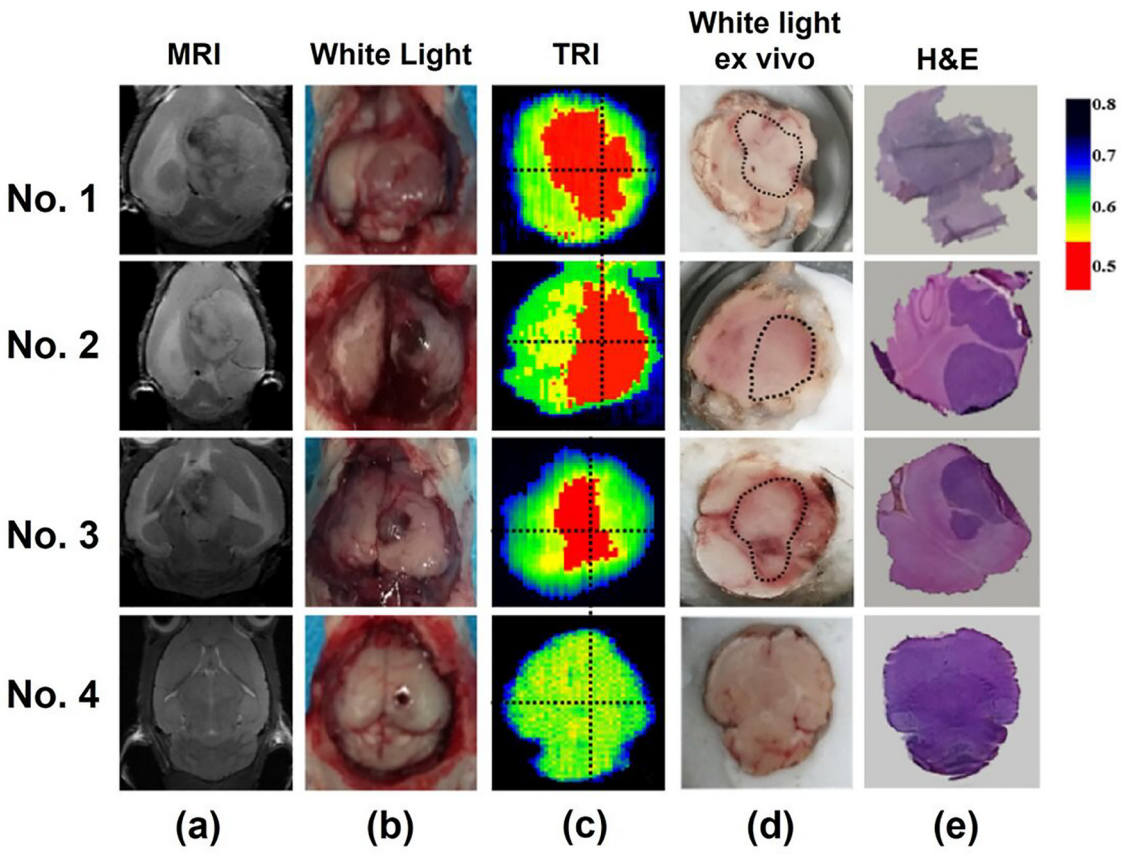

FIG. 26. Brains of mice with glioma (1–3) and a healthy mouse (4) imaged *in vivo* with MRI (a), visible light (b) and THz (c) and *ex vivo* images (d), and histological results (e) of the same regions. Reproduced with permission from Wu *et al.*, Biomed. Opt. Express **10**, 3953 (2019).[309] Copyright 2019 Optical Society of America.

drier skin, as shown in Figs. 28(b)–28(f). As part of the further analysis of these results, they found that by using a three color coding system for the pixels based on the water content, it was possible to identify a potential threshold for diabetic foot diagnosis.[332,333] They coded pixels with water content above 55.8% as green, those between 47% and 55.8% as yellow, and those below 47% as red. They defined a threshold parameter as

$$G - R = \%\text{Green Pixels} - \%\text{Red Pixels}. \tag{7}$$

Plotting this variable for diabetic and nondiabetic subjects, they found that all healthy subjects had $G - R > 18\%$ whereas 82% of diabetic subjects had $G - R < 18\%$. The most recent results on this front[334] dealt with a much larger cohort that includes 98 nondiabetics and 80 diabetics. This is probably the largest human population ever imaged with THz for medical research purposes. The diabetics were classified according to their clinical history as well as neurological and vascular assessments of their feet. First, the new study shows that patients with a history of ulceration or amputation or with peripheral neuropathy can be distinguished from those without these problems using the THz technique. Second, it provides clear indication that the skin dehydration of the feet of diabetic patients is related to the neurological "feedback loop" that regulates the hydration of the feet, rather than the irrigation. It should be noted that this is the only known application presently under research in which the pressure applied to the region by the imaging window mimics the normal environmental conditions for the tissue being tested, making this application unique among THz *in vivo* investigations.

Finally, there has also been some speculation on the ability of THz measurements to identify changes in blood glucose levels. For example, Cherkasova *et al.* investigated the sensitivity of THz measurements to glycerol when injected, ingested, or topically applied to the skin.[335,336] They measured some changes in the skin following the increase in blood glucose. Additionally, Chen *et al.* performed a series of near-field measurements on capillaries in the ears of diabetic mice.[95] They were able to identify the capillaries in the ear of a mouse from the image by the higher absorption coefficient value in the capillary compared to the surrounding tissue. They monitored the changes in the THz images of the ears of diabetic mice and observed changes in the measured absorption coefficient. However, in these studies, it is not possible to isolate the observed changes to be solely linked to changes in the blood glucose. These approaches to blood glucose measurement still lack the accuracy and specificity to replace current techniques and new methods need to be developed to enable THz devices to measure blood which is often too deep below the surface of the skin to be accessed by THz radiation.

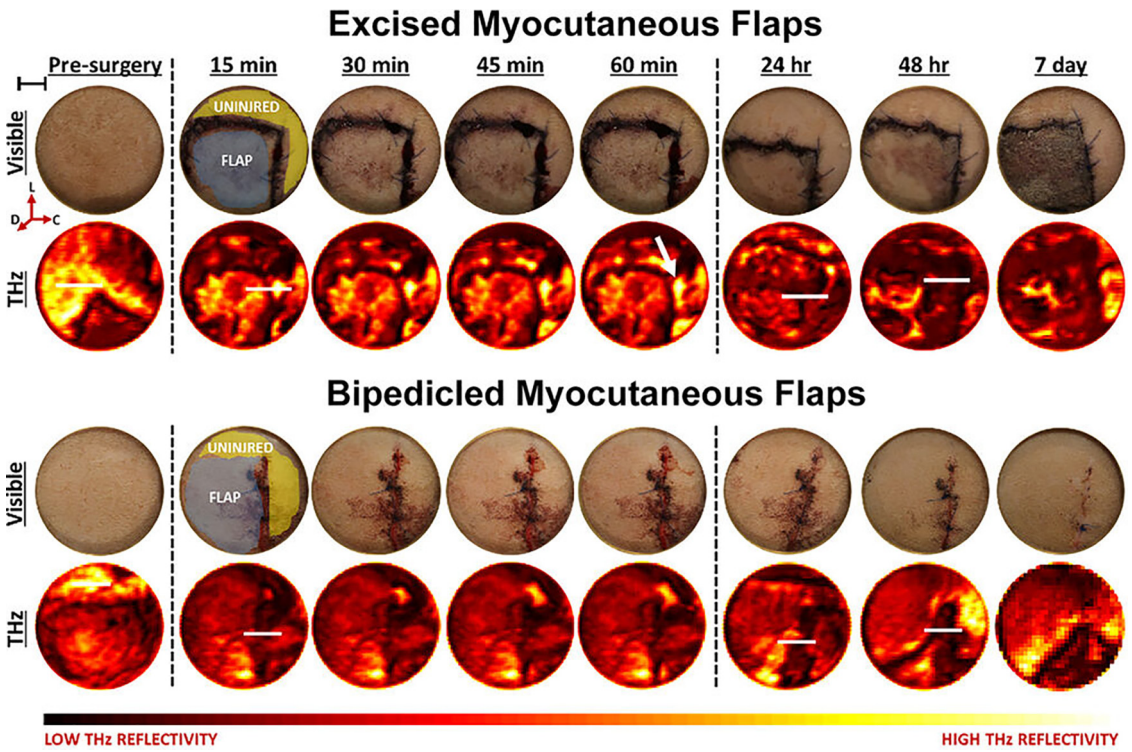

FIG. 27. The visible and THz images of fully and partially excised skin flaps, respectively, increasing time following the procedure. Reproduced with permission from Bajwa *et al.*, Biomed. Opt. Express **8**, 460 (2017).[330] Copyright 2016 Optical Society of America.

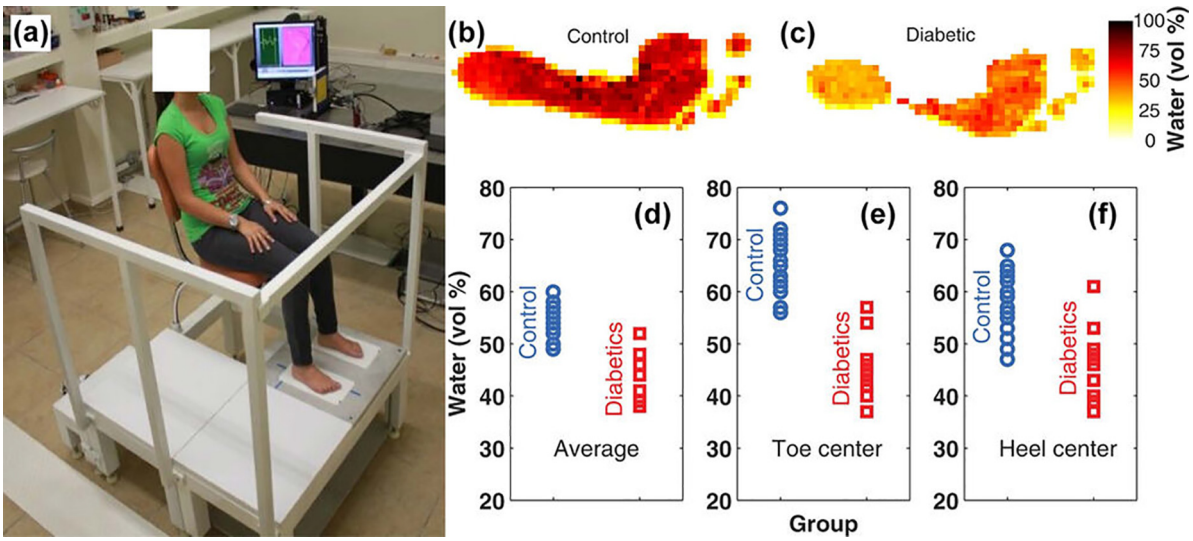

FIG. 28. Assessing diabetic foot syndrome with THz imaging: (a) the experimental setup used to image the foot with the skin in contact with an imaging window; (b) THz images of the water content of the feet of healthy and diabetic subjects; and (c) the distribution of the water content in the different foot regions for healthy and diabetic subjects. Reproduced with permission from Hernandez-Cardoso *et al.*, Sci. Rep. **7**, 42124 (2017).[331] Copyright 2017 Authors, licensed under a Creative Commons Attribution (CC BY) license.

It should also be noted that work has recently been performed exploring the potential of THz spectroscopy to differentiate between diabetic and nondiabetic blood samples by processing the blood to form blood plasma pellets.[337,338] A change in the refractive index of around 10% was observed between pellets from diabetic and nondiabetic subjects. This approach enables the removal of the effect of water from the THz spectra while also producing samples which can be stored at room temperature for a long time, making it possible to transport and/or repeat the measurements in the future if needed.

8. Passive in vivo imaging

It should also be mentioned that the potential of THz imaging has been investigated using the THz radiation produced by the body itself, rather than using a THz emitter to illuminate the sample and measure the reflected response, an image of the region of interest is taken at THz frequencies. For example, Berlovskaya *et al.* measured the background THz radiation emitted by subjects to obtain IR-THz images and explored the possibility of using these images to identify the psychoemotional state of a subject using noncontact imaging.[339] They measured 38 subjects in cases of electrical stimulation, cognitive load, and physical exercise. Through the classification of the pixels in the image into different clusters, they could observe differences in the stress responses of different subjects; some appeared to have an increased blood supply under stress while others had a decrease. They were also able to observe the periodic patterns in the region around the nose caused by breathing.

Another study was performed using a THz detector to obtain measurements of the radiation emitted by the human body in the frequency range of 0.1–1.5 THz.[340] The system was raster scanned to acquire an image of the human hand. In the image, the fingers can be clearly observed as there was sufficient sensitivity provided by the detector despite the low temperature contrast between the human body and the room temperature background.

Owda *et al.* performed a series of simulations of the emissivity of human skin in the frequency range from 30 to 300 GHz and found that the emissivity of skin is expected to decrease with increasing skin hydration.[341] They then measured the skin of 30 subjects in four regions; the inner and outer wrist and the volar and dorsal forearm. The study revealed differences in the measurements of male and female skin and also in the different regions measured. This study was extended further as 60 subjects were then measured in six regions on the arm and hand using the same approach to passive sensing.[342] They extended the parameters being investigated to also include ethnicity and body mass index. This technique has potential for being used in security as it is able to measure the emissivity of human skin and would be able to identify regions which have abnormalities indicating the presence of concealed objects.

VI. NEW ADVANCES IN DATA ANALYSIS

As discussed in Sec. III, most biosamples exhibit no absorption fingerprints in the THz region; hence, there is usually no distinct feature for convenient sample classification or identification. Separation between two different sample classes usually relies on small dielectric differences at some particular frequencies. Fortunately, mainly promoted by the commercialized THz-TDS systems, broadband THz measurements are now widely available, which provide multidimensional data in the time, frequency, and even spatial domains. These data not only offer comprehensive information, but also introduce difficulties in data analysis. For example, the refractive indices or absorption coefficients at particular frequencies, the amplitude in the time domain, and the pulse position can all potentially provide a contrast between two sample classes. It is difficult to decide which parameters should be used without an accurate prior knowledge. Advanced data analysis comprehensively taking this high-dimensional information into account is in high demand to achieve a better accuracy.

Usually, the data analysis for THz biomedical research is a binary classification problem, such as deciding whether a signal is reflected from the cancerous area or the normal area.[295] Multi-class classification may be required in some cases, such as determining the degree of cancer or injuries.[61] For continuous variations, such as the concentration of protein solutions, it becomes a regression problem.[343] In either case, the essential data processing typically contains three steps: (a) data acquisition; (b) feature extraction; and (c) classification, as depicted in the flowchart in Fig. 29. We overview the recent investigations which apply these techniques for THz biomedical research. Table II summarizes the system used for data acquisition, feature extraction methods, classifiers, and their applications. For the data acquisition, most measurements are based on THz-TDS systems owing to the advantageous broadband information.[344–346] A VNA has also been used, which also offers a broadband signal in the frequency-domain.[347] Using these systems, refractive indices or absorption coefficients which represent the sample properties independent of the measurement setup can be used for further processing. Time-domain amplitudes, transmission spectra, and other measured values can also be utilized, but they are specifically related to the measurement configuration. If imaging was performed, useful information may also be found from the spatial features. However, usually due to the limited number of samples and the small field of view, spatial information is rarely used. For THz images scanned by a broadband system, we generally look for features in each pixel that contain a full waveform. This is different from the classification for visible pictures, which is mainly based on the spatial patterns.

The goal of the second step is to extract features that can maximize the difference between two/multiple targeted classes. This step can be skipped by directly sending some measured values or sample properties to the classifier without further extraction. For example, Li *et al.* used the spectral magnitudes in the whole effective bandwidth to classify glucose and lactose spectra under various imperfect conditions, in order to remove the influence from the environment.[344] Cassar *et al.* used the refractive index at 0.55 THz to differentiate between benign and malignant breast carcinoma, making the classification straightforward by directly thresholding the refractive index with morphological dilation.[348] Zahid *et al.* compared the classifying accuracy for features selected from the time domain, frequency domain, and time–frequency domain, respectively, showing that they all provided a good accuracy for water content estimation in living plant leaves.[347] In these studies, directly taking the raw features had the advantage of a clear physical meaning. For example, if two classes can be differentiated by the transmission, the contrast is known to be from a difference in their transparency. However, sending large dimensional data for classification has a poor efficiency, which complicates the algorithm and increases the computational difficulties. Reducing the dimension by selecting some of the values requires prior knowledge on the origin

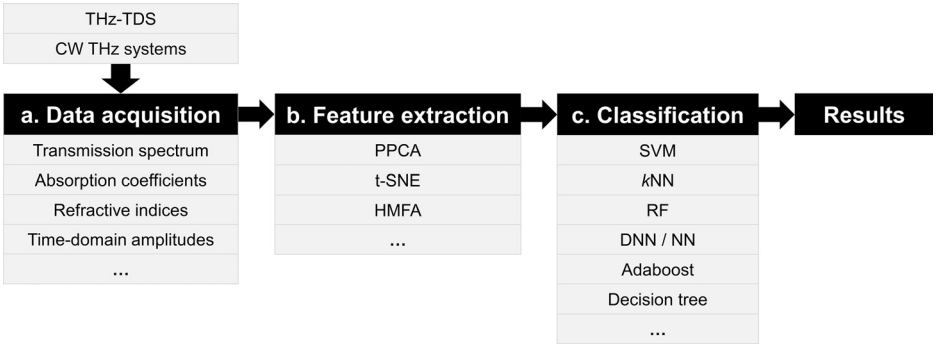

FIG. 29. Flowchart of the common approach to data analysis for THz biomedical applications.

of contrast and may miss other useful features. A more widely used strategy is to perform an additional feature extraction process to the raw data. This step extracts features with the greatest contrast and reduces the number of parameters. Principle component analysis (PPCA, to be distinguished from PCA referring to photoconductive antenna) is the most widely used method. In PPCA, a collection of input features is decomposed by a few orthogonal vectors (i.e., principle components) to describe the major variations of the data. By projecting the input data to the linearly uncorrelated principle components, the dimension can be efficiently reduced while the most informative features are kept. For example, applying PPCA to the absorption coefficient or transmission spectra extracts the key attenuation features. Examples can be found in the classification of exhaled air from patients with diabetes mellitus and healthy volunteers,[349] as well as classifying tissues of melanoma and nevus,[346] normal and prostate cancer,[350] and different concentrations of bovine serum albumin (BSA) solutions.[343] Other measured values can also be dimensionally reduced by PPCA. For example, Li *et al.* introduced wavelet transformation as the alternative to the Fourier transform due to its merit of multi-scale resolution for nonstationary signals.[351] They adopted the energy to Shannon entropy ratios (ESERs) from the wavelet packet transform for PPCA. In some experiments, PPCA may still offer too

TABLE II. Methods and algorithms used for different biomedical applications.

Data acquisition	Feature extraction	Classification	Application	Year, Reference
THz-TDS magnitude spectra	···	SVM, DNN	Glucose/lactose classification	2020, Li *et al.*[344]
THz-TDS refractive index	···	Morphological dilation + thresholding	Breast carcinoma delineation	2021, Cassar *et al.*[348]
VNA features of different domains	···	SVM, *k*NN, decision tree	Water content in leafs	2019, Zahid *et al.*[347]
THz-TDS absorption spectra	PPCA	···	Exhaled air from diabetes mellitus patients	2020, Kistenev *et al.*[349]
THz-TDS absorption spectra	PPCA	···	Melanoma and nevus tissue	2020, Kistenev *et al.*[346]
THz-TDS absorption spectra	PPCA	SVM	Prostate cancer grading	2020, Knyazkova *et al.*[350]
THz-TDS transmission spectra	PPCA	SVR	BSA concentration	2018, Sun *et al.*[343]
THz-TDS ESER	PPCA	SVM, *k*NN, ensemble	Breast invasive ductal carcinoma	2020, Liu *et al.*[351]
THz-TDS absorption spectra	PPCA + t-test	K-means, SVM	Human gastric normal and tumor tissues	2014, Hou *et al.*[295]
THz-TDS17 parameters	PPCA + decision tree	NN, SVM	Colon cancer diagnosis	2013, Eadie *et al.*[352]
THz-TDS refractive index and absorption spectra	MIC + PPCA	RF, Adaboost	Mouse liver injury	2019, Huang *et al.*[353]
THz-TDS absorption spectra	PPCA, t-SNE	SVM, RF, NBM, XGBoost	Protein conformation	2020, Cao *et al.*[354]
THz-TDS absorption spectra	HMFA	···	Gastric cancer	2018, Cao *et al.*[345]
THz-TDS complex spectra	SIT	···	Metastatic lymph nodes	2017, Park *et al.*[355]
CW THz imaging intensity	ReliefF	SVM, *k*NN, RF	Traumatic brain injury	2018, Shi *et al.*[61]

many parameters for the classification. To further reduce the dimension, Hou *et al.* used a t-test method to evaluate the significance of each individual principle component, and found the first four important components provide the best performance.[295] Similarly, Eadie *et al.* applied the decision tree method, which was originally designed for classification, to evaluate the importance of the features extracted from PPCA.[352] They finally selected eight parameters for the classifications. Huang *et al.* used another method of maximal information coefficient (MIC) to select the frequency points that provide the best contrast first, before applying PPCA.[353] MIC is a kind of the method which can find the relationship between two variants.[356] They showed a higher accuracy compared to the results without applying MIC. Apart from PPCA, features can also be extracted by other methods. For example, Cao *et al.* compared the PPCA with t-distributed stochastic neighbor embedding (t-SNE).[354] They claimed that the t-SNE method is better at dimensional reduction for spectral data. The results showed the outperformed accuracy in classifying the protein conformation states by t-SNE. Modified hard modeling factor analysis (HMFA) is an unmixing method decomposing the absorption spectrum into combinations of multiple weighted peak functions, thus the broadband absorption is represented by the weights of the discrete peaks.[357] This method was applied to extract the absorption features of the gastric cancer samples.[345] Park *et al.* used spectroscopic integration technique (SIT) such that each signal is represented by a single feature value. They showed an enhanced contrast in different levels of metastatic lymph nodes.[355] Shi *et al.* imaged different degrees of traumatic brain injury by a CW THz system. The gray histogram of the region of interest was taken from the measurement, and the features were extracted by ReliefF algorithm for further classifications.[61]

With the features from the measured values or the extraction methods, it is possible to do classification manually by comparing the tested sample with the statistical results. However, this is usually very difficult and subjective for high-dimensional data. A classifier is generally required for an automatic and accurate classification. Machine-learning (ML) based methods have become very popular in the recent decade, due to their successful application in many other fields especially for image recognition. ML can be classified into two types: supervised and unsupervised learning methods. The former type requires a manually labeled dataset to train or "supervise" the algorithm, such that the algorithm is built to maximize the difference between different targeted classes. This method is more commonly used in THz applications since a prior knowledge about the class of the measured sample is usually available. The major concern for supervised learning is that the sample size should be large enough for a generalized and accurate training and testing. Unsupervised learning automatically clusters the unlabeled data without human involvement. The best merit is that training is not required. However, unsupervised learning methods output an unknown number of classes, and the algorithm is usually more complicated.

Among various supervised ML methods, support vector machine (SVM) is most widely used. SVM maps the low-dimensional input data into a high-dimensional space where an optimal hyperplane boundary separating the two classes can be constructed. Successful classifications of glucose and lactose,[344] human gastric normal and tumor tissues[295] and traumatic brain injury,[61] etc., can be found in Table II. Most of these applications show accuracies higher than 90%, demonstrating reliability suitable for THz biomedical applications. From the simplicity perspective, the method of *k*-nearest neighbor (*k*NN) could be the best choice which has also been widely adapted. It classifies a tested sample by a plurality vote of its *k*-nearest neighbors in the training set and decides its class by the most common class observed. The comparison with SVM shows similar performance in various applications.[61,347,351] Random forest (RF) is another supervised ML method by using multiple decision trees.[358] The class of a tested sample is decided by the majority class of the multiple trees. Therefore, it usually provides a better accuracy than a single decision tree. Applications in mouse liver tissues,[353] traumatic brain injury,[61] and protein conformation evaluation[354] have all shown good accuracy. Many other methods are available, such as deep neural network (DNN) or neural network (NN),[344,352] support vector regression (SVR),[343] Adaboost,[353] decision tree,[347] naive Bayes model (NBM) and extreme gradient boosting (XGBoost),[354] Ensemble,[351] etc. They have all demonstrated high precision in different applications.

The examples discussed present the promising applications of advanced data analysis, especially using ML methods in THz biomedical applications. They provide a solution to extract the contrast between two targeted classes by considering high-dimensional features. However, a few improvements should be made in the future. First, a larger dataset should be constructed for ML. Currently, many of the datasets are rather small which is not very convincing for generalization and application. On the other hand, a larger dataset will be more comprehensive to represent the features of the data, benefiting the downstream classifier on improving the performance. Second, the numerous feature extraction methods and classifiers applied in different applications make it confusing for people to decide which one should be selected. A topical study on the technical comparisons of these methods and algorithms is needed to provide general guidance on their usages in THz biomedical studies. A recent review on ML techniques for THz applications has been reported by Park *et al.*,[359] which provides technical details and comparisons between different ML methods. In addition, data-driven methods like DNN or convolutional neural network which map the input directly to the output could be offered as a solution without the need of feature extraction. Third, although most of the classifiers achieve relatively high accuracy in classifications, an even better performance is needed for clinical applications. Some of the studies outlined above have compared multiple classifiers in a task to decide which one performs best. Actually, the performance can be further improved by combining two or multiple methods, with the decision made according to the majority. In any case, the decision of ML is made by a set of purely mathematical calculations. The algorithm performs a bit like a black box so care must be taken, particularly for biomedical applications, so that interpretable results are produced. For example, differentiating samples simply by their different absorptions can be explained by their different water concentration. However, differentiating them by a set of features with complicated rules is difficult to link to their physical properties. Therefore, being able to provide physical data interpretation is important to push it forward to clinical usage.

VII. CHALLENGES AND FUTURE PERSPECTIVES

Despite significant progress being made on both the techniques and applications aspects of THz biophotonics, new challenges are emerging with the expansion of applications. In this section, we summarize four major challenges that remain for THz biophotonics: the

issue of high water-absorption, the low flexibility of THz systems, the slow imaging speed, and the lack of methodology standards.

A. High THz absorption by water

The high THz absorption by water is a big obstacle for THz technology to be used in biomedical applications. The penetration depth of THz light in skin (which is approximately 70% water by volume) is limited to a wavelength comparable level, namely, less than 500 μm at 1 THz.[17] For comparison, traditional biophotonic techniques, such as OCT and diffuse optical spectroscopic imaging (DOSI),[360] have a penetration depth of around 5 mm in skin and eyes. Increasing the SNR by using a brighter source can improve the detectable depth. Pickwell–MacPherson compared the penetration depth of skin, water, and adipose as a function of SNR and showed a near 1-mm penetration depth for skin when a SNR of 100 000 can be achieved.[361] Using an intense source to alleviate the absorption issue for liquid samples has been demonstrated by Havenith's group. In their work, they used a p-Ge laser with a sufficiently high power to maximize the penetration distance and hence improve the accuracy. This motivates development of high-power THz sources to enhance the capability for absorptive nonliving samples. Indeed, solid-state devices and THz QCLs have both been improving their output powers at the same time as extending their higher/lower operating frequency limits. However, for *in vivo* applications thermal effects by intense sources can produce unwanted side effects in living biosystems, see Sec. IV.

THz spectroscopy is an important tool for exploring and understanding many fundamental molecular dynamics. It is most ideal to characterize the properties of the samples by mimicking their solvent environment; hence, the biggest challenge comes from the high absorption of water that makes the tiny changes induced by the molecules, such as the folding or conformational changes of proteins, difficult to measure precisely. The same issue was found for most reported biosensors, which have high-Q resonances in measuring low-loss samples but suffer significantly from the damping effect for absorptive samples. As a result, MM, resonant waveguides and THz SPPs usually only work as refractive index sensors. Designing configurations sensitive to high absorption samples could be another approach. We have shown the good sensitivity of the Si-ATR configuration to water in Sec. II B 1.[76,77] A similar configuration has also been adopted in the study of hydration shells of molecules of different weights.[216] Resonant sensors specifically designed for absorptive samples would also be very useful for detecting trace amounts of aqueous samples. Improving the accuracy of measuring highly absorptive liquids is a long-term but important topic that will have a great impact on many applications.

B. Low flexibility of THz systems

The high absorption by water means that measurements of *in vivo* tissues need to be performed in a reflection geometry. Most biological samples are "smooth" compared to the long wavelength of THz waves; thus, they behave similar to mirrors in that there is only specular reflection. The drawback is that unlike optical cameras that can easily capture the diffuse light without a precise illumination source, THz waves need to be measured accurately in the direction of the reflected beam and the detected signal will be very sensitive to small alignment variations. For *in vivo* measurements, a pre-aligned window making good contact with the measured area is usually used to mitigate against this, as it flattens the area being investigated and ensures there are no phase errors. As a result, most *in vivo* measurements have been limited to soft and hairless skin regions, such as the volar forearm, hands, and feet because they can be measured noninvasively with good contact with the imaging window. However, although there have been a few experiments of animal intraoperative measurements which are also based on a window-contact modality,[154,309] diseases are seldom in body areas that can be flattened and contacted by a window. This has made it nearly impossible to investigate using present THz imaging systems for cancer detection. Therefore, configurations with high flexibility that can quickly adjust the alignment according to the measured surface profile are urgently needed. For example, the configurations introduced in Sec. II B 4 were developed for this purpose. Further improvements using advanced sensors, mechanical components, and algorithms are on the horizon. With increased flexibility, the areas accessible for THz *in vivo* measurements will be greatly extended. This is a necessary step to progress THz technology from laboratory-based investigations to clinical applications. Another potential solution is to use passive imaging techniques and detect the THz emission from the body itself. At the moment, such technology is tailored to security screening to image large targets with a low sensitivity, as the main purpose is to distinguish hidden metal objects. Technically it is difficult to achieve medical-level sensitivity because the thermal noise at THz frequencies generates a lot of electrical noise. Such systems are also bulky and have limited frequency outputs. For example, the TS4-SC by Thruvision weighs 24 kg with a size of $61 \times 61 \times 25\,\mathrm{cm}^3$ and measures the intensity at 0.25 THz only. This is currently far away from the capabilities needed to perform studies investigating the origin of THz contrast in diseased tissues. However, depending on the results from broadband studies with other systems, passive technology could potentially be tailored for biomedical applications in the future.

C. Slow imaging speed

Developing fast THz-imaging technologies is an essential step before large-scale clinical studies can be performed. For example, close to real-time interpretation would be needed to enable the determination of cancer margins. This is because it is difficult to keep a patient sufficiently still for long periods of time and there is also a need to remove any time-induced variation on an image, such as occlusion. The acquisition time for certain parameters is longer than for others and also depends on the approach used to acquire the data. For example, if spectroscopic information is needed from a TDS source, it will take longer than if acquired from a CW source, but in the research phase, we do not know which frequencies will give the best contrast. Measuring a broadband response at this stage will help determine and optimize which sources and detectors can be used in the future. Recently, bolometer-array THz cameras working at room temperature over a broadband frequency have been combined with digital holography to provide amplitude and phase information,[64,362] with a frame rate of 5 and 3.5 Hz, respectively. The ultimate limit of frame rate is set by the camera, which can reach a video rate for current commercial products, while in practice the speed and field of view are further restricted by the power of the source. This detector technology combined with a frequency selective source has the potential of being used in hospital settings. As a source, THz QCLs are potentially viable since

they emit a single frequency that is tunable at discrete frequencies with suitable powers (>10 mW), with recent developments increasing the working temperature (see Sec. II A 2). However, it should be noted that the operating frequency of QCLs is usually too high (>2 THz); hence, the penetration depth is too small for biomedical applications. Commercial difference frequency photomixers emit powers of around 50 μW,[363] which is too weak for such bolometer arrays.

Another possible technique is to use a single-pixel camera combined with a pulsed time-domain THz system (see Sec. II A 1).[364] Although this technique obtains the image information in serial as opposed to in parallel, compared with detector arrays, Ref. 364 has achieved six frames-per-second real-time imaging of a 32 × 32 sample plotting the max amplitude. A follow-up publication showed that they can obtain a 32 × 32 image over a 10 ps time-interval in 2.6 s of acquisition,[365] which is around ten times faster than current commercial THz time-domain imaging systems. In the optical regime, a single-pixel camera was able to display a 101 × 103 video with 72 frames-per-second in real-time;[366] hence, this technology can certainly be fast enough with sufficient signal and a fast modulator. In this imaging modality, the fundamental acquisition speed is limited by the response time of the spatial modulator, and a recent overview of spatial THz modulators for single-pixel cameras is given in Ref. 98.

It is worth mentioning here that a new technology for CW single-wavelength imaging proposed by Weatherill's group.[367,368] They utilized alkali atomic vapors in the Rydberg state, which refers the atoms being excited to very a high energy level where the energy levels are closely spaced, such that their difference could be equal to the energy of a THz photon. In their recent work,[368] the detection is based on stimulating the emission of green light with THz photons. The most promising aspect of this technology is the very high efficiency that each THz photon has a 52.4% chance of being converted to a 535 nm photon. This provides the ability to achieve an ultrafast THz frame rate up to 3 kHz by using a low-power THz source of 17 μW. However, the emission mechanism means that the limitation of this technology is that it is only responsible for a narrow THz bandwidth for a specific Rydberg state.

D. Lack of methodology standards

The lack of commonly accepted measurement standards has resulted in diversity of the methodology, including the systems, configurations, experimental protocols, and processing methods. Even for the relatively standard THz-TDS transmission measurement of solid samples, divergence among different groups around the world was found in an international comparison study.[369] Biomedical samples and applications are further complicated by having more variables than solid-phase materials, which undoubtedly makes it more difficult to establish common standards. Therefore, focused research on specific applications is needed to reduce the divergence gradually. For example, in skin studies there is no agreement in the modeling of the skin, and structures of single-layer, bilayer, bilayer with continuous water-content or birefringence have been applied. There are also control variables affecting the THz response. For sensing applications, a standardization of the techniques used to detect the quantities of interest is also needed. Some work has been done to address these issues. For *in vivo* skin measurements, there have been investigations into the optical model of the skin as well as how different control variables affect the THz response of skin.[9,110] Similarly, the topical review on ML provides a subjective comparison among numerous ML algorithms.[359] These efforts pave the way to improve the data accuracy as well as the comparability between different studies.

Finally, any bioeffects due to exposure to THz radiation at different powers will have to be considered. While THz photons are non-ionizing, they do have effects on biological matter as discussed in Sec. IV. However, the exact mechanism of how THz radiation interacts with living biosystems is currently not experimentally established. The theoretical framework is that a Fröhlich condensate state is formed, and this perturbs the biochemical kinetics; however, there is only a single experimental study from 2015 that is thought to have observed such a Fröhlich condensate in single isolated lysozyme protein,[191] which is far from a living organism. Without an adequate understanding of how THz waves affect biomatter, any attempt to establish safety protocols will be a precarious empirical challenge.

VIII. CONCLUSIONS

In this review, we have given a detailed overview regarding aspects relating to the fundamental instrumentation, interaction theories, radiation concerns, biomedical applications, and advanced data analysis. We emphasize the importance of having a comprehensive understanding of these aspects in order to gain a clear perspective of this interdisciplinary area. THz systems have been developed into various configurations to study samples ranging from molecules to cells and tissues and been applied in areas ranging from fundamental physical and chemical investigations to pathological diagnosis. THz instrumentation is becoming more widespread and different techniques have been developed and applied for specific applications. This has also promoted investigations into the biological effects of THz radiation. New challenges and difficulties have arisen from these applications and they push forward the further improvement of the techniques. As we summarized in Sec. VII, although we have seen tremendous progress being made to improve different aspects over the years, there are still several significant obstacles in between THz technology and its mature application to medicine. Thus, there is still a long way to go, but we envisage that further developments in biophotonics will gradually shorten the distance between research and clinical practice.

ACKNOWLEDGMENTS

This work was partially supported by the Research Grants Council of Hong Kong (Project No. 14206717), the Engineering and Physical Sciences Research Council (EPSRC) (No. EP/S021442/1) and the Royal Society Wolfson Merit Award (EPM), and the National Natural Science Foundation of China (No. 61988102).

AUTHOR DECLARATIONS

Conflict of Interest

The authors have no conflicts to disclose.

DATA AVAILABILITY

Data sharing is not applicable to this article as no new data were created or analyzed in this study.

REFERENCES

[1]H. Yada, M. Nagai, and K. Tanaka, "Origin of the fast relaxation component of water and heavy water revealed by terahertz time-domain attenuated total reflection spectroscopy," Chem. Phys. Lett. **464**, 166–170 (2008).

[2]B. B. Hu and M. C. Nuss, "Imaging with terahertz waves," Opt. Lett. **20**, 1716 (1995).
[3]B. M. Fischer, M. Walther, and P. U. Jepsen, "Far-infrared vibrational modes of DNA components studied by terahertz time-domain spectroscopy," Phys. Med. Biol. **47**, 3807–3814 (2002).
[4]Y. Ueno, R. Rungsawang, I. Tomita, and K. Ajito, "Quantitative measurements of amino acids by terahertz time-domain transmission spectroscopy," Anal. Chem. **78**, 5424–5428 (2006).
[5]C. Yu, S. Fan, Y. Sun, and E. Pickwell-MacPherson, "The potential of terahertz imaging for cancer diagnosis: A review of investigations to date," Quant. Imaging Med. Surg. **2**, 33–45 (2012).
[6]Y. Peng, C. Shi, X. Wu, Y. Zhu, and S. Zhuang, "Terahertz imaging and spectroscopy in cancer diagnostics: A technical review," BME Front. **2020**, 2547609.
[7]K. I. Zaytsev, I. N. Dolganova, N. V. Chernomyrdin, G. M. Katyba, A. A. Gavdush, O. P. Cherkasova, G. A. Komandin, M. A. Shchedrina, A. N. Khodan, D. S. Ponomarev, I. V. Reshetov, V. E. Karasik, M. Skorobogatiy, V. N. Kurlov, and V. V. Tuchin, "The progress and perspectives of terahertz technology for diagnosis of neoplasms: A review," J. Opt. **22**, 013001 (2020).
[8]A. I. Nikitkina, P. Y. Bikmulina, E. R. Gafarova, N. V. Kosheleva, Y. M. Efremov, E. A. Bezrukov, D. V. Butnaru, I. N. Dolganova, N. V. Chernomyrdin, O. P. Cherkasova, A. A. Gavdush, and P. S. Timashev, "Terahertz radiation and the skin: A review," J. Biomed. Opt. **26**, 043005 (2021).
[9]J. Wang, H. Lindley-hatcher, X. Chen, and E. PickwellâMacPherson, "THz sensing of human skin: A review of skin modeling approaches," Sensors **21**, 3624 (2021).
[10]S. Fan, Y. He, B. S. Ung, and E. Pickwell-Macpherson, "The growth of biomedical terahertz research," J. Phys. D **47**, 374009 (2014).
[11]X. Yang, X. Zhao, K. Yang, Y. Liu, Y. Liu, W. Fu, and Y. Luo, "Biomedical applications of terahertz spectroscopy and imaging," Trends Biotechnol. **34**, 810–824 (2016).
[12]Q. Sun, Y. He, K. Liu, S. Fan, E. P. J. Parrott, and E. Pickwell-MacPherson, "Recent advances in terahertz technology for biomedical applications," Quant. Imaging Med. Surg. **7**, 345–355 (2017).
[13]M. Tonouchi, "Cutting-edge terahertz technology," Nat. Photonics **1**, 97–105 (2007).
[14]X.-C. Zhang and J. Xu, *Introduction to THz Wave Photonics* (Springer, New York, 2010).
[15]D. H. Auston and K. P. Cheung, "Coherent time-domain far-infrared spectroscopy," J. Opt. Soc. Am. B **2**, 606–612 (1985).
[16]Y. Hirota, R. Hattori, M. Tani, and M. Hangyo, "Polarization modulation of terahertz wave by multipole type photoconductive antenna," Opt. Express **14**, 4486 (2006).
[17]E. P. J. Parrott, S. M. Y. Sy, T. Blu, V. P. Wallace, and E. Pickwell-MacPherson, "Terahertz pulsed imaging *in vivo*: Measurements and processing methods," J. Biomed. Opt. **16**, 106010 (2011).
[18]Z. B. Harris, M. E. Khani, and M. Hassan Arbab, "Terahertz portable handheld spectral reflection (PHASR) scanner," IEEE Access **8**, 228024–228031 (2020).
[19]Y. B. Ji, E. S. Lee, S.-H. Kim, J.-H. Son, and T.-I. Jeon, "A miniaturized fiber-coupled terahertz endoscope system," Opt. Express **17**, 17082 (2009).
[20]J. Wang, H. Lindley-Hatcher, K. Liu, and E. Pickwell-MacPherson, "Evaluation of transdermal drug delivery using terahertz pulsed imaging," Biomed. Opt. Express **11**, 4484 (2020).
[21]X. Chen, E. P. J. Parrott, Z. Huang, H.-P. Chan, and E. Pickwell-MacPherson, "Robust and accurate terahertz time-domain spectroscopic ellipsometry," Photonics Res. **6**, 768–775 (2018).
[22]K.-E. Peiponon, J. A. Zeitler, and M. Kuwata-Gonokami, *Terahertz Spectroscopy and Imaging* (Springer, 2012), Vol. 171.
[23]A. Bonvalet, M. Joffre, J. L. Martin, and A. Migus, "Generation of ultrabroadband femtosecond pulses in the mid-infrared by optical rectification of 15 fs light pulses at 100 MHz repetition rate," Appl. Phys. Lett. **67**, 2907 (1995).
[24]B. Braaf, M. G. O. Gräfe, N. Uribe-Patarroyo, B. E. Bouma, B. J. Vakoc, J. F. de Boer, S. Donner, and J. Weichsel, *High Resolution Imaging in Microscopy and Ophthalmology* (Springer, 2019), pp. 161–179.
[25]J. A. Fülöp, S. Tzortzakis, and T. Kampfrath, "Laser-driven strong-field terahertz sources," Adv. Opt. Mater. **8**, 1900681 (2020).
[26]J. Zhao, E. Yiwen, K. Williams, X. C. Zhang, and R. W. Boyd, "Spatial sampling of terahertz fields with sub-wavelength accuracy via probe-beam encoding," Light **8**, 55 (2019).
[27]L. Olivieri, J. S. Totero Gongora, A. Pasquazi, and M. Peccianti, "Time-resolved nonlinear ghost imaging," ACS Photonics **5**, 3379–3388 (2018).
[28]L. Olivieri, J. S. Gongora, L. Peters, V. Cecconi, A. Cutrona, J. Tunesi, R. Tucker, A. Pasquazi, and M. Peccianti, "Hyperspectral terahertz microscopy via nonlinear ghost imaging," Optica **7**, 186–191 (2020).
[29]T. Kampfrath, M. Battiato, P. Maldonado, G. Eilers, J. Nötzold, S. Mährlein, V. Zbarsky, F. Freimuth, Y. Mokrousov, S. Blügel, M. Wolf, I. Radu, P. M. Oppeneer, and M. Münzenberg, "Terahertz spin current pulses controlled by magnetic heterostructures," Nat. Nanotechnol. **8**, 256–260 (2013).
[30]E. T. Papaioannou and R. Beigang, "THz spintronic emitters: A review on achievements and future challenges," Nanophotonics **10**, 1243–1257 (2021).
[31]T. Seifert, S. Jaiswal, U. Martens, J. Hannegan, L. Braun, P. Maldonado, F. Freimuth, A. Kronenberg, J. Henrizi, I. Radu, E. Beaurepaire, Y. Mokrousov, P. M. Oppeneer, M. Jourdan, G. Jakob, D. Turchinovich, L. M. Hayden, M. Wolf, M. Münzenberg, M. Kläui, and T. Kampfrath, "Efficient metallic spintronic emitters of ultrabroadband terahertz radiation," Nat. Photonics **10**, 483–488 (2016).
[32]S. C. Chen, Z. Feng, J. Li, W. Tan, L. H. Du, J. Cai, Y. Ma, K. He, H. Ding, Z. H. Zhai, Z. R. Li, C. W. Qiu, X. C. Zhang, and L. G. Zhu, "Ghost spintronic THz-emitter-array microscope," Light **9**, 99 (2020).
[33]Y. Wu, M. Elyasi, X. Qiu, M. Chen, Y. Liu, L. Ke, and H. Yang, "High-performance THz emitters based on ferromagnetic/nonmagnetic heterostructures," Adv. Mater. **29**, 1603031 (2017).
[34]T. Seifert, S. Jaiswal, M. Sajadi, G. Jakob, S. Winnerl, M. Wolf, M. Kläui, and T. Kampfrath, "Ultrabroadband single-cycle terahertz pulses with peak fields of 300 kV cm^{-1} from a metallic spintronic emitter," Appl. Phys. Lett. **110**, 252402 (2017).
[35]I. Mehdi, J. V. Siles, C. Lee, and E. Schlecht, "THz diode technology: Status, prospects, and applications," Proc. IEEE **105**, 990–1007 (2017).
[36]M. Naftaly, R. G. Clarke, D. A. Humphreys, and N. M. Ridler, "Metrology state-of-the-art and challenges in broadband phase-sensitive terahertz measurements," Proc. IEEE **105**, 1151–1165 (2017).
[37]P. Tan, J. Huang, K. F. Liu, Y. Q. Xiong, and M. W. Fan, "Terahertz radiation sources based on free electron lasers and their applications," Sci. China Inf. Sci. **55**, 107–125 (2012).
[38]G. N. Kulipanov, E. G. Bagryanskaya, E. N. Chesnokov, Y. Y. Choporova, V. V. Gerasimov, Y. V. Getmanov, S. L. Kiselev, B. A. Knyazev, V. V. Kubarev, S. E. Peltek, V. M. Popik, T. V. Salikova, M. A. Scheglov, S. S. Seredniakov, O. A. Shevchenko, A. N. Skrinsky, S. L. Veber, and N. A. Vinokurov, "Novosibirsk free electron laser-facility description and recent experiments," IEEE Trans. Terahertz Sci. Technol. **5**, 798–809 (2015).
[39]A. Doria, G. P. Gallerano, E. Giovenale, G. Messina, A. Lai, A. Ramundo-Orlando, V. Sposato, M. D'Arienzo, A. Perrotta, M. Romanò, M. Sarti, M. R. Scarfì, I. Spassovsky, and O. Zeni, "THz radiation studies on biological systems at the ENEA FEL facility," Infrared Phys. Technol. **45**, 339–347 (2004).
[40]S. Yamazaki, M. Harata, Y. Ueno, M. Tsubouchi, K. Konagaya, Y. Ogawa, G. Isoyama, C. Otani, and H. Hoshina, "Propagation of THz irradiation energy through aqueous layers: Demolition of actin filaments in living cells," Sci. Rep. **10**, 9008 (2020).
[41]Y. U. Jeong, G. M. Kazakevitch, H. J. Cha, S. H. Park, and B. C. Lee, "Demonstration of a wide-band compact free electron laser to the THz imaging of bio samples," Nucl. Instrum. Methods Phys. Res., Sect. A **575**, 58–62 (2007).
[42]P. Chevalier, A. Amirzhan, F. Wang, M. Piccardo, S. G. Johnson, F. Capasso, and H. O. Everitt, "Widely tunable compact terahertz gas lasers," Science **366**, 856–860 (2019).
[43]A. Khalatpour, A. K. Paulsen, C. Deimert, Z. R. Wasilewski, and Q. Hu, "High-power portable terahertz laser systems," Nat. Photonics **15**, 16–20 (2021).
[44]K. Murate and K. Kawase, "Perspective: Terahertz wave parametric generator and its applications," J. Appl. Phys. **124**, 160901 (2018).

[45]A. D. Rakić, T. Taimre, K. Bertling, Y. L. Lim, P. Dean, A. Valavanis, and D. Indjin, "Sensing and imaging using laser feedback interferometry with quantum cascade lasers," Appl. Phys. Rev. **6**, 021320 (2019).
[46]C. Baker, I. S. Gregory, M. J. Evans, W. R. Tribe, E. H. Linfield, and M. Missous, "All-optoelectronic terahertz system using low-temperature-grown InGaAs photomixers," Opt. Express **13**, 9639 (2005).
[47]M. Wan, J. J. Healy, and J. T. Sheridan, "Terahertz phase imaging and biomedical applications," Opt. Laser Technol. **122**, 105859 (2020).
[48]R. Guo, K. Akiyama, H. Minamide, and H. Ito, "Frequency-agile terahertz-wave spectrometer for high-resolution gas sensing," Appl. Phys. Lett. **90**, 121127 (2007).
[49]T. Hagelschuer, M. Wienold, H. Richter, L. Schrottke, H. T. Grahn, and H.-W. Hübers, "Real-time gas sensing based on optical feedback in a terahertz quantum-cascade laser," Opt. Express **25**, 30203 (2017).
[50]J. A. Zeitler, P. F. Taday, D. A. Newnham, M. Pepper, K. C. Gordon, and T. Rades, "Terahertz pulsed spectroscopy and imaging in the pharmaceutical setting—A review," J. Pharm. Pharmacol. **59**, 209–223 (2007).
[51]F. Keilmann and R. Hillenbrand, "Near-field microscopy by elastic light scattering from a tip," Philos. Trans. R. Soc. London, Ser. A **362**, 787–805 (2004).
[52]H.-G. von Ribbeck, M. Brehm, D. W. van der Weide, S. Winnerl, O. Drachenko, M. Helm, and F. Keilmann, "Spectroscopic THz near-field microscope," Opt. Express **16**, 3430 (2008).
[53]B. Li, D. Wang, L. Rong, C. Zhai, Y. Wang, and J. Zhao, "Application of continuous-wave terahertz computed tomography for the analysis of chicken bone structure," Opt. Eng. **57**, 023105 (2018).
[54]A. Dobroiu, M. Yamashita, Y. N. Ohshima, Y. Morita, C. Otani, and K. Kawase, "Terahertz imaging system based on a backward-wave oscillator," Appl. Opt. **43**, 5637 (2004).
[55]J. Y. Lu, C. C. Kuo, C. M. Chiu, H. W. Chenc, C. L. Pan, and C. K. Sun, "THz interferometric imaging using subwavelength plastic fiber based THz endoscopes," Opt. Express **16**, 2494–2501 (2008).
[56]H. Chen, S. Ma, X. Wu, W. Yang, and T. Zhao, "Diagnose human colonic tissues by terahertz near-field imaging," J. Biomed. Opt. **20**, 036017 (2015).
[57]Z. D. Taylor, J. Garritano, S. Sung, N. Bajwa, D. B. Bennett, B. Nowroozi, P. Tewari, J. W. Sayre, J. P. Hubschman, S. X. Deng, E. R. Brown, and W. S. Grundfest, "THz and mm-wave sensing of corneal tissue water content: *In vivo* sensing and imaging results," IEEE Trans. Terahertz Sci. Technol. **5**, 184–196 (2015).
[58]S. Sung, S. Selvin, N. Bajwa, S. Chantra, B. Nowroozi, J. Garritano, J. Goell, A. D. Li, S. X. Deng, E. R. Brown, W. S. Grundfest, and Z. D. Taylor, "THz imaging system for *in vivo* human cornea," IEEE Trans. Terahertz Sci. Technol. **8**, 27–37 (2018).
[59]L. Rong, T. Latychevskaia, C. Chen, D. Wang, Z. Yu, X. Zhou, Z. Li, H. Huang, Y. Wang, and Z. Zhou, "Terahertz in-line digital holography of human hepatocellular carcinoma tissue," Sci. Rep. **5**, 8445 (2015).
[60]P. Doradla, K. Alavi, C. Joseph, and R. Giles, "Detection of colon cancer by continuous-wave terahertz polarization imaging technique," J. Biomed. Opt. **18**, 090504 (2013).
[61]J. Shi, Y. Wang, T. Chen, D. Xu, H. Zhao, L. Chen, C. Yan, L. Tang, Y. He, H. Feng, and J. Yao, "Automatic evaluation of traumatic brain injury based on terahertz imaging with machine learning," Opt. Express **26**, 6371–6381 (2018).
[62]P. H. Siegel and R. J. Dengler, "Terahertz heterodyne imager for biomedical applications," Proc. SPIE **5354**, 1–9 (2004).
[63]S. M. Kim, F. Hatami, J. S. Harris, A. W. Kurian, J. Ford, D. King, G. Scalari, M. Giovannini, N. Hoyler, J. Faist, and G. Harris, "Biomedical terahertz imaging with a quantum cascade laser," Appl. Phys. Lett. **88**, 153903 (2006).
[64]M. Locatelli, M. Ravaro, S. Bartalini, L. Consolino, M. S. Vitiello, R. Cicchi, F. Pavone, and P. D. Natale, "Real-time terahertz digital holography with a quantum cascade laser," Sci. Rep. **5**, 13566 (2015).
[65]Y. L. Lim, T. Taimre, K. Bertling, P. Dean, D. Indjin, A. Valavanis, S. P. Khanna, M. Lachab, H. Schaider, T. W. Prow, H. Peter Soyer, S. J. Wilson, E. H. Linfield, A. G. Davies, and A. D. Rakić, "High-contrast coherent terahertz imaging of porcine tissue via swept-frequency feedback interferometry," Biomed. Opt. Express **5**, 3981 (2014).
[66]P. Knobloch, C. Schildknecht, T. Kleine-Ostmann, M. Koch, S. Hoffmann, M. Hofmann, E. Rehberg, M. Sperling, K. Donhuijsen, G. Hein, and K. Pierz, "Medical THz imaging: An investigation of histo-pathological samples," Phys. Med. Biol. **47**, 3875–3884 (2002).
[67]K. J. Siebert, T. Löffler, H. Quast, M. Thomson, T. Bauer, R. Leonhardt, S. Czasch, and H. G. Roskos, "All-optoelectronic continuous wave THz imaging for biomedical applications," Phys. Med. Biol. **47**, 3743–3748 (2002).
[68]K. Kawase, Y. Ogawa, Y. Watanabe, and H. Inoue, "Non-destructive terahertz imaging of illicit drugs using spectral fingerprints," Opt. Express **11**, 2549 (2003).
[69]Y. Wang, H. Minamide, M. Tang, T. Notake, and H. Ito, "Study of water concentration measurement in thin tissues with terahertz-wave parametric source," Opt. Express **18**, 15504 (2010).
[70]D. B. Bennett, W. Li, Z. D. Taylor, W. S. Grundfest, and E. R. Brown, "Stratified media model for terahertz reflectometry of the skin," IEEE Sens. J. **11**, 1253–1262 (2010).
[71]W. Zhang, E. R. Brown, L. Viveros, K. P. Burris, and C. N. Stewart, "Narrow terahertz attenuation signatures in Bacillus thuringiensis," J. Biophotonics **7**, 818–824 (2014).
[72]I. Ozheredov, M. Prokopchuk, M. Mischenko, T. Safonova, P. Solyankin, A. Larichev, A. Angeluts, A. Balakin, and A. Shkurinov, "*In vivo* THz sensing of the cornea of the eye," Laser Phys. Lett. **15**, 055601 (2018).
[73]A. Tamminen, M. Baggio, I. Nefedova, Q. Sun, S. Presnyakov, J. Ala-laurinaho, E. Brown, V. Wallace, E. Macpherson, T. Maloney, N. Kravchenko, M. Salkola, S. Deng, and Z. Taylor, "Extraction of thickness and water content gradients in hydrogel-based, water-backed corneal phantoms via submillimeter wave reflectometry," IEEE Trans. Terahertz Sci. Technol. **11**(6), 647–659 (2021).
[74]A. Pashkin, M. Kempa, H. Němec, F. Kadlec, and P. Kužel, "Phase-sensitive time-domain terahertz reflection spectroscopy," Rev. Sci. Instrum. **74**, 4711–4717 (2003).
[75]X. Chen, E. P. Parrott, B. S. Ung, and E. Pickwell-Macpherson, "A robust baseline and reference modification and acquisition algorithm for accurate THz imaging," IEEE Trans. Terahertz Sci. Technol. **7**, 493–501 (2017).
[76]U. Møller, "Terahertz spectroscopy applied to food model systems," Ph.D. thesis (Tedhnical University of Denmark, 2009).
[77]P. U. Jepsen, D. G. Cooke, and M. Koch, "Terahertz spectroscopy and imaging—Modern techniques and applications," Laser Photonics Rev. **5**, 124–166 (2011).
[78]Q. Sun, K. Liu, X. Chen, X. Liu, A. I. Hernandez-Serrano, and E. Pickwell-MacPherson, "Utilizing multilayer structures to enhance terahertz characterization of thin films ranging from aqueous solutions to histology slides," Opt. Lett. **44**, 2149–2152 (2019).
[79]H. Fujiwara, *Spectroscopic Ellipsometry Principles and Applications* (John Wiley & Sons, 2007).
[80]T. Hofmann, C. M. Herzinger, A. Boosalis, T. E. Tiwald, J. a. Woollam, and M. Schubert, "Variable-wavelength frequency-domain terahertz ellipsometry," Rev. Sci. Instrum. **81**, 023101 (2010).
[81]M. Yamashita, H. Takahashi, T. Ouchi, and C. Otani, "Ultra-broadband terahertz time-domain ellipsometric spectroscopy utilizing GaP and GaSe emitters and an epitaxial layer transferred photoconductive detector," Appl. Phys. Lett. **104**, 051103 (2014).
[82]N. Matsumoto, T. Hosokura, T. Nagashima, and M. Hangyo, "Measurement of the dielectric constant of thin films by terahertz time-domain spectroscopic ellipsometry," Opt. Lett. **36**, 265–267 (2011).
[83]M. Neshat and N. Armitage, "Terahertz time-domain spectroscopic ellipsometry: Instrumentation and calibration," Opt. Express **20**, 29063–29075 (2012).
[84]X. Chen, Q. Sun, J. Wang, H. Lindley-Hatcher, and E. PickwellâMacPherson, "Exploiting complementary terahertz ellipsometry configurations to probe the hydration and cellular structure of skin *in vivo*," Adv. Photonics Res. **2**, 2000024 (2021).
[85]M. Eisele, T. L. Cocker, M. A. Huber, M. Plankl, L. Viti, D. Ercolani, L. Sorba, M. S. Vitiello, and R. Huber, "Ultrafast multi-terahertz nano-spectroscopy with sub-cycle temporal resolution," Nat. Photonics **8**, 841–845 (2014).
[86]K. Okada, K. Serita, Q. Cassar, H. Murakami, G. MacGrogan, J.-P. Guillet, P. Mounaix, and M. Tonouchi, "Terahertz near-field microscopy of ductal carcinoma *in situ* (DCIS) of the breast," J. Phys. **2**, 044008 (2020).
[87]F. Blanchard, A. Doi, T. Tanaka, H. Hirori, H. Tanaka, Y. Kadoya, and K. Tanaka, "Real-time terahertz near-field microscope," Opt. Express **19**, 8277 (2011).

[88]L. E. Barr, P. Karlsen, S. M. Hornett, I. R. Hooper, M. Mrnka, C. R. Lawrence, D. B. Phillips, and E. Hendry, "Super-resolution imaging for sub-IR frequencies based on total internal reflection," Optica **8**, 88 (2021).
[89]R. I. Stantchev, J. C. Mansfield, R. S. Edginton, P. Hobson, F. Palombo, and E. Hendry, "Subwavelength hyperspectral THz studies of articular cartilage," Sci. Rep. **8**, 6924 (2018).
[90]C.-M. Chiu, H.-W. Chen, Y.-R. Huang, Y.-J. Hwang, W.-J. Lee, H.-Y. Huang, and C.-K. Sun, "All-terahertz fiber-scanning near-field microscopy," Opt. Lett. **34**, 1084 (2009).
[91]H. Chen, W.-J. Lee, H.-Y. Huang, C.-M. Chiu, Y.-F. Tsai, T.-F. Tseng, J.-T. Lu, W.-L. Lai, and C.-K. Sun, "Performance of THz fiber-scanning near-field microscopy to diagnose breast tumors," Opt. Express **19**, 19523–19531 (2011).
[92]T.-F. Tseng, S.-C. Yang, Y.-T. Shih, Y.-F. Tsai, T.-D. Wang, and C.-K. Sun, "Near-field sub-THz transmission-type image system for vessel imaging *in-vivo*," Opt. Express **23**, 25058–25071 (2015).
[93]P. Hillger, R. Jain, J. Grzyb, W. Förster, B. Heinemann, G. MacGrogan, P. Mounaix, T. Zimmer, and U. R. Pfeiffer, "A 128-pixel system-on-a-chip for real-time super-resolution terahertz near-field imaging," IEEE J. Solid-State Circuits **53**, 3599–3612 (2018).
[94]U. R. Pfeiffer, P. Hillger, R. Jain, J. Grzyb, T. Bucher, Q. Cassar, G. MacGrogan, J.-P. Guillet, P. Mounaix, and T. Zimmer, "*Ex vivo* breast tumor identification: Advances toward a silicon-based terahertz near-field imaging sensor," IEEE Microwave Mag. **20**, 32–46 (2019).
[95]H. Chen, Y. Zhang, X. Li, X. Chen, S. Ma, X. Wu, T. Qiu, and W. Zhang, "*In vivo* non-invasive diagnosis of glucose level in type-2 diabetes mouse by THz near-field imaging," J. Infrared, Millimeter, Terahertz Waves **40**, 456–465 (2019).
[96]G. M. Gibson, S. D. Johnson, and M. J. Padgett, "Single-pixel imaging 12 years on: A review," Opt. Express **28**, 28190 (2020).
[97]R. I. Stantchev, D. B. Phillips, P. Hobson, S. M. Hornett, M. J. Padgett, and E. Hendry, "Compressed sensing with near-field THz radiation," Optica **4**, 989 (2017).
[98]R. I. Stantchev and E. Pickwell-MacPherson, "Spatial terahertz-light modulators for single-pixel cameras," in *Terahertz Technology* (IntechOpen, 2021).
[99]Y. Malevich, S. Ergoktas, M. G. Bakan, P. Steiner, and C. Kocabas, "Video-speed graphene modulator arrays for terahertz imaging applications," ACS Photonics **7**, 2374–2380 (2020).
[100]C. Baker, W. R. Tribe, B. E. Cole, and M. C. Kemp, "Developments in people screening using terahertz technology," Proc. SPIE **5616**, 61–68 (2004).
[101]C. Baker, W. R. Tribe, T. Lo, B. E. Cole, S. Chandler, and M. C. Kemp, "People screening using terahertz technology," Proc. SPIE **5790**, 1–10 (2005).
[102]M. R. Grootendorst, A. J. Fitzgerald, S. G. Brouwer de Koning, A. Santaolalla, A. Portieri, M. Van Hemelrijck, M. R. Young, J. Owen, M. Cariati, M. Pepper, V. P. Wallace, S. E. Pinder, and A. Purushotham, "Use of a handheld terahertz pulsed imaging device to differentiate benign and malignant breast tissue," Biomed. Opt. Express **8**, 2932 (2017).
[103]B. Schulkin, D. Brigada, J. S. James, T. Tongue, and X. C. Zhang, "Progress toward handheld THz sensing," in *36th International Conference on Infrared, Millimeter, and Terahertz Waves (IRMMW-THz 2011)* (IEEE, 2011), pp. 1–2.
[104]G. J. Wilmink, B. L. Ibey, T. Tongue, B. Schulkin, N. Laman, X. G. Peralta, C. C. Roth, C. Z. Cerna, B. D. Rivest, J. E. Grundt, and W. P. Roach, "Development of a compact terahertz time-domain spectrometer for the measurement of the optical properties of biological tissues," J. Biomed. Opt. **16**, 047006 (2011).
[105]Y. B. Ji, I.-S. Moon, H. S. Bark, S. H. Kim, D. W. Park, S. K. Noh, Y.-M. Huh, J.-S. Suh, S. J. Oh, and T.-I. Jeon, "Terahertz otoscope and potential for diagnosing otitis media," Biomed. Opt. Express **7**, 1201 (2016).
[106]P. Doradla, K. Alavi, C. Joseph, and R. Giles, "Single-channel prototype terahertz endoscopic system," J. Biomed. Opt. **19**, 080501 (2014).
[107]E.-M. M. Stübling, A. Rehn, T. Siebrecht, Y. Bauckhage, L. Öhrström, P. Eppenberger, J. C. Balzer, F. Rühli, and M. Koch, "Application of a robotic THz imaging system for sub-surface analysis of ancient human remains," Sci. Rep. **9**, 3390 (2019).
[108]Q. Sun, E. P. Parrott, Y. He, and E. Pickwell-MacPherson, "*In vivo* THz imaging of human skin: Accounting for occlusion effects," J. Biophotonics **11**, e201700111 (2018).
[109]J. Wang, R. I. Stantchev, Q. Sun, T.-W. Chiu, A. T. Ahuja, and E. P. MacPherson, "THz *in vivo* measurements: The effects of pressure on skin reflectivity," Biomed. Opt. Express **9**, 6467 (2018).
[110]H. Lindley-Hatcher, A. I. Hernandez-Serrano, Q. Sun, J. Wang, J. Cebrian, L. Blasco, and E. Pickwell-Macpherson, "A robust protocol for *in vivo* THz skin measurements," J. Infrared, Millimeter, Terahertz Waves **40**, 980–989 (2019).
[111]S. Sung, A. Li, S. X. Deng, E. Brown, W. S. Grundfest, Z. D. Taylor, S. Dabironezare, N. Llombart, S. Selvin, N. Bajwa, S. Chantra, B. Nowroozi, J. Garritano, and J. Goell, "Optical system design for noncontact, normal incidence, THz imaging of *in vivo* human cornea," IEEE Trans. Terahertz Sci. Technol. **8**, 1–12 (2018).
[112]A. Chen, A. Virk, Z. Harris, A. Abazari, R. Honkanen, and M. H. Arbab, "Non-contact terahertz spectroscopic measurement of the intraocular pressure through corneal hydration mapping," Biomed. Opt. Express **12**, 3438–3449 (2021).
[113]F. Ellrich, M. Bauer, N. Schreiner, A. Keil, T. Pfeiffer, J. Klier, S. Weber, J. Jonuscheit, F. Friederich, and D. Molter, "Terahertz quality inspection for automotive and aviation industries," J. Infrared, Millimeter, Terahertz Waves **41**, 470–489 (2020).
[114]T. Pfeiffer, S. Weber, J. Klier, S. Bachtler, D. Molter, J. Jonuscheit, and G. Von Freymann, "Terahertz thickness determination with interferometric vibration correction for industrial applications," Opt. Express **26**, 12558–12568 (2018).
[115]E. Stübling, Y. Bauckhage, E. Jelli, B. Fischer, B. Globisch, M. Schell, A. Heinrich, J. C. Balzer, and M. Koch, "A THz tomography system for arbitrarily shaped samples," J. Infrared, Millimeter, Terahertz Waves **38**, 1179–1182 (2017).
[116]K. Krügener, E.-M. Stübling, R. Jachim, B. Kietz, M. Koch, and W. Viöl, "THz tomography for detecting damages on wood caused by insects," Appl. Opt. **58**, 6063–6066 (2019).
[117]M. Mikerov, R. Shrestha, P. van Dommelen, D. M. Mittleman, and M. Koch, "Analysis of ancient ceramics using terahertz imaging and photogrammetry," Opt. Express **28**, 22255–22263 (2020).
[118]S.-J. Nam, Y. J. Lim, J. H. Nam, H. S. Lee, Y. Hwang, J. Park, and H. J. Chun, "3D reconstruction of small bowel lesions using stereo camera-based capsule endoscopy," Sci. Rep. **10**, 6025 (2020).
[119]T.-H. Lin, "Automatic 3D color shape measurement system based on a stereo camera," Appl. Opt. **59**, 2086–2096 (2020).
[120]P. H. Siegel, "Technology in biology and medicine," IEEE Trans. Terahertz Sci. Technol. **52**, 2438–2447 (2004).
[121]N. V. Chernomyrdin, A. S. Kucheryavenko, G. S. Kolontaeva, G. M. Katyba, I. N. Dolganova, P. A. Karalkin, D. S. Ponomarev, V. N. Kurlov, I. V. Reshetov, M. Skorobogatiy, V. V. Tuchin, and K. I. Zaytsev, "Reflection-mode continuous-wave 0.15 λ-resolution terahertz solid immersion microscopy of soft biological tissues," Appl. Phys. Lett. **113**, 111102 (2018).
[122]A. A. Gavdush, N. V. Chernomyrdin, K. M. Malakhov, S.-I. T. Beshplav, I. N. Dolganova, A. V. Kosyrkova, P. V. Nikitin, G. R. Musina, G. M. Katyba, I. V. Reshetov, O. P. Cherkasova, G. A. Komandin, V. E. Karasik, A. A. Potapov, V. V. Tuchin, and K. I. Zaytsev, "Terahertz spectroscopy of gelatin-embedded human brain gliomas of different grades: A road toward intraoperative THz diagnosis," J. Biomed. Opt. **24**, 027001 (2019).
[123]M. D. King and T. M. Korter, "Noncovalent interactions between modified cytosine and guanine DNA base pair mimics investigated by terahertz spectroscopy and solid-state density functional theory," J. Phys. Chem. A **115**, 14391–14396 (2011).
[124]T. M. Korter, R. Balu, M. B. Campbell, M. C. Beard, S. K. Gregurick, and E. J. Heilweil, "Terahertz spectroscopy of solid serine and cysteine," Chem. Phys. Lett. **418**, 65–70 (2006).
[125]P. C. Upadhya, Y. C. Shen, A. G. Davies, and E. H. Linfield, "Terahertz time-domain spectroscopy of glucose and uric acid," J. Biol. Phys. **29**, 117–121 (2003).
[126]Y. C. Shen, P. C. Upadhya, E. H. Linfield, and A. G. Davies, "Temperature-dependent low-frequency vibrational spectra of purine and adenine," Appl. Phys. Lett. **82**, 2350–2352 (2003).
[127]J. Neu, E. A. Stone, J. A. Spies, G. Storch, A. S. Hatano, B. Q. Mercado, S. J. Miller, and C. A. Schmuttenmaer, "Terahertz spectroscopy of tetrameric peptides," J. Phys. Chem. Lett. **10**, 2624–2628 (2019).

[128]R. J. Falconer and A. G. Markelz, "Terahertz spectroscopic analysis of peptides and proteins," J. Infrared, Millimeter, Terahertz Waves **33**, 973–988 (2012).
[129]M. R. Kutteruf, C. M. Brown, L. K. Iwaki, M. B. Campbell, T. M. Korter, and E. J. Heilweil, "Terahertz spectroscopy of short-chain polypeptides," Chem. Phys. Lett. **375**, 337–343 (2003).
[130]A. G. Markelz, A. Roitberg, and E. J. Heilweil, "Pulsed terahertz spectroscopy of DNA, bovine serum albumin and collagen between 0.1 and 2.0 THz," Chem. Phys. Lett. **320**, 42–48 (2000).
[131]M. Walther, B. M. Fischer, and P. U. Jepsen, "Noncovalent intermolecular forces in polycrystalline and amorphous saccharides in the far infrared," Chem. Phys. **288**, 261–268 (2003).
[132]S. Warnecke, J. X. Wu, Ã. Rinnan, M. Allesø, F. van den Berg, P. U. Jepsen, and S. B. Engelsen, "Quantifying crystalline α-lactose monohydrate in amorphous lactose using terahertz time domain spectroscopy and near infrared spectroscopy," Vib. Spectrosc. **102**, 39–46 (2019).
[133]D. C. Elton, "The origin of the Debye relaxation in liquid water and fitting the high frequency excess response," Phys. Chem. Chem. Phys. **19**, 18739–18749 (2017).
[134]C. Rønne, L. Thrane, P. O. Åstrand, A. Wallqvist, K. V. Mikkelsen, and S. R. Keiding, "Investigation of the temperature dependence of dielectric relaxation in liquid water by THz reflection spectroscopy and molecular dynamics simulation," J. Chem. Phys. **107**, 5319–5331 (1997).
[135]P. U. Jepsen, U. Møller, and H. Merbold, "Investigation of aqueous alcohol and sugar solutions with reflection terahertz time-domain spectroscopy," Opt. Express **15**, 14717 (2007).
[136]E. Pickwell, B. E. Cole, A. J. Fitzgerald, M. Pepper, and V. P. Wallace, "In vivo study of human skin using pulsed terahertz radiation," Phys. Med. Biol. **49**, 1595–1607 (2004).
[137]E. Pickwell, B. E. Cole, A. J. Fitzgerald, V. P. Wallace, and M. Pepper, "Simulation of terahertz pulse propagation in biological systems," Appl. Phys. Lett. **84**, 2190–2192 (2004).
[138]E. Pickwell, A. J. Fitzgerald, B. E. Cole, P. F. Taday, R. J. Pye, T. Ha, M. Pepper, and V. P. Wallace, "Simulating the response of terahertz radiation to basal cell carcinoma using ex vivo spectroscopy measurements," J. Biomed. Opt. **10**, 064021 (2005).
[139]M. H. Arbab, T. C. Dickey, D. P. Winebrenner, A. Chen, M. B. Klein, and P. D. Mourad, "Terahertz reflectometry of burn wounds in a rat model," Biomed. Opt. Express **2**, 2339 (2011).
[140]M. H. Arbab, D. P. Winebrenner, T. C. Dickey, A. Chen, M. B. Klein, and P. D. Mourad, "Terahertz spectroscopy for the assessment of burn injuries in vivo," J. Biomed. Opt. **18**, 077004 (2013).
[141]A. J. Fitzgerald, E. Pickwell-MacPherson, and V. P. Wallace, "Use of finite difference time domain simulations and Debye theory for modelling the terahertz reflection response of normal and tumour breast tissue," PLoS One **9**, e99291 (2014).
[142]A. A. Gavdush, N. V. Chernomyrdin, G. A. Komandin, I. N. Dolganova, P. V. Nikitin, G. R. Musina, G. M. Katyba, A. S. Kucheryavenko, I. V. Reshetov, A. A. Potapov, V. V. Tuchin, and K. I. Zaytsev, "Terahertz dielectric spectroscopy of human brain gliomas and intact tissues *ex vivo*: Double-Debye and double-overdamped-oscillator models of dielectric response," Biomed. Opt. Express **12**, 69 (2021).
[143]C. B. Reid, G. Reese, A. P. Gibson, and V. P. Wallace, "Terahertz time-domain spectroscopy of human blood," IEEE Trans. Terahertz Sci. Technol. **3**, 774–778 (2013).
[144]B. C. Truong, H. D. Tuan, V. P. Wallace, A. J. Fitzgerald, and H. T. Nguyen, "The potential of the double Debye parameters to discriminate between basal cell carcinoma and normal skin," IEEE Trans. Terahertz Sci. Technol. **5**, 990–998 (2015).
[145]B. C. Truong, H. D. Tuan, A. J. Fitzgerald, V. P. Wallace, and H. T. Nguyen, "A dielectric model of human breast tissue in terahertz regime," IEEE Trans. Biomed. Eng. **62**, 699–707 (2015).
[146]J. C. Maxwell-Garnett, "XII. Colours in metal glasses and in metallic films," Philos. Trans. R. Soc. London, Ser. A **203**, 385–420 (1904).
[147]M. Scheller, C. Jansen, and M. Koch, "Applications of effective medium theories in the terahertz regime," in *Recent Optical and Photonic Technologies* (IntechOpen, 2010), pp. 231–250.
[148]G. G. Hernandez-Cardoso, A. K. Singh, and E. Castro-Camus, "Empirical comparison between effective medium theory models for the dielectric response of biological tissue at terahertz frequencies," Appl. Opt. **59**, D6 (2020).
[149]Y. He, K. Liu, C. Au, Q. Sun, E. P. Parrott, and E. Pickwell-MacPherson, "Determination of terahertz permittivity of dehydrated biological samples," Phys. Med. Biol. **62**, 8882–8893 (2017).
[150]M. Borovkova, M. Khodzitsky, P. Demchenko, O. Cherkasova, A. Popov, and I. Meglinski, "Terahertz time-domain spectroscopy for non-invasive assessment of water content in biological samples," Biomed. Opt. Express **9**, 2266–2276 (2018).
[151]J. Wang, Q. Sun, R. I. Stantchev, T.-W. Chiu, A. T. Ahuja, and E. PickwellâMacPherson, "*In vivo* terahertz imaging to evaluate scar treatment strategies: Silicone gel sheeting," Biomed. Opt. Express **10**, 3584–3590 (2019).
[152]Q. Sun, R. I. Stantchev, J. Wang, E. P. Parrott, A. Cottenden, T. W. Chiu, A. T. Ahuja, and E. Pickwell-MacPherson, "*In vivo* estimation of water diffusivity in occluded human skin using terahertz reflection spectroscopy," J. Biophotonics **12**, e201800145 (2019).
[153]Y. Kaneoke, M. Furuse, S. Inao, K. Saso, K. Yoshida, Y. Motegi, M. Mizuno, and A. Izawa, "Spin-lattice relaxation times of bound water—Its determination and implications for tissue discrimination," Magn. Reson. Imaging **5**, 415–420 (1987).
[154]Y. B. Ji, S. J. Oh, S. G. Kang, J. Heo, S. H. Kim, Y. Choi, S. Song, H. Y. Son, S. H. Kim, J. H. Lee, S. J. Haam, Y. M. Huh, J. H. Chang, C. Joo, and J. S. Suh, "Terahertz reflectometry imaging for low and high grade gliomas," Sci. Rep. **6**, 36040 (2016).
[155]S. Sy, S. Huang, Y. X. J. Wang, J. Yu, A. T. Ahuja, Y. T. Zhang, and E. Pickwell-MacPherson, "Terahertz spectroscopy of liver cirrhosis: Investigating the origin of contrast," Phys. Med. Biol. **55**, 7587–7596 (2010).
[156]A. J. Fitzgerald, V. P. Wallace, M. Jimenez-Linan, L. Bobrow, R. J. Pye, A. D. Purushotham, and D. D. Arnone, "Terahertz pulsed imaging of human breast tumors," Radiology **239**, 533–540 (2006).
[157]F. Wahaia, G. Valusis, L. M. Bernardo, A. Almeida, J. A. Moreira, P. C. Lopes, J. MacUtkevic, I. Kasalynas, D. Seliuta, R. Adomavicius, R. Henrique, and M. Lopes, "Detection of colon cancer by terahertz techniques," J. Mol. Struct. **1006**, 77–82 (2011).
[158]S. J. Oh, S.-H. Kim, Y. B. Ji, K. Jeong, Y. Park, J. Yang, D. W. Park, S. K. Noh, S.-G. Kang, Y.-M. Huh, J.-H. Son, and J.-S. Suh, "Study of freshly excised brain tissues using terahertz imaging," Biomed. Opt. Express **5**, 2837 (2014).
[159]S. Yamaguchi, Y. Fukushi, O. Kubota, T. Itsuji, T. Ouchi, and S. Yamamoto, "Origin and quantification of differences between normal and tumor tissues observed by terahertz spectroscopy," Phys. Med. Biol. **61**, 6808–6820 (2016).
[160]International Commission on Non-Ionizing Radiation Protection, "Guidelines for limiting exposure to time-varying electric, magnetic, and electromagnetic fields (up to 300 GHz)," Health Phys. **74**, 494–522 (1998).
[161]Secretariat Laser Institute of America, *American National Standard for Safe Use of Lasers* (Laser Institute of America, 2014).
[162]G. J. Wilmink and J. E. Grundt, "Invited review article: Current state of research on biological effects of terahertz radiation," J. Infrared, Millimeter, Terahertz Waves **32**, 1074–1122 (2011).
[163]T. T. L. Kristensen, W. Withayachumnankul, P. U. Jepsen, and D. Abbott, "Modeling terahertz heating effects on water," Opt. Express **18**, 4727–4739 (2010).
[164]B. S. Alexandrov, V. Gelev, A. R. Bishop, A. Usheva, and K. Ã. Rasmussen, "DNA breathing dynamics in the presence of a terahertz field," Phys. Lett. A **374**, 1214–1217 (2010).
[165]S. M. Chitanvis, "Can low-power electromagnetic radiation disrupt hydrogen bonds in dsDNA?," J. Polym. Sci., Part B **44**, 2740–2747 (2006).
[166]H. Fröhlich, "The biological effects of microwaves and related questions," in *Advances in Electronics and Electron Physics*, Advances in Electronics and Electron Physics Vol. 53, edited by L. Marton and C. Marton (Academic Press, 1980), pp. 85–152.
[167]G. P. Gallerano, E. Grosse, R. Korenstein, M. Dressel, W. Mantele, M. R. Scarfi, A. C. Cefalas, P. Taday, R. H. Clothier, and P. Jepsen, "THz-BRIDGE: A European project for the study of the interaction of terahertz radiation with biological systems," in Infrared and Millimeter Waves, Conference Digest of the 2004 Joint 29th International Conference on 2004 and 12th International Conference on Terahertz Electronics, 2004.

[168]O. P. Cherkasova, D. S. Serdyukov, A. S. Ratushnyak, E. F. Nemova, E. N. Kozlov, Y. V. Shidlovskii, K. I. Zaytsev, and V. V. Tuchin, "Effects of terahertz radiation on living cells: A review," Opt. Spectrosc. **128**, 855–866 (2020).
[169]L. Zhao, Y.-H. Hao, and R.-Y. Peng, "Advances in the biological effects of terahertz wave radiation," Mil. Med. Res. **1**, 26 (2014).
[170]A. Ramundo Orlando and G. P. Gallerano, "Terahertz radiation effects and biological applications," J. Infrared, Millimeter, Terahertz Waves **30**, 1308–1318 (2009).
[171]V. I. Fedorov, N. Y. Weisman, E. F. Nemova, and N. A. Nikolaev, "Terahertz radiation influence on stressed drosophila life span," Biophysics **59**, 458–463 (2014).
[172]V. I. Fedorov and N. Y. Weisman, "The development of F_1 progeny from mature egg cells after terahertz radiation of parental drosophila," Biophysics **62**, 460–465 (2017).
[173]V. I. Fedorov and N. Y. Weisman, "The lifespan of the F_1 progeny of drosophila females exposed to terahertz radiation of low intensity," Biophysics **60**, 835–842 (2015).
[174]L. V. Titova, A. K. Ayesheshim, A. Golubov, D. Fogen, R. Rodriguez-Juarez, F. A. Hegmann, and O. Kovalchuk, "Intense THz pulses cause H2AX phosphorylation and activate DNA damage response in human skin tissue," Biomed. Opt. Express **4**, 559–568 (2013).
[175]T. Tachizaki, R. Sakaguchi, S. Terada, K.-I. Kamei, and H. Hirori, "Terahertz pulse-altered gene networks in human induced pluripotent stem cells," Opt. Lett. **45**, 6078–6081 (2020).
[176]C. M. Hough, D. N. Purschke, C. Huang, L. V. Titova, O. V. Kovalchuk, B. J. Warkentin, and F. A. Hegmann, "Intense terahertz pulses inhibit *Ras signaling* and other cancer-associated signaling pathways in human skin tissue models," J. Phys.: Photonics **3**, 034004 (2021).
[177]K.-T. Kim, J. Park, S. J. Jo, S. Jung, O. S. Kwon, G. P. Gallerano, W.-Y. Park, and G.-S. Park, "High-power femtosecond-terahertz pulse induces a wound response in mouse skin," Sci. Rep. **3**, 2296 (2013).
[178]A. Ramundo-Orlando, G. P. Gallerano, P. Stano, A. Doria, E. Giovenale, G. Messina, M. Cappelli, M. D'Arienzo, and I. Spassovsky, "Permeability changes induced by 130 GHz pulsed radiation on cationic liposomes loaded with carbonic anhydrase," Bioelectromagnetics **28**, 587–598 (2007).
[179]A. A. Angeluts, A. B. Gapeyev, M. N. Esaulkov, O. G. Kosareva, S. N. Matyunin, M. M. Nazarov, T. N. Pashovkin, P. M. Solyankin, O. P. Cherkasova, and A. P. Shkurinov, "Study of terahertz-radiation-induced DNA damage in human blood leukocytes," Quantum Electron. **44**, 247–251 (2014).
[180]V. Franchini, S. Ceccuzzi, A. Doria, G. P. Gallerano, E. Giovenale, G. L. Ravera, A. De Amicis, S. De Sanctis, S. Di Cristofaro, E. Regalbuto, E. Coluzzi, J. Marinaccio, A. Sgura, R. Bei, M. Benvenuto, A. Modesti, L. Masuelli, and F. Lista, "Biological effects of 25 to 150 GHz radiation after in vitro exposure of human fibroblasts: A comparison of experimental results," J. Infrared, Millimeter, Terahertz Waves **39**, 899–911 (2018).
[181]I. Echchgadda, J. E. Grundt, C. Z. Cerna, C. C. Roth, B. L. Ibey, and G. J. Wilmink, "Terahertz stimulate specific signaling pathways in human cells," in 39th International Conference on Infrared, Millimeter, and Terahertz Waves (IRMMW-THz), 2014.
[182]G. J. Wilmink, B. L. Ibey, C. L. Roth, R. L. Vincelette, B. D. Rivest, C. B. Horn, J. Bernhard, D. Roberson, and W. P. Roach, "Determination of death thresholds and identification of terahertz (THz)-specific gene expression signatures," in *Optical Interactions with Tissues and Cells XXI*, edited by E. D. Jansen and R. J. Thomas (SPIE, 2010), Vol. 7562, pp. 131–138.
[183]I. Echchgadda, C. Z. Cerna, M. A. Sloan, D. P. Elam, and B. L. Ibey, "Effects of different terahertz frequencies on gene expression in human keratinocytes," in *Optical Interactions With Tissue and Cells XXVI*, edited by E. D. Jansen (SPIE, 2015), Vol. 9321, pp. 147–155.
[184]V. K. Kiseliov, V. I. Makolinets, N. A. Mitryaeva, and V. P. Radionov, "Application of terahertz lasers setup for the investigation of the influence of HHF-radiation on the tumor processes," in 37th International Conference on Infrared, Millimeter, and Terahertz Waves, 2012.
[185]V. K. Kiseliov, V. I. Makolinets, N. A. Mitryaeva, and V. P. Radionov, "Application of terahertz laser technology to investigate the influence of HHF radiation on the tumor process," Telecommun. Radio Eng. **71**, 1617–1626 (2012).
[186]J. Bock, Y. Fukuyo, S. Kang, M. L. Phipps, L. B. Alexandrov, K. Ã. Rasmussen, A. R. Bishop, E. D. Rosen, J. S. Martinez, H.-T. Chen, G. Rodriguez, B. S. Alexandrov, and A. Usheva, "Mammalian stem cells reprogramming in response to terahertz radiation," PLoS One **5**, e15806 (2010).
[187]M. Mizuno, H. Kitahara, K. Sasaki, M. Tani, M. Kojima, Y. Suzuki, T. Tasaki, Y. Tatematsu, M. Fukunari, and K. Wake, "Dielectric property measurements of corneal tissues for computational dosimetry of the eye in terahertz band *in vivo* and *in vitro*," Biomed. Opt. Express **12**, 1295 (2021).
[188]M. Kojima, Y. Suzuki, T. Tasaki, Y. Tatematsu, M. Mizuno, M. Fukunari, and H. Sasaki, "Clinical course of high-frequency millimeter-wave (162 GHz) induced ocular injuries and investigation of damage thresholds," J. Infrared, Millimeter, Terahertz Waves **41**, 834–845 (2020).
[189]O. Cherkasova, M. Surovtseva, A. Lykov, O. Kazakov, A. Kabakov, O. Poveshchenko, A. Poveshchenko, D. Serdyukov, S. Kuznetsov, and A. Letyagin, "Studying the effect of 0.14 THz radiation on human dermal fibroblasts," AIP Conf. Proc. **2098**, 020004 (2019).
[190]O. Zeni, G. P. Gallerano, A. Perrotta, M. Romanò, A. Sannino, M. Sarti, M. DâArienzo, A. Doria, E. Giovenale, A. Lai, G. Messina, and M. R. Scarfì, "Cytogenetic observations in human peripheral blood leukocytes following in vitro exposure to THz radiation: A pilot study," Health Phys. **92**, 349–357 (2007).
[191]I. V. Lundholm, H. Rodilla, W. Y. Wahlgren, A. Duelli, G. Bourenkov, J. Vukusic, R. Friedman, J. Stake, T. Schneider, and G. Katona, "Terahertz radiation induces non-thermal structural changes associated with Fröhlich condensation in a protein crystal," Struct. Dyn. **2**, 54702 (2015).
[192]E. P. Parrott and J. A. Zeitler, "Terahertz time-domain and low-frequency Raman spectroscopy of organic materials," Appl. Spectrosc. **69**, 1–25 (2015).
[193]K. M. Tych, A. D. Burnett, C. D. Wood, J. E. Cunningham, A. R. Pearson, A. G. Davies, and E. H. Linfield, "Applying broadband terahertz time-domain spectroscopy to the analysis of crystalline proteins: A dehydration study," J. Appl. Crystallogr. **44**, 129–133 (2011).
[194]B. Born, S. J. Kim, S. Ebbinghaus, M. Gruebele, and M. Havenith, "The terahertz dance of water with the proteins: The effect of protein flexibility on the dynamical hydration shell of ubiquitin," Faraday Discuss. **141**, 161–173 (2008).
[195]J. S. Melinger, N. Laman, S. S. Harsha, S. F. Cheng, and D. Grischkowsky, "High-resolution waveguide terahertz spectroscopy of partially oriented organic polycrystalline films," J. Phys. Chem. A **111**, 10977–10987 (2007).
[196]J. S. Melinger, N. Laman, S. S. Harsha, and D. Grischkowsky, "Line narrowing of terahertz vibrational modes for organic thin polycrystalline films within a parallel plate waveguide," Appl. Phys. Lett. **89**, 251110 (2006).
[197]B. M. Fischer, M. Hoffmann, H. Helm, R. Wilk, F. Rutz, T. Kleine-Ostmann, M. Koch, and P. U. Jepsen, "Terahertz time-domain spectroscopy and imaging of artificial RNA," Opt. Express **13**, 5205 (2005).
[198]M. Brucherseifer, M. Nagel, P. H. Bolívar, and H. Kurz, "Label-free probing of the binding state of DNA by time-domain terahertz sensing," Appl. Phys. Lett. **77**, 4049 (2000).
[199]R. Rungsawang, Y. Ueno, I. Tomita, and K. Ajito, "Angle-dependent terahertz time-domain spectroscopy of amino acid single crystals," J. Phys. Chem. B **110**, 21259–21263 (2006).
[200]A. Markelz, S. Whitmire, J. Hillebrecht, and R. Birge, "THz time domain spectroscopy of biomolecular conformational modes," Phys. Med. Biol. **47**, 3797–3805 (2002).
[201]C. Zhang, E. Tarhan, A. K. Ramdas, A. M. Weiner, and S. M. Durbin, "Broadened far-infrared absorption spectra for hydrated and dehydrated myoglobin," J. Phys. Chem. B **108**, 10077–10082 (2004).
[202]J. A. Zeitler, D. A. Newnham, P. F. Taday, C. J. Strachan, M. Pepper, K. C. Gordon, and T. Rades, "Temperature dependent terahertz pulsed spectroscopy of carbamazepine," Thermochim. Acta **436**, 71–77 (2005).
[203]J. R. Knab, J. Y. Chen, Y. He, and A. G. Markelz, "Terahertz measurements of protein relaxational dynamics," Proc. IEEE **95**, 1605–1610 (2007).
[204]X. Li, T. Globus, B. Gelmont, L. C. Salay, and A. Bykhovski, "Terahertz absorption of DNA decamer duplex," J. Phys. Chem. A **112**, 12090–12096 (2008).
[205]M. U. Heyden, G. Schwaab, E. Bründermann, X. Yu, D. M. Leitner, and M. Havenith, "Solute-induced retardation of water dynamics probed directly by

terahertz spectroscopy," Proc. Natl. Acad. Sci. U. S. A. **103**, 12301–12306 (2006).
[206]S. Ebbinghaus, J. K. Seung, M. Heyden, X. Yu, U. Heugen, M. Gruebele, D. M. Leitner, and M. Havenith, "An extended dynamical hydration shell around proteins," Proc. Natl. Acad. Sci. U. S. A. **104**, 20749–20752 (2007).
[207]S. Ebbinghaus, J. K. Seung, M. Heyden, X. Yu, M. Gruebele, D. M. Leitner, and M. Havenith, "Protein sequence- and pH-dependent hydration probed by terahertz spectroscopy," J. Am. Chem. Soc. **130**, 2374–2375 (2008).
[208]T. Q. Luong, P. K. Verma, R. K. Mitra, and M. Havenith, "Do hydration dynamics follow the structural perturbation during thermal denaturation of a protein: A terahertz absorption study," Biophys. J. **101**, 925–933 (2011).
[209]S. J. Kim, B. Born, M. Havenith, and M. Gruebele, "Real-time detection of protein-water dynamics upon protein folding by terahertz absorption spectroscopy," Angew. Chem.-Int. Ed. **47**, 6486–6489 (2008).
[210]M. Heyden, S. Ebbinghaus, and M. Havenith, "Terahertz spectroscopy as a tool to study hydration dynamics," in *Encyclopedia of Analytical Chemistry* (Wiley Online Library, 2010).
[211]V. Conti Nibali and M. Havenith, "New insights into the role of water in biological function: Terahertz absorption spectroscopy and molecular dynamics simulations studies of the solvation dynamics of biomolecules," J. Am. Chem. Soc. **136**, 12800–12807 (2014).
[212]A. Tamminen, M. Baggio, I. Nefedova, Q. Sun, J. Anttila, J. Ala-laurinaho, E. Brown, V. Wallace, E. Macpherson, T. Maloney, M. Salkola, S. Deng, and Z. Taylor, "Submillimeter-wave permittivity measurements of bound water in collagen hydrogels via frequency domain spectroscopy," IEEE Trans. Terahertz Sci. Technol. **11**, 538–547 (2021).
[213]T. Arikawa, M. Nagai, and K. Tanaka, "Characterizing hydration state in solution using terahertz time-domain attenuated total reflection spectroscopy," Chem. Phys. Lett. **457**, 12–17 (2008).
[214]J. W. Bye, S. Meliga, D. Ferachou, G. Cinque, J. A. Zeitler, and R. J. Falconer, "Analysis of the hydration water around bovine serum albumin using terahertz coherent synchrotron radiation," J. Phys. Chem. A **118**, 83–88 (2014).
[215]O. Sushko, R. Dubrovka, and R. S. Donnan, "Sub-terahertz spectroscopy reveals that proteins influence the properties of water at greater distances than previously detected," J. Chem. Phys. **142**, 055101 (2015).
[216]M. Grognot and G. Gallot, "Relative contributions of core protein and solvation shell in the terahertz dielectric properties of protein solutions," J. Phys. Chem. B **121**, 9508–9512 (2017).
[217]M. Hishida and K. Tanaka, "Long-range hydration effect of lipid membrane studied by terahertz time-domain spectroscopy," Phys. Rev. Lett. **106**, 158102 (2011).
[218]W. Xu, L. Xie, and Y. Ying, "Mechanisms and applications of terahertz metamaterial sensing: A review," Nanoscale **9**, 13864–13878 (2017).
[219]J. F. O'Hara, W. Withayachumnankul, and I. Al-Naib, "A review on thin-film sensing with terahertz waves," J. Infrared, Millimeter, Terahertz Waves **33**, 245–291 (2012).
[220]N. I. Zheludev and Y. S. Kivshar, "From metamaterials to metadevices," Nat. Mater. **11**, 917–924 (2012).
[221]W. Withayachumnankul and D. Abbott, "Metamaterials in the terahertz regime," IEEE Photonics J. **1**, 99–118 (2009).
[222]T. Chen, S. Li, and H. Sun, "Metamaterials application in sensing," Sensors **12**, 2742–2765 (2012).
[223]R. Singh, W. Cao, I. Al-Naib, L. Cong, W. Withayachumnankul, and W. Zhang, "Ultrasensitive terahertz sensing with high-*Q* Fano resonances in metasurfaces," Appl. Phys. Lett. **105**, 171101 (2014).
[224]H. Tao, A. C. Strikwerda, M. Liu, J. P. Mondia, E. Ekmekci, K. Fan, D. L. Kaplan, W. J. Padilla, X. Zhang, R. D. Averitt, and F. G. Omenetto, "Performance enhancement of terahertz metamaterials on ultrathin substrates for sensing applications," Appl. Phys. Lett. **97**, 261909 (2010).
[225]H. Tao, L. R. Chieffo, M. A. Brenckle, S. M. Siebert, M. Liu, A. C. Strikwerda, K. Fan, D. L. Kaplan, X. Zhang, R. D. Averitt, and F. G. Omenetto, "Metamaterials on paper as a sensing platform," Adv. Mater. **23**, 3197–3201 (2011).
[226]S. Y. Chiam, R. Singh, J. Gu, J. Han, W. Zhang, and A. A. Bettiol, "Increased frequency shifts in high aspect ratio terahertz split ring resonators," Appl. Phys. Lett. **94**, 064102 (2009).
[227]K. Meng, S. J. Park, A. D. Burnett, T. Gill, C. D. Wood, M. Rosamond, L. H. Li, L. Chen, D. R. Bacon, J. R. Freeman, P. Dean, Y. H. Ahn, E. H. Linfield, A. G. Davies, and J. E. Cunningham, "Increasing the sensitivity of terahertz split ring resonator metamaterials for dielectric sensing by localized substrate etching," Opt. Express **27**, 23164 (2019).
[228]D. K. Lee, J. H. Kang, J. S. Lee, H. S. Kim, C. Kim, J. Hun Kim, T. Lee, J. H. Son, Q. H. Park, and M. Seo, "Highly sensitive and selective sugar detection by terahertz nano-antennas," Sci. Rep. **5**, 15459 (2015).
[229]R. Zhang, Q. Chen, K. Liu, Z. Chen, K. Li, X. Zhang, J. Xu, and E. Pickwell-Macpherson, "Terahertz microfluidic metamaterial biosensor for sensitive detection of small-volume liquid samples," IEEE Trans. Terahertz Sci. Technol. **9**, 209–214 (2019).
[230]S. Yang, C. Tang, Z. Liu, B. Wang, C. Wang, J. Li, L. Wang, and C. Gu, "Simultaneous excitation of extremely high-Q-factor trapped and octupolar modes in terahertz metamaterials," Opt. Express **25**, 15938 (2017).
[231]L. Cong, S. Tan, R. Yahiaoui, F. Yan, W. Zhang, and R. Singh, "Experimental demonstration of ultrasensitive sensing with terahertz metamaterial absorbers: A comparison with the metasurfaces," Appl. Phys. Lett. **106**, 031107 (2015).
[232]R. Yahiaoui, S. Tan, L. Cong, R. Singh, F. Yan, and W. Zhang, "Multispectral terahertz sensing with highly flexible ultrathin metamaterial absorber," J. Appl. Phys. **118**, 083103 (2015).
[233]W. Xu, L. Xie, J. Zhu, L. Tang, R. Singh, C. Wang, Y. Ma, H. T. Chen, and Y. Ying, "Terahertz biosensing with a graphene-metamaterial heterostructure platform," Carbon **141**, 247–252 (2019).
[234]R. Wang, W. Xu, D. Chen, R. Zhou, Q. Wang, W. Gao, J. Kono, L. Xie, and Y. Ying, "Ultrahigh-sensitivity molecular sensing with carbon nanotube terahertz metamaterials," ACS Appl. Mater. Interfaces **12**, 40629–40634 (2020).
[235]W. Xu, L. Xie, J. Zhu, X. Xu, Z. Ye, C. Wang, Y. Ma, and Y. Ying, "Gold nanoparticle-based terahertz metamaterial sensors: Mechanisms and applications," ACS Photonics **3**, 2308–2314 (2016).
[236]K. Liu, R. Zhang, Y. Liu, X. Chen, K. Li, and E. Pickwell-MacPherson, "Gold nanoparticle enhanced detection of EGFR with terahertz metamaterial biosensor," Biomed. Opt. Express **12**, 1559–1567 (2021).
[237]J. F. O'Hara, R. Singh, I. Brener, E. Smirnova, J. Han, A. J. Taylor, and W. Zhang, "Thin-film sensing with planar terahertz metamaterials: Sensitivity and limitations," Opt. Express **16**, 1786 (2008).
[238]H. R. Park, K. J. Ahn, S. Han, Y. M. Bahk, N. Park, and D. S. Kim, "Colossal absorption of molecules inside single terahertz nanoantennas," Nano Lett. **13**, 1782–1786 (2013).
[239]H. R. Park, X. Chen, N. C. Nguyen, J. Peraire, and S. H. Oh, "Nanogap-enhanced terahertz sensing of 1 nm thick ($\lambda/10^6$) dielectric films," ACS Photonics **2**, 417–424 (2015).
[240]W. Withayachumnankul, J. F. OâHara, W. Cao, I. Al-Naib, and W. Zhang, "Limitation in thin-film sensing with transmission-mode terahertz time-domain spectroscopy," Opt. Express **22**, 972 (2014).
[241]Z. Bai, Y. Liu, R. Kong, T. Nie, Y. Sun, H. Li, T. Sun, C. Pandey, Y. Wang, H. Zhang, Q. Song, G. Liu, M. Kraft, W. Zhao, X. Wu, and L. Wen, "Near-field terahertz sensing of HeLa cells and *Pseudomonas* based on monolithic integrated metamaterials with a spintronic terahertz emitter," ACS Appl. Mater. Interfaces **12**, 35895–35902 (2020).
[242]R. Singh, I. A. I. Al-Naib, M. Koch, and W. Zhang, "Asymmetric planar terahertz metamaterials," Opt. Express **18**, 13044 (2010).
[243]S. J. Park, S. A. Yoon, and Y. H. Ahn, "Dielectric constant measurements of thin films and liquids using terahertz metamaterials," RSC Adv. **6**, 69381–69386 (2016).
[244]F. Miyamaru, K. Hattori, K. Shiraga, S. Kawashima, S. Suga, T. Nishida, M. W. Takeda, and Y. Ogawa, "Highly sensitive terahertz sensing of glycerol-water mixtures with metamaterials," J. Infrared, Millimeter, Terahertz Waves **35**, 198–207 (2014).
[245]R. Mendis and D. Grischkowsky, "Undistorted guided-wave propagation of subpicosecond terahertz pulses," Opt. Lett. **26**, 846–848 (2001).
[246]R. Menais and D. Grischkowsky, "THz interconnect with low-loss and low-group velocity dispersion," IEEE Microwave Wireless Compon. Lett. **11**, 444–446 (2001).
[247]J. Zhang and D. Grischkowsky, "Waveguide terahertz time-domain spectroscopy of nanometer water layers," Opt. Lett. **29**, 1617 (2004).
[248]N. Laman, S. S. Harsha, D. Grischkowsky, and J. S. Melinger, "High-resolution waveguide THz spectroscopy of biological molecules," Biophys. J. **94**, 1010–1020 (2008).

[249]S. S. Harsha, N. Laman, and D. Grischkowsky, "High-Q terahertz Bragg resonances within a metal parallel plate waveguide," Appl. Phys. Lett. **94**, 091118 (2009).
[250]R. Mendis, V. Astley, J. Liu, and D. M. Mittleman, "Terahertz microfluidic sensor based on a parallel-plate waveguide resonant cavity," Appl. Phys. Lett. **95**, 171113 (2009).
[251]E. S. Lee, Y. B. Ji, and T. I. Jeon, "Terahertz band gap properties by using metal slits in tapered parallel-plate waveguides," Appl. Phys. Lett. **97**, 1993–1998 (2010).
[252]H. S. Bark, J. Zha, E. S. Lee, and T.-I. Jeon, "Thin layer terahertz sensing using two-channel parallel-plate waveguides," Opt. Express **22**, 16738 (2014).
[253]J. Cabello-Sanchez, V. Drakinskiy, J. Stake, and H. Rodilla, "On-chip characterization of high-loss liquids between 750 and 1100 GHz," IEEE Trans. Terahertz Sci. Technol. **11**, 113–116 (2021).
[254]H. Rodilla, A. Kim, J. Vukusic, G. D. Jeffries, K. Vukusic, A. Jesorka, and J. Stake, in 2014 39th International Conference on Infrared, Millimeter, and Terahertz waves (IRMMW-THz), 2014.
[255]M. B. Byrne, J. Cunningham, K. Tych, A. D. Burnett, M. R. Stringer, C. D. Wood, L. Dazhang, M. Lachab, E. H. Linfield, and A. G. Davies, "Terahertz vibrational absorption spectroscopy using microstrip-line waveguides," Appl. Phys. Lett. **93**, 182904 (2008).
[256]T. Ohkubo, M. Onuma, J. Kitagawa, and Y. Kadoya, "Micro-strip-line-based sensing chips for characterization of polar liquids in terahertz regime," Appl. Phys. Lett. **88**, 212511 (2006).
[257]C. Wood, J. Cunningham, I. C. Hunter, P. Tosch, E. H. Linfield, and A. G. Davies, "On-chip pulsed terahertz systems and their applications," Int. J. Infrared Millimeter Waves **27**, 557–569 (2006).
[258]M. Nagel, P. Haring Bolivar, M. Brucherseifer, H. Kurz, A. Bosserhoff, and R. Büttner, "Integrated THz technology for label-free genetic diagnostics," Appl. Phys. Lett. **80**, 154–156 (2002).
[259]F. Fan, X. Zhang, S. Li, D. Deng, N. Wang, H. Zhang, and S. Chang, "Terahertz transmission and sensing properties of microstructured PMMA tube waveguide," Opt. Express **23**, 27204 (2015).
[260]J. C. Ginn, R. L. Jarecki, E. A. Shaner, and P. S. Davids, "Infrared plasmons on heavily-doped silicon," J. Appl. Phys. **110**, 043110 (2011).
[261]A. Otto, "Excitation of nonradiative surface plasma waves in silver by the method of frustrated total reflection," Z. Phys. A **216**, 398–410 (1968).
[262]E. Kretschmann and H. Raether, "Radiative decay of non radiative surface plasmons excited by light," Z. Naturforsch. A **23**, 2135–2136 (1968).
[263]K. J. Willis, S. C. Hagness, and I. Knezevic, "A generalized Drude model for doped silicon at terahertz frequencies derived from microscopic transport simulation," Appl. Phys. Lett. **102**, 122113 (2013).
[264]R. Soref, R. E. Peale, and W. Buchwald, "Longwave plasmonics on doped silicon and silicides," Opt. Express **16**, 6507 (2008).
[265]H. Hirori, M. Nagai, and K. Tanaka, "Destructive interference effect on surface plasmon resonance in terahertz attenuated total reflection," Opt. Express **13**, 10801 (2005).
[266]J. Chochol, K. Postava, M. Čada, and J. Pištora, "Experimental demonstration of magnetoplasmon polariton at InSb(InAs)/dielectric interface for terahertz sensor application," Sci. Rep. **7**, 13117 (2017).
[267]J. Homola and M. Piliarik, *Surface Plasmon Resonance (SPR) Sensors* (Springer, Berlin/Heidelberg, 2006), pp. 45–67.
[268]B. A. Prabowo, A. Purwidyantri, and K. C. Liu, "Surface plasmon resonance optical sensor: A review on light source technology," Biosensors **8**, 80 (2018).
[269]C. H. Gan, "Analysis of surface plasmon excitation at terahertz frequencies with highly doped graphene sheets via attenuated total reflection," Appl. Phys. Lett. **101**, 111609 (2012).
[270]Y. Huang, S. Zhong, Y. Shen, L. Yao, Y. Yu, and D. Cui, "Graphene insulator stack based ultrasensitive terahertz sensor with surface plasmon resonance," IEEE Photonics J. **9**, 5900911 (2017).
[271]J. Saxler, J. Gómez Rivas, C. Janke, H. P. Pellemans, P. H. Bolívar, and H. Kurz, "Time-domain measurements of surface plasmon polaritons in the terahertz frequency range," Phys. Rev. B **69**, 155427 (2004).
[272]T. H. Isaac, W. L. Barnes, and E. Hendry, "Determining the terahertz optical properties of subwavelength films using semiconductor surface plasmons," Appl. Phys. Lett. **93**, 241115 (2008).
[273]T. Yang, Y. Li, R. Stantchev, Y. Zhu, Y. Qin, X. Zhou, and W. Huang, "Detection of defects on the surface of a semiconductor by terahertz surface plasmon polaritons," Appl. Opt. **55**, 4139–4144 (2016).
[274]W. X. Tang, H. C. Zhang, H. F. Ma, W. X. Jiang, and T. J. Cui, "Concept, theory, design, and applications of spoof surface plasmon polaritons at microwave frequencies," Adv. Opt. Mater. **7**, 1800421 (2019).
[275]J. Gómez Rivas, M. Kuttge, P. Haring Bolivar, H. Kurz, and J. A. Sánchez-Gil, "Propagation of surface plasmon polaritons on semiconductor gratings," Phys. Rev. Lett. **93**, 256804 (2004).
[276]C. R. Williams, S. R. Andrews, S. A. Maier, A. I. Fernández-Domínguez, L. Martín-Moreno, and F. J. García-Vidal, "Highly confined guiding of terahertz surface plasmon polaritons on structured metal surfaces," Nat. Photonics **2**, 175–179 (2008).
[277]S. Li, M. M. Jadidi, T. E. Murphy, and G. Kumar, "Terahertz surface plasmon polaritons on a semiconductor surface structured with periodic V-grooves," Opt. Express **21**, 7041 (2013).
[278]B. Ng, J. Wu, S. M. Hanham, A. I. Fernández-Domínguez, N. Klein, Y. F. Liew, M. B. Breese, M. Hong, and S. A. Maier, "Spoof plasmon surfaces: A novel platform for THz sensing," Adv. Opt. Mater. **1**, 543–548 (2013).
[279]Y. Huang, S. Zhong, T. Shi, Y.-C. Shen, and D. Cui, "HR-Si prism coupled tightly confined spoof surface plasmon polaritons mode for terahertz sensing," Opt. Express **27**, 34067 (2019).
[280]Y. Huang, S. Zhong, T. Shi, Y. C. Shen, and D. Cui, "Terahertz plasmonic phase-jump manipulator for liquid sensing," Nanophotonics **9**, 3011–3021 (2020).
[281]S. Fan, B. Ung, E. P. Parrott, and E. Pickwell-Macpherson, "Gelatin embedding: A novel way to preserve biological samples for terahertz imaging and spectroscopy," Phys. Med. Biol. **60**, 2703 (2015).
[282]H. Hoshina, A. Hayashi, N. Miyoshi, F. Miyamaru, and C. Otani, "Terahertz pulsed imaging of frozen biological tissues," Appl. Phys. Lett. **94**, 123901 (2009).
[283]Y. C. Sim, J. Y. Park, K.-M. Ahn, C. Park, and J.-H. Son, "Terahertz imaging of excised oral cancer at frozen temperature," Biomed. Opt. Express **4**, 1413–1421 (2013).
[284]Y. He, B. S.-Y. Ung, E. P. J. Parrott, A. T. Ahuja, and E. Pickwell-MacPherson, "Freeze-thaw hysteresis effects in terahertz imaging of biomedical tissues," Biomed. Opt. Express **7**, 4711 (2016).
[285]Y. Sun, B. M. Fischer, and E. Pickwell-MacPherson, "Effects of formalin fixing on the terahertz properties of biological tissues," J. Biomed. Opt. **14**, 064017 (2009).
[286]G. M. Png, J. W. Choi, B. W. Ng, S. P. Mickan, D. Abbott, and X. C. Zhang, "The impact of hydration changes in fresh bio-tissue on THz spectroscopic measurements," Phys. Med. Biol. **53**, 3501–3517 (2008).
[287]R. M. Woodward, B. E. Cole, V. P. Wallace, R. J. Pye, D. D. Arnone, E. H. Linfield, and M. Pepper, "Terahertz pulse imaging in reflection geometry of human skin cancer and skin tissue," Phys. Med. Biol. **47**, 3853 (2002).
[288]V. P. Wallace, A. J. Fitzgerald, S. Shankar, N. Flanagan, R. Pye, J. Cluff, and D. D. Arnone, "Terahertz pulsed imaging of basal cell carcinoma *ex vivo* and *in vivo*," Br. J. Dermatol. **151**, 424–432 (2004).
[289]V. P. Wallace, A. J. Fitzgerald, E. Pickwell, R. J. Pye, P. F. Taday, N. Flanagan, and T. Ha, "Terahertz pulsed spectroscopy of human basal cell carcinoma," Appl. Spectrosc. **60**, 1127–1133 (2006).
[290]C. S. Joseph, R. Patel, V. A. Neel, R. H. Giles, and A. N. Yaroslavsky, "Imaging of *ex vivo* nonmelanoma skin cancers in the optical and terahertz spectral regions," J. Biophotonics **7**, 295–303 (2014).
[291]P. C. Ashworth, E. Pickwell-MacPherson, E. Provenzano, S. E. Pinder, A. D. Purushotham, M. Pepper, and V. P. Wallace, "Terahertz pulsed spectroscopy of freshly excised human breast cancer," Opt. Express **17**, 12444–12454 (2009).
[292]A. J. Fitzgerald, S. Pinder, A. D. Purushotham, P. O'sKelly, P. C. Ashworth, and V. P. Wallace, "Classification of terahertz-pulsed imaging data from excised breast tissue," J. Biomed. Opt. **17**, 016005 (2012).
[293]S. Yamaguchi, Y. Fukushi, O. Kubota, T. Itsuji, T. Ouchi, and S. Yamamoto, "Brain tumor imaging of rat fresh tissue using terahertz spectroscopy," Sci. Rep. **6**, 30124 (2016).
[294]G. R. Musina, P. V. Nikitin, N. V. Chernomyrdin, I. N. Dolganova, A. A. Gavdush, G. A. Komandin, D. S. Ponomarev, A. A. Potapov, I. V. Reshetov, V. V. Tuchin, and K. I. Zaytsev, "Prospects of terahertz technology in

diagnosis of human brain tumors—A review," J. Biomed. Photonics Eng. **6**, 020201 (2020).
[295]D. Hou, X. Li, J. Cai, Y. Ma, X. Kang, P. Huang, and G. Zhang, "Terahertz spectroscopic investigation of human gastric normal and tumor tissues," Phys. Med. Biol. **59**, 5423–5440 (2014).
[296]S. Preu, G. H. Dhler, S. Malzer, L. J. Wang, and A. C. Gossard, "Tunable, continuous-wave Terahertz photomixer sources and applications," J. Appl. Phys. **109**, 061301 (2011).
[297]F. Formanek, M.-A. Brun, and A. Yasuda, "Contrast improvement of terahertz images of thin histopathologic sections," Biomed. Opt. Express **2**, 58 (2011).
[298]F. Wahaia, I. Kasalynas, R. Venckevicius, D. Seliuta, G. Valusis, A. Urbanowicz, G. Molis, F. Carneiro, C. D. Carvalho Silva, and P. L. Granja, "Terahertz absorption and reflection imaging of carcinoma-affected colon tissues embedded in paraffin," J. Mol. Struct. **1107**, 214–219 (2016).
[299]C. B. Reid, A. Fitzgerald, G. Reese, R. Goldin, P. Tekkis, P. S. O'Kelly, E. Pickwell-Macpherson, A. P. Gibson, and V. P. Wallace, "Terahertz pulsed imaging of freshly excised human colonic tissues," Phys. Med. Biol. **56**, 4333–4353 (2011).
[300]E. Jung, M. Lim, K. Moon, Y. Do, S. Lee, H. Han, H. J. Choi, K. S. Cho, and K. R. Kim, "Terahertz pulse imaging of micro-metastatic lymph nodes in early-stage cervical cancer patients," J. Opt. Soc. Korea **15**, 155–160 (2011).
[301]W. G. Yeo, O. Gurel, N. Srinivasan, P. D. King, N. K. Nahar, S. Park, N. L. Lehman, and K. Sertel, "Terahertz imaging and electromagnetic model of axon demyelination in Alzheimer's disease," IEEE Trans. Terahertz Sci. Technol. **7**, 711–721 (2017).
[302]Z. D. Taylor, J. Garritano, S. Sung, N. Bajwa, D. B. Bennett, B. Nowroozi, P. Tewari, J. Sayre, J. P. Hubschman, S. Deng, E. R. Brown, and W. S. Grundfest, "THz and mm-wave sensing of corneal tissue water content: Electromagnetic modeling and analysis," IEEE Trans. Terahertz Sci. Technol. **5**, 170–183 (2015).
[303]D. B. Bennett, Z. D. Taylor, P. Tewari, R. S. Singh, M. O. Culjat, W. S. Grundfest, D. J. Sassoon, R. D. Johnson, J.-P. Hubschman, and E. R. Brown, "Terahertz sensing in corneal tissues," J. Biomed. Opt. **16**, 057003 (2011).
[304]S. J. Oh, S.-H. Kim, K. Jeong, Y. Park, Y.-M. Huh, J.-H. Son, and J.-S. Suh, "Measurement depth enhancement in terahertz imaging of biological tissues," Opt. Express **21**, 21299 (2013).
[305]S. J. Oh, J. Kang, I. Maeng, J.-S. Suh, Y.-M. Huh, S. Haam, and J.-H. Son, "Nanoparticle-enabled terahertz imaging for cancer diagnosis," Opt. Express **17**, 3469 (2009).
[306]J. Dong, H. Breitenborn, R. Piccoli, L. V. Besteiro, P. You, D. Caraffini, Z. M. Wang, A. O. Govorov, R. Naccache, F. Vetrone, L. Razzari, and R. Morandotti, "Terahertz three-dimensional monitoring of nanoparticle-assisted laser tissue soldering," Biomed. Opt. Express **11**, 2254–2267 (2020).
[307]K. W. Kim, K.-S. Kim, H. Kim, S. H. Lee, J.-H. Park, J.-H. Han, S.-H. Seok, J. Park, Y. Choi, Y. I. Kim, J. K. Han, and J.-H. Son, "Terahertz dynamic imaging of skin drug absorption," Opt. Express **20**, 9476 (2012).
[308]K. W. Kim, H. Kim, J. Park, J. K. Han, and J. H. Son, "Terahertz tomographic imaging of transdermal drug delivery," IEEE Trans. Terahertz Sci. Technol. **2**, 99–106 (2012).
[309]L. Wu, D. Xu, Y. Wang, B. Liao, Z. Jiang, L. Zhao, Z. Sun, N. Wu, T. Chen, H. Feng, and J. Yao, "Study of *in vivo* brain glioma in a mouse model using continuous-wave terahertz reflection imaging," Biomed. Opt. Express **10**, 3953 (2019).
[310]S. Huang, P. C. Ashworth, K. W. C. Kan, Y. Chen, V. P. Wallace, Y.-T. Zhang, and E. Pickwell-MacPherson, "Improved sample characterization in terahertz reflection imaging and spectroscopy: Erratum," Opt. Express **19**, 24782 (2011).
[311]B. E. Cole, R. M. Woodward, D. A. Crawley, V. P. Wallace, D. D. Arnone, and M. Pepper, Jr., "Terahertz imaging and spectroscopy of human skin *in vivo*," in *Commercial and Biomedical Applications of Ultrashort Pulse Lasers; Laser Plasma Generation and Diagnostics*, edited by R. F. Haglund, J. Neev, and R. F. Wood (SPIE, 2001), Vol. 4276, pp. 1–10.
[312]H. Lindley-Hatcher, A. I. Hernandez-Serrano, J. Wang, J. Cebrian, J. Hardwicke, and E. Pickwell-MacPherson, "Evaluation of *in vivo* THz sensing for assessing human skin hydration," J. Phys. **3**, 014001 (2020).
[313]K. I. Zaytsev, A. A. Gavdush, N. V. Chernomyrdin, and S. O. Yurchenko, "Highly accurate *in vivo* terahertz spectroscopy of healthy skin: Variation of refractive index and absorption coefficient along the human body," IEEE Trans. Terahertz Sci. Technol. **5**, 817–827 (2015).
[314]I. Echchgadda, J. E. Grundt, M. Tarango, B. L. Ibey, T. Tongue, M. Liang, H. Xin, and G. J. Wilmink, "Using a portable terahertz spectrometer to measure the optical properties of *in vivo* human skin," in Proceedings Vol. 8585, Terahertz and Ultrashort Electromagnetic Pulses for Biomedical Applications, 85850J, 2013.
[315]P. Tewari, C. P. Kealey, D. B. Bennett, N. Bajwa, K. S. Barnett, R. S. Singh, M. O. Culjat, A. Stojadinovic, W. S. Grundfest, and Z. D. Taylor, "*In vivo* terahertz imaging of rat skin burns," J. Biomed. Opt. **17**, 040503 (2012).
[316]S. Fan, B. S. Y. Ung, E. P. J. Parrott, V. P. Wallace, and E. Pickwell-Macpherson, "*In vivo* terahertz reflection imaging of human scars during and after the healing process," J. Biophotonics **10**, 1143–1151 (2017).
[317]P. Tewari, J. Garritano, N. Bajwa, S. Sung, H. Huang, D. Wang, W. Grundfest, D. B. Ennis, D. Ruan, E. Brown, E. Dutson, M. C. Fishbein, and Z. Taylor, "Methods for registering and calibrating *in vivo* terahertz images of cutaneous burn wounds," Biomed. Opt. Express **10**, 322–337 (2019).
[318]N. Bajwa, S. Sung, J. Garritano, B. Nowroozi, P. Tewari, D. B. Ennis, J. Alger, W. Grundfest, and Z. Taylor, "*In vivo* confirmation of hydration based contrast mechanisms for terahertz medical imaging using MRI," in *Proceedings SPIE 9199, Terahertz Emitters, Receivers, and Applications V*, edited by M. Razeghi, A. N. Baranov, J. M. Zavada, and D. Pavlidis (SPIE, 2014), p. 91990U.
[319]N. Bajwa, S. Sung, D. B. Ennis, M. C. Fishbein, B. N. Nowroozi, D. Ruan, A. MacCabi, J. Alger, M. A. John, W. S. Grundfest, and Z. D. Taylor, "Terahertz imaging of cutaneous edema: Correlation with magnetic resonance imaging in burn wounds," IEEE Trans. Biomed. Eng. **64**, 2682–2694 (2017).
[320]O. B. Osman, T. J. Tan, S. Henry, A. Warsen, N. Farr, A. M. McClintic, Y.-N. Wang, S. Arbabi, and M. H. Arbab, "Differentiation of burn wounds in an *in vivo* porcine model using terahertz spectroscopy," Biomed. Opt. Express **11**, 6528 (2020).
[321]A. Chen, O. B. Osman, Z. B. Harris, A. Abazri, R. Honkanen, and M. H. Arbab, "Investigation of water diffusion dynamics in corneal phantoms using terahertz time-domain spectroscopy," Biomed. Opt. Express **11**, 1284 (2020).
[322]J. A. Castoro, A. A. Bettelheim, and F. A. Bettelheim, "Water gradients across bovine cornea," Invest. Ophthalmol. Visual Sci. **29**, 963–968 (1988).
[323]W. Grundfest, Z. Taylor, J. Garritano, B. Nowroozi, N. Bajwa, and S. Sung, "THz sensing of corneal tissue water content," U.S. patent 10,939,844 (2021).
[324]I. Ozheredov, T. Safonova, E. Sikach, M. Mischenko, M. Prokopchuk, A. Larichev, Y. Listopadskaya, and A. Shkurinov, "Potential clinical applications of terahertz reflectometry for the assessment of the tear film stability," Opt. Eng. **59**, 061622 (2020).
[325]E. A. Kekkonen, A. A. Konovko, Y. S. Lee, I. M. Lee, I. A. Ozherdov, K. H. Park, T. N. Safonova, E. I. Sikach, and A. P. Shkurinov, "Assessment of the degree of hydration of ocular surface tissues using THz reflectometry," Quantum Electron. **50**, 61–68 (2020).
[326]K. I. Zaytsev, K. G. Kudrin, V. E. Karasik, I. V. Reshetov, and S. O. Yurchenko, "*In vivo* terahertz spectroscopy of pigmentary skin nevi: Pilot study of non-invasive early diagnosis of dysplasia," Appl. Phys. Lett. **106**, 053702 (2015).
[327]K. I. Zaytsev, K. G. Kudrin, I. V. Reshetov, A. A. Gavdush, N. V. Chernomyrdin, V. E. Karasik, and S. O. Yurchenko, "*In vivo* spectroscopy of healthy skin and pathology in terahertz frequency range," J. Phys. **584**, 012023 (2015).
[328]K. I. Zaytsev, N. V. Chernomyrdin, K. G. Kudrin, A. A. Gavdush, P. A. Nosov, S. O. Yurchenko, and I. V. Reshetov, "*In vivo* terahertz pulsed spectroscopy of dysplastic and non-dysplastic skin nevi," J. Phys. **735**, 012076 (2016).
[329]H. Chen, T.-H. Chen, T.-F. Tseng, J.-T. Lu, C.-C. Kuo, S.-C. Fu, W.-J. Lee, Y.-F. Tsai, Y.-Y. Huang, E. Y. Chuang, Y.-J. Hwang, and C.-K. Sun, "High-sensitivity *in vivo* THz transmission imaging of early human breast cancer in a subcutaneous xenograft mouse model," Opt. Express **19**, 21552–21562 (2011).
[330]N. Bajwa, J. Au, R. Jarrahy, S. Sung, M. C. Fishbein, D. Riopelle, D. B. Ennis, T. Aghaloo, M. A. St. John, W. S. Grundfest, and Z. D. Taylor, "Non-invasive

terahertz imaging of tissue water content for flap viability assessment," Biomed. Opt. Express **8**, 460 (2017).
[331]G. G. Hernandez-Cardoso, S. C. Rojas-Landeros, M. Alfaro-Gomez, A. I. Hernandez-Serrano, I. Salas-Gutierrez, E. Lemus-Bedolla, A. R. Castillo-Guzman, H. L. Lopez-Lemus, and E. Castro-Camus, "Terahertz imaging for early screening of diabetic foot syndrome: A proof of concept," Sci. Rep. **7**, 42124 (2017).
[332]G. G. Hernandez-Cardoso, M. Alfaro-Gomez, S. C. Rojas-Landeros, I. Salas-Gutierrez, and E. Castro-Camus, "Diabetic foot early diagnosis and statistical analysis by spectral terahertz reflection images," in *Terahertz Emitters, Receivers, and Applications IX*, edited by M. Razeghi and A. N. Baranov (SPIE, 2018), Vol. 10756, p. 10756X.
[333]G. G. Hernandez-Cardoso, M. Alfaro-Gomez, S. C. Rojas-Landeros, I. Salas-Gutierrez, and E. Castro-Camus, "Pixel statistical analysis of diabetic vs. non-diabetic foot-sole spectral terahertz reflection images," J. Infrared, Millimeter, Terahertz Waves **39**, 879–886 (2018).
[334]G. G. Hernandez-Cardoso, L. F. Amador-Medina, G. Gutierrez-Torres, E. S. Reyes-Reyes, C. A. Benavides Martínez, C. Cardona Espinoza, J. Arce Cruz, I. Salas-Gutierrez, B. O. Murillo-Ortíz, and E. Castro-Camus, "Terahertz imaging demonstrates its diagnostic potential and reveals a relationship between cutaneous dehydration and neuropathy for diabetic foot syndrome patients," Sci. Rep. **12**, 3110 (2022).
[335]O. P. Cherkasova, M. M. Nazarov, E. E. Berlovskaya, A. A. Angeluts, A. M. Makurenkov, and A. P. Shkurinov, "Studying human and animal skin optical properties by terahertz time-domain spectroscopy," Bull. Russ. Acad. Sci.: Phys. **80**, 479–483 (2016).
[336]O. Cherkasova, M. Nazarov, and A. Shkurinov, "Noninvasive blood glucose monitoring in the terahertz frequency range," Opt. Quantum Electron. **48**, 217 (2016).
[337]M. S. Kulya, E. L. Odlyanitskiy, Q. Cassar, I. A. Mustafin, V. N. Trukhin, P. G. Gavrilova, D. V. Korolev, Y. A. Kononova, N. S. Balbekin, P. Mounaix, J. P. Guillet, N. V. Petrov, and O. A. Smolyanskaya, "Fast terahertz spectroscopic holographic assessment of optical properties of diabetic blood plasma," J. Infrared, Millimeter, Terahertz Waves **41**, 1041–1056 (2020).
[338]A. A. Lykina, M. M. Nazarov, M. R. Konnikova, I. A. Mustafin, V. L. Vaks, V. A. Anfertev, E. G. Domracheva, M. B. Chernyaeva, Y. V. Kistenev, D. A. Vrazhnov, V. V. Prischepa, Y. A. Kononova, D. V. Korolev, O. P. Cherkasova, A. P. Shkurinov, A. Y. Babenko, and O. A. Smolyanskaya, "Terahertz spectroscopy of diabetic and non-diabetic human blood plasma pellets," J. Biomed. Opt. **26**, 043006 (2021).
[339]E. E. Berlovskaya, O. P. Cherkasova, I. A. Ozheredov, T. V. Adamovich, E. S. Isaychev, S. A. Isaychev, A. M. Makurenkov, A. N. Varaksin, S. B. Gatilov, N. I. Kurenkov, A. M. Chernorizov, and A. P. Shkurinov, "New approach to terahertz diagnostics of human psychoemotional state," Quantum Electron. **49**, 70–77 (2019).
[340]D. Čibiraitė-Lukenskienė, K. Ikamas, T. Lisauskas, V. Krozer, H. G. Roskos, and A. Lisauskas, "Passive detection and imaging of human body radiation using an uncooled field-effect transistor-based THz detector," Sensors **20**, 4087 (2020).
[341]A. Y. Owda, N. Salmon, S. W. Harmer, S. Shylo, N. J. Bowring, N. D. Rezgui, and M. Shah, "Millimeter-wave emissivity as a metric for the non-contact diagnosis of human skin conditions," Bioelectromagnetics **38**, 559–569 (2017).
[342]A. Y. Owda, N. Salmon, and N. D. Rezgui, "Electromagnetic signatures of human skin in the millimeter wave band 80–100 GHz," Prog. Electromagn. Res. B **80**, 79–99 (2018).
[343]Y. Sun, P. Du, X. Lu, P. Xie, Z. Qian, S. Fan, and Z. Zhu, "Quantitative characterization of bovine serum albumin thin-films using terahertz spectroscopy and machine learning methods," Biomed. Opt. Express **9**, 2917 (2018).
[344]K. Li, X. Chen, R. Zhang, and E. Pickwell-Macpherson, "Classification for glucose and lactose terahertz spectrums based on SVM and DNN methods," IEEE Trans. Terahertz Sci. Technol. **10**, 617–623 (2020).
[345]Y. Cao, P. Huang, X. Li, W. Ge, D. Hou, and G. Zhang, "Terahertz spectral unmixing based method for identifying gastric cancer," Phys. Med. Biol. **63**, 035016 (2018).
[346]Y. V. Kistenev, A. V. Borisov, A. I. Knyazkova, V. V. Nikolaev, A. Samarinova, N. A. Navolokin, D. K. Tuchina, and V. V. Tuchin, "Differential diagnostics of paraffin-embedded tissues by IR-THz spectroscopy and machine learning," in *Tissue Optics and Photonics* (International Society for Optics and Photonics, 2020), Vol. 11363, pp. 1–7.
[347]A. Zahid, H. T. Abbas, A. Ren, A. Zoha, H. Heidari, S. A. Shah, M. A. Imran, A. Alomainy, and Q. H. Abbasi, "Machine learning driven non-invasive approach of water content estimation in living plant leaves using terahertz waves," Plant Methods **15**, 138 (2019).
[348]Q. Cassar, S. Caravera, G. MacGrogan, T. Bücher, P. Hillger, U. Pfeiffer, T. Zimmer, J. P. Guillet, and P. Mounaix, "Terahertz refractive index-based morphological dilation for breast carcinoma delineation," Sci. Rep. **11**, 1–16 (2021).
[349]Y. V. Kistenev, A. V. Teteneva, T. V. Sorokina, A. I. Knyazkova, O. A. Zakharova, A. Cuisset, V. L. Vaks, E. G. Domracheva, M. B. Chernyaeva, V. A. Anfertâev, E. S. Sim, I. Y. Yanina, V. V. Tuchin, and A. V. Borisov, "Diagnosis of diabetes based on analysis of exhaled air by terahertz spectroscopy and machine learning," Opt. Spectrosc. **128**, 809–814 (2020).
[350]A. I. Knyazkova, A. V. Borisov, L. V. Spirina, and Y. V. Kistenev, "Paraffin-embedded prostate cancer tissue grading using terahertz spectroscopy and machine learning," J. Infrared, Millimeter, Terahertz Waves **41**, 1089–1104 (2020).
[351]W. Liu, R. Zhang, Y. Ling, H. Tang, R. She, G. Wei, X. Gong, and Y. Lu, "Automatic recognition of breast invasive ductal carcinoma based on terahertz spectroscopy with wavelet packet transform and machine learning," Biomed. Opt. Express **11**, 971 (2020).
[352]L. H. Eadie, C. B. Reid, A. J. Fitzgerald, and V. P. Wallace, "Optimizing multi-dimensional terahertz imaging analysis for colon cancer diagnosis," Expert Syst. Appl. **40**, 2043–2050 (2013).
[353]P. Huang, Y. Cao, J. Chen, W. Ge, D. Hou, and G. Zhang, "Analysis and inspection techniques for mouse liver injury based on terahertz spectroscopy," Opt. Express **27**, 26014 (2019).
[354]C. Cao, Z. Zhang, X. Zhao, and T. Zhang, "Terahertz spectroscopy and machine learning algorithm for non-destructive evaluation of protein conformation," Opt. Quantum Electron. **52**, 225 (2020).
[355]J. Y. Park, H. J. Choi, H. Cheon, S. W. Cho, S. Lee, and J.-H. Son, "Terahertz imaging of metastatic lymph nodes using spectroscopic integration technique," Biomed. Opt. Express **8**, 1122 (2017).
[356]D. Reshef, Y. Reshef, H. Finucane, S. Grossman, G. Mcvean, P. Turnbaugh, E. Lander, M. Mitzenmacher, and P. Sabeti, "Detecting novel associations in large data sets," Science **334**, 1518–1524 (2011).
[357]E. Kriesten, F. Alsmeyer, A. Bardow, and W. Marquardt, "Fully automated indirect hard modeling of mixture spectra," Chemom. Intell. Lab. Syst. **91**, 181–193 (2008).
[358]L. Breiman, "Random forests," Mach. Learn. **45**, 5–32 (2001).
[359]H. Park and J. H. Son, "Machine learning techniques for THz imaging and time-domain spectroscopy," Sensors **21**, 1186 (2021).
[360]A. E. Cerussi, V. W. Tanamai, D. Hsiang, J. Butler, R. S. Mehta, and B. J. Tromberg, "Diffuse optical spectroscopic imaging correlates with final pathological response in breast cancer neoadjuvant chemotherapy," Philos. Trans. R. Soc. A **369**, 4512–4530 (2011).
[361]E. Pickwell-MacPherson, "Practical considerations for *in vivo* THz imaging," Terahertz Sci. Technol. **3**, 163–171 (2010).
[362]M. Yamagiwa, T. Ogawa, T. Minamikawa, D. G. Abdelsalam, K. Okabe, N. Tsurumachi, Y. Mizutani, T. Iwata, H. Yamamoto, and T. Yasui, "Real-time amplitude and phase imaging of optically opaque objects by combining full-field off-axis terahertz digital holography with angular spectrum reconstruction," J. Infrared, Millimeter, Terahertz Waves **39**, 561–572 (2018).
[363]See https://www.toptica.com/products/terahertz-systems/frequency-domain/terascan/ for "Toptica."
[364]R. I. Stantchev, X. Yu, T. Blu, and E. Pickwell-macpherson, "Real-time terahertz imaging with a single-pixel detector," Nat. Commun. **11**, 2535 (2020).
[365]R. I. Stantchev, K. Li, and E. Pickwell-MacPherson, "Rapid imaging of pulsed terahertz radiation with spatial light modulators and neural networks," ACS Photonics **8**, 3150–3155 (2021).

[366]E. Hahamovich, S. Monin, Y. Hazan, and A. Rosenthal, "Single pixel imaging at megahertz switching rates via cyclic Hadamard masks," Nat. Commun. **12**, 4516 (2021).
[367]C. G. Wade, N. Šibali, N. R. De Melo, J. M. Kondo, C. S. Adams, and K. J. Weatherill, "Real-time near-field terahertz imaging with atomic optical fluorescence," Nat. Photonics **11**, 40–43 (2017).
[368]L. A. Downes, A. R. MacKellar, D. J. Whiting, C. Bourgenot, C. S. Adams, and K. J. Weatherill, "Full-field terahertz imaging at kilohertz frame rates using atomic vapor," Phys. Rev. X **10**, 011027 (2020).
[369]M. Naftaly, "An international intercomparison of THz time-domain spectrometers," in *2016 41st International Conference on Infrared, Millimeter, and Terahertz Waves (IRMMW-THz)* (IEEE, 2016), pp. 1–2.